Hybrid synchronous condenser system design and control for enhanced grid services

Nuhic, Mirza

Publication date:
2022

Document Version
Publisher's PDF, also known as Version of record

Technical University of Denmark

Mirza Nuhic

Hybrid synchronous condenser system design and control for enhanced grid services

Dissertation, January 2022

Kongens Lyngby, Denmark

Center for Electric Power and Energy
Department of Electrical Engineering

DANMARKS TEKNISKE UNIVERSITET
Center for Electric Power and Energy (CEE)
DTU Electrical Engineering

Hybrid synchronous condenser system design and control for enhanced grid services

Hybrid synkron kondensatorsystem design og kontrol til forbedrede net tjenester

Dissertation, by Mirza Nuhic

Supervisors:
Guangya Yang, Technical University of Denmark
Cornel Brozio, Scottish Power
Richard Rivas, Hitachi ABB

DTU - Technical University of Denmark, Kongens Lyngby - January 2022

Hybrid synchronous condenser system design and control for enhanced grid services

This thesis was prepared by:
Mirza Nuhic

Supervisors:
Guangya Yang, Technical University of Denmark
Cornel Brozio, Scottish Power
Richard Rivas, Hitachi ABB

Dissertation Examination Committee:
Senior Researcher Yi Zong (Chairman)
Department of Electrical Engineering, Technical University of Denmark, Denmark

Professor Bikash Pal
Imperial College London, Great Britain

Lead Power System Specialist Lukasz Kocewiak
Ãrstad, Denmark

Center for Electric Power and Energy (CEE)
DTU Electrical Engineering
Elektrovej, Building 325
DK-2800 Kgs. Lyngby
Denmark

Tel: (+45) 4525 3500
Fax: (+45) 4588 6111
E-mail: cee@elektro.dtu.dk

Release date: January 2022

Edition: Draft V01

Class: Internal

Field: Electrical Engineering

Remarks: The dissertation is presented to the Department of Electrical Engineering of the Technical University of Denmark in partial fulfillment of the requirements for the degree of Doctor of Philosophy.

ISBN: 000-00-00000-00-0

Preface

This thesis is prepared at the Department of Electrical Engineering of the Technical University of Denmark in partial fulfilment of the requirements for acquiring the degree of Doctor of Philosophy in Engineering. The Ph.D. project was funded by the project Phoenix project, funded by Ofgem under Network Innovation Competition programme, Project Direction ref: SPT / Phoenix / 16 December 2016 (https://www.spenergynetworks.co.uk/pages/phoenix.aspx)..

This dissertation summarizes the work carried out by the author during his Ph.D. project. It started on 01st April 2018, and it was completed on 20th January 2022. During this period, he was hired by the Technical University of Denmark as a Ph.D. student at the Center for Electric Power and Energy (CEE).

The thesis is composed of 4 scientific papers, 2 of which have been peer-reviewed and published, whereas the remaining 2 are to be submitted.

Mirza Nuhic
January 2022

Acknowledgements

First and foremost, I want to express my deepest gratitude to and appreciation of Guangya Yang. His great support, encouragement, patience, and extensive knowledge have been invaluable in my academic career at DTU starting from my master thesis and throughout my Ph.D. thesis. His enthusiasm for my project and his kind support is something that I will always cherish. In addition, I have appreciated and enjoyed the team spirit, which he has created in his research team, and which I have been so lucky to have been a part of for the past 5-6 years.

I would also like to thank my co-supervisors Cornel Brozio, Scottish Power and Richard Rivas, Hitachi ABB, for their valuable feedback during the study.

Finally, I thank the Phoenix project team members at Hitachi ABB Power Grids, National Grid ESO, and SP energy networks for stimulating inputs and discussions. I am very grateful that I had this opportunity to have a close cooperation with the industry.

I am forever grateful to Kanakesh Vatta Kkuni for our close collaboration and inspiring discussions. I also want to thank my other friends and colleagues at CEE, who made my time at DTU as a Ph.D. student enjoyable; Sujay, Anubav, Tiago, Georgious, Jin, Pengda, Mohammed, Jundi, Ha, Aysegul, Jacob, Theis, Jochen, Allesandro, and many others. A special thank you goes to Daniel and Ana.

I want to show my appreciation for the administrative and laboratory staff at DTU who were a big help during my project. Thank you, Anne, LÃ¦rke, Christina, Bjarni, Magnus, Jesper and Per Munch. I especially want to thank Arne Hejde Nielsen and Spyros Chatzivasileiads for their kind support for my Ph.D.

Finally, I want to thank all my friends and extended family from Bosnia and Denmark for being a great support during my Ph.D. journey, and for never losing their faith in me. I want to thank my parents, Enisa and Nedim, my sister, Amra, and my mother-in-law for their invaluable support. Last but not least, I would like to thank my wife, Nina, for her patience, her enthusiasm, and unconditional love.

Mirza Nuhic

Kongens Lyngby, Denmark, 2022

Table of Contents

Figurer

Tabeller

Abstract

One of the major challenges for the future power systems is decommissioning of synchronous machine-based generation, which will result in reduced overall strength of the system. For example, as the number of synchronous machines in the generation mix subsides, the inertia in the system will reduce, making the frequency more susceptible to large swings in the face of disturbances, significantly affecting the voltage control, as well as the short-circuit power levels. The total renewable energy capacity of the world has increased by ca. 260 GW in 2020 as compared to the previous year, taking the total capacity to ca. 2800 GW. The share of the renewable energy in the energy mix is expected to continue to rise, making it a necessity to address the problems previously mentioned.

Phasing out of conventional synchronous machines means that other technologies will have to be able to provide and replicate their functions and capabilities in terms of voltage and frequency control, short-circuit power, inertia, oscillation damping etc. The most common technology is the power converter interfaced renewable energy. Flexibility of power converter control is one of the major advantages of this technology in bringing the necessary functions to the system and providing similar characteristics as a conventional generation. However, there are some obstacles that cannot be overcome by only power converter based renewable energy sources due to the physical and economical aspects of the technology. In that regard, battery systems and supercapacitors can introduce that additional active power and provide a range of beneficial functions. In addition, synchronous condensers have been identified as a technology that can contribute with high levels of short-circuit power and provide inertia that will inevitably reduce in converter dominated power systems.

This thesis proposes a hybrid synchronous condenser (HSC) solution consisting of a synchronous condenser, battery energy storage system (BESS), and a hybrid controller for the combined system. This system is designed with the goal to integrate and combine the benefits of both technologies with regards to provision of ancillary services. Furthermore, the capabilities of the different technologies and control strategies are analyzed and compared in order to quantify the contribution in terms of voltage and frequency support. The criteria for the comparison are based on the speed of the response, overloading capability, and performance in weak and strong grids. The idea was to test each technology and control strategy against voltage and frequency disturbance, voltage angle jump, and short circuit contribution.

Based on this, we propose a control design that can provide damping for torsional oscillations. The oscillation damping controller is integrated within the HSC system, where the active damping is provided by BESS, while the synchronous condenser contributes only passively. Each oscillating mode has a dedicated controller loop, and the interaction between different frequencies is minimal. The outputs are added together to form a single input to the current controller of the VSC. Each loop consists of a filter, gain, and phase compensator. The parameter tuning is performed by applying a simulation-based approach, where we ran simulations for each parameter set and evaluated

the fitness function, utilizing a particle swarm method for optimization. The performance of the controller was first evaluated using a small signal perturbance on the mechanical torque and measuring the speed deviation and the electrical torque deviation to obtain the damping profile of the system.

At last a control method is proposed for maximizing the inertial contribution of the HSC system by using BESS to compensate the active power oscillation of HSC caused by the synchronous condenser. During a disturbance, the synchronous condenser will provide oscillating active power to the system, and periodically inject and absorb reactive power. By compensating the absorbed active power of the condenser with BESS, one can maximize the inertial contribution of the HSC system. The input signal for the controller is the measured active power output from the synchronous condenser, which means that we avoid a more complicated solution by using the rotor speed of the condenser. The controller loop consists of derivatives of the active power, gain, and the phase compensator. The analysis includes estimation of energy storage that is necessary relative to the size of the synchronous condenser, as well as performance evaluation in case of using a flywheel.

All the proposed controllers are validated by performing a hardware in the loop test and measuring the speed deviation of the affected generators. It is found from the thesis that the investigated HSC design can provide a wide range of services to the need of the stability of the power grids now and in the future, with several potentials yet to explore. However, in order to roll out the technology, it is also essential to further develop the current ancillary service market in order to quantify the value of the services and justify the investment in this technology, albeit this work is out of the scope of the thesis. From the technical standpoint, the aim of the project, which was to investigate and demonstrate the effect of HSC, has been actualized.

Resumé

En af de store udfordringer for fremtidens el-systemer er nedlukning af synkron maskinbaseret produktion, hvilket vil resultere i reduceret overordnet styrke af systemet. For eksempel, efterhånden som antallet af synkronmaskiner i generationsblandingen aftager, vil inertien i systemet reduceres, hvilket vil gøre frekvensen mere modtagelig for store udsving i tilfælde af forstyrrelser, væsentligt påvirke spændingsstyringen, samt kortslutningseffekt niveauerne. Verdens samlede vedvarende energikapacitet er steget med ca. 260 GW i 2020 sammenlignet med året før, hvilket bringer den samlede kapacitet til ca. 2800 GW. Andelen af vedvarende energi i energimixet forventes fortsat at stige, hvilket gør det nødvendigt at løse de tidligere nævnte problemer.

Udfasning af konventionelle synkronmaskiner betyder, at andre teknologier skal kunne levere og replikere deres funktioner og muligheder i form af spændings- og frekvensstyring, kortslutningseffekt, inerti, oscillationsdæmpning osv. Den mest almindelige teknologi er strømkonverteren interagerende med vedvarende energi. Fleksibiliteten ved styring af strømkonvertere er en af de største fordele ved denne teknologi ved at bringe de nødvendige funktioner til systemet og give lignende egenskaber som en konventionel generation. Der er dog nogle forhindringer, som ikke kun kan overvindes af strømkonverter-baserede vedvarende energikilder på grund af teknologiens fysiske og økonomiske aspekter. I den forbindelse kan batterisystemer og superkondensatorer introducere den ekstra aktive effekt og give en række fordelagtige funktioner. Derudover er synkrone kondensatorer blevet identificeret som en teknologi, der kan bidrage med høje niveauer af kortslutningseffekt og give inerti, der uundgåeligt vil reducere i konverterdominerede strømsystemer.

Denne afhandling foreslår en hybrid synkron kondensator (HSC) løsning bestående af en synkron kondensator, batteri energilagringssystem (BESS) og en hybrid controller til det kombinerede system. Dette system er designet med det mål at integrere og kombinere fordelene ved begge teknologier med hensyn til levering af hjælpetjenester. Ydermere er mulighederne af de forskellige teknologier og kontrolstrategier analyseret og sammenlignet for at kunne kvantificere bidraget i form af spændings- og frekvensunderstøttelse. Kriterierne for sammenligningen er baseret på responshastighed, overbelastningsevne, samt ydeevne i svage og stærke net. Ideen var at teste hver teknologi og kontrolstrategi mod spændings- og frekvensforstyrrelser, spændingsvinkelspring og kortslutningsbidrag.

På baggrund af dette foreslår vi et styringsdesign, der kan give dæmpning for torsions oscillationer. Oscillationsdæmpningsregulatoren er integreret i HSC-systemet, hvor den aktive dæmpning leveres af BESS, mens den synkrone kondensator kun bidrager passivt. Hver oscillerende tilstand har en dedikeret controller-loop, og interaktionen mellem forskellige frekvenser er minimal. Outputs lægges sammen for at danne et enkelt input til VSC'ens strømstyring. Hvert loop består af et filter, forstærkning og en fasekompensator. Parameterjusteringen udføres ved at anvende en simulationsbaseret tilgang, hvor vi kørte simuleringer for hvert parametersæt og evaluerede fitnessfunktionen ved at bruge en partikelsværmmetode til optimering. Styringens ydeevne blev først evalueret ved hjælp af en lille signalforstyrrelse på det mekaniske drejningsmoment og

måling af hastighedsafvigelsen og den elektriske drejningsmomentafvigelse for at opnå systemets dæmpningsprofil.

Endelig foreslås en kontrolmetode til at maksimere inertibidraget fra HSC-systemet ved at bruge BESS til at kompensere den aktive effektoscillation af HSC forårsaget af den synkrone kondensator. Under en forstyrrelse vil den synkrone kondensator give oscillerende aktiv effekt til systemet og periodisk indsprøjte og absorbere reaktiv effekt. Ved at kompensere kondensatorens absorberede aktive effekt med BESS, kan man maksimere inertibidraget fra HSC-systemet. Input signalet til controlleren er den målte aktive effekt output fra den synkrone kondensator, hvilket betyder, at vi undgår en mere kompliceret løsning ved at bruge kondensatorens rotorhastighed. Controller-loopet består af derivater af den aktive effekt, forstærkningen og fasekompensatoren. Analysen omfatter estimering af energilagring, der er nødvendig i forhold til størrelsen af den synkrone kondensator, samt ydelsesevaluering i tilfælde af brug af et svinghjul.

Alle de foreslåede controllers valideres ved at udføre en hardware i loop-testen og måle hastighedsafvigelsen for de berørte generatorer. Det fremgår af afhandlingen, at det undersøgte HSC-design kan levere en bred vifte af tjenester til behovet for stabiliteten af elnettene nu og i fremtiden, med adskillige potentialer endnu at udforske. Men for at udrulle teknologien er det også væsentligt at videreudvikle det nuværende marked for hjælpetjenester for at kvantificere værdien af tjenesterne og retfærdiggøre investeringen i denne teknologi, selvom dette arbejde er uden for afhandlingens rammer. Rent teknisk er formålet med projektet, som var at undersøge og demonstrere effekten af HSC, blevet aktualiseret.

systemets dÃ¦mpningsprofil. Endelig foreslÃ¥s en kontrolmetode til at maksimere inertibidraget fra HSC-systemet ved at bruge BESS til at kompensere den aktive effektoscillation af HSC forÃ¥rsaget af den synkrone kondensator. Under en forstyrrelse vil den synkrone kondensator give oscillerende aktiv effekt til systemet og periodisk indsprÃ¸jte og absorbere reaktiv effekt. Ved at kompensere kondensatorens absorberede aktive effekt med BESS, kan man maksimere inertibidraget fra HSC-systemet. Input signalet til controlleren er den mÃ¥lte aktive effekt output fra den synkrone kondensator, hvilket betyder, at vi undgÃ¥r en mere kompliceret lÃ¸sning ved at bruge kondensatorens rotorhastighed. Controller-loopet bestÃ¥r af derivater af den aktive effekt, forstÃ¦rkningen og fasekompensatoren. Analysen omfatter estimering af energilagring, der er nÃ¸dvendig i forhold til stÃ¸rrelsen af den synkrone kondensator, samt ydelsesevaluering i tilfÃ¦lde af brug af et svinghjul. Alle de foreslÃ¥ede controllers valideres ved at udfÃ¸re en hardware i loop-testen og mÃ¥le hastighedsafvigelsen for de berÃ¸rte generatorer. Det fremgÃ¥r af afhandlingen, at det undersÃ¸gte HSC-design kan levere en bred vifte af tjenester til behovet for stabiliteten af elnettene nu og i fremtiden, med adskillige potentialer endnu at udforske. Men for at udrulle teknologien er det ogsÃ¥ vÃ¦sentligt at videreudvikle det nuvÃ¦rende marked for hjÃ¦lpetjenester for at kvantificere vÃ¦rdien af tjenesterne og retfÃ¦rdiggÃ¸re investeringen i denne teknologi, selvom dette arbejde er uden for afhandlingens rammer. Rent teknisk er formÃ¥let med projektet, som var at undersÃ¸ge og demonstrere effekten af HSC, blevet aktualiseret.

Acronyms

Definitions

This section states and clarifies some definitions of functions, roles and responsibilities that are referred to in this thesis.

Definition 1: bla bla bla

Definition 2: bla bla bla

KAPITEL 1

Introduction

1.1 Background

One of the serious challenges for the future power systems is decommissioning of conventional power plants consisting of large synchronous machines, which provide substantial levels of inertia, short circuit level, voltage and frequency controllability among others. The increasing penetration of renewable energy, which is interfaced to the grid by power converters that inherently do not posses the capabilities of synchronous machines, will eventually lead to significant issues for power system operators and overall stability of the power systems if left unaddressed. Phasing out synchronous machines implies the importance of replacing their role with other technologies that are capable to replicate the same functions in terms of frequency and voltage support, inertia, oscillation damping, short-circuit levels, etc. In conventional power systems, inertia is provided by the kinetic energy stored in large rotating machines [5]. Larger disturbance in power balance can result in a significant system frequency deviation, which is countered by a release of kinetic energy stored in the rotating masses of synchronous generators [6]. The trend of decreasing inertia levels have been observed in numerous national power systems, for example as shown in [1] and [7]. In UK, the average inertia across the next 10 years is set to decline, as the Fig. 1.1 clearly shows.

In low inertia system, frequency is more susceptible to rapid changes due to loss of generation, which can trigger loss of mains protection relays and potentially lead to a total collapse. For example, some relays in UK are set for 0.125 Hz/s RoCoF limit, which means that loss of 1000 MW requires 200 GVAs of inertia to stay within the limits of RoCoF (0.125 Hz/s). The trend of decreasing

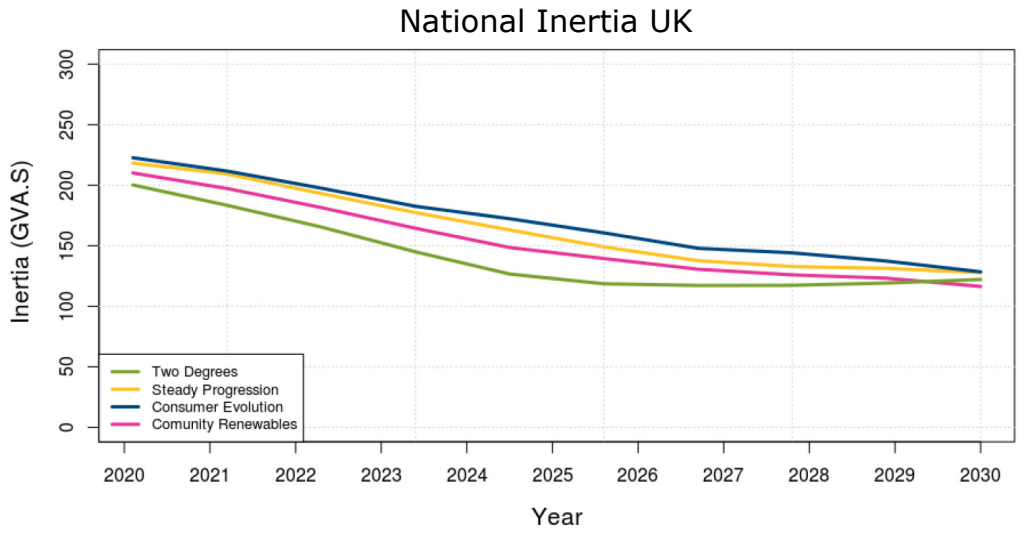

Figur 1.1: UK Inertia Trend up to 2030, Adapted from [1]

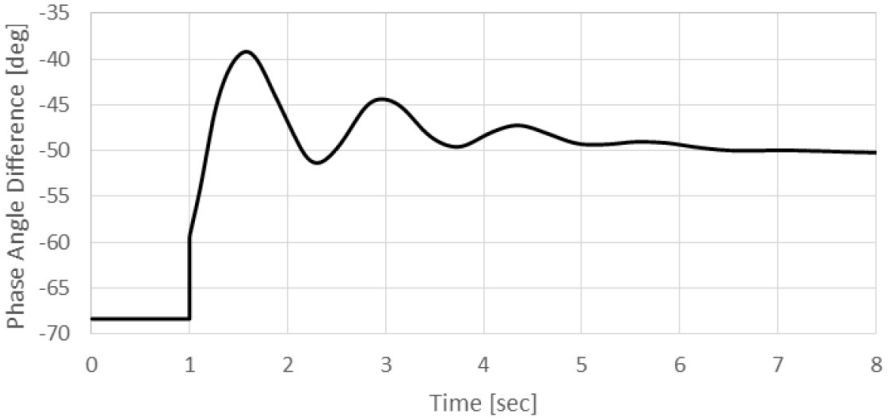

Figur 1.2: Bus Phase Angle Jump During Line Re-energization Following a Fault; Adapted from [2]

inertia levels in power systems is an opportunity to unlock fast frequency response from new technologies and particularly from power converter interfaced renewable energy sources.

Decreasing number of synchronous machines will not solely affect inertia in the system, but the short-circuit level as well and have a significant impact on the overall strength of the power system. There is a minimum threshold of system strength that is needed for the power system to remain in stable conditions and return to a steady state after a significant disturbance. The sensitivity of the power system to various disturbances depends largely on the strength of the system, and one of the indices to evaluate the strength of a particular power system was the short-circuit ratio (SCR). In the same way that inertia levels in the system determine the volatility of frequency deviation, the short-circuit levels have significant impact on voltage stability [8]. The shortfalls of SCR rest in the fact that it does not take into consideration the interaction between the power converter interfaced power plants, current saturated operation, and the differences in control strategies [9]. Additionally, significant number of power converter controllers are designed for applications in strong power grids, making it imperative to reevaluate and redesign the performance in low inertia systems.

As previously discussed, in low inertia systems with high penetration of converter-based renewable sources, the changes of system parameters can be significant and occur rapidly. Therefore, it is of high importance that the power converter control strategies are designed in such a way to be able to resist these rapid changes, stay connected to the grid, and provide support to the grid. For example, an event of undesirable tripping of solar plant occurred in North America in January 2019 [2]. A line tripped following a fault, and upon re-energizing the line, load flow changed by nearly 1000 MW, and resulted in a bus phase jump as shown in Fig. 1.2. The solar plant tripped because the phase angle threshold between the grid and Phase-Locked-Loop (PLL) exceeded the preset value. Unnecessary tripping of power plants can significantly degrade the stability margin of the system and potentially lead to blackouts, and that is specifically exemplified in weaker, low inertia system.

It is therefore of high significance to investigate and design new solutions that can potentially address the problems that will be faced in future power converter dominated power system.

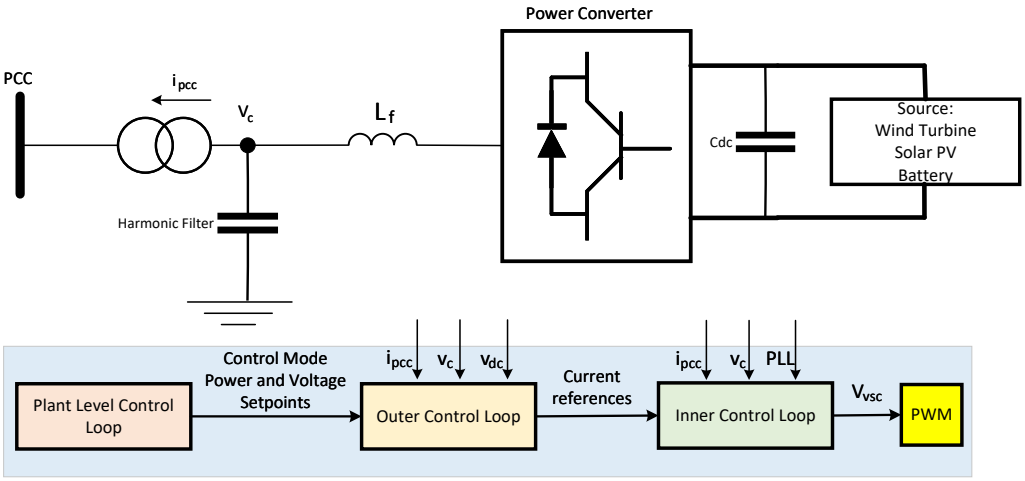

Figur 1.3: Control Loop Structure of Grid-Following converter

1.1.1 Basic Control Structure and Control Strategies of Power Converters

Missing diagram (Figure 3) of VSC structure with loop description

The most common power converter control structure is shown in Fig. 1.3 In principle, it contains three levels of control:

- High level control: This control level is mainly reserved for the power system operators for steady state or quasi-dynamic operations where it includes selections of the grid management functions such as frequency and voltage support functions, power control functions (active and reactive power set-points), or any functions that are required for a particular unit or the power plant.
- Outer control loop: This level of control includes the characteristics and parameters for the voltage and frequency support functions, active and reactive power control methods, fault-ride-through strategy, DC voltage control, as well as supplementary control functions like oscillation damping, harmonic suppression, etc.
- Inner control loop: The inner or current control loop regulates the output of the current or voltage at the terminal of the converter. It also includes the current limiting function, which is vital for power converter protection.

Power converters are usually synchronised with the grid by utilising the Phase-Locked-Loop. Phase locked loop measures the voltages at the inverter terminal, extracts the phase of the system voltage, and regulates the frequency and the phase of its output to follow the grid phase. This type of converters are known as grid-following converters, as they need a set frequency and phase to operate. The advantage of this type of control is that it can provide tight power and current control during normal and dynamic situations. Until today, all the major converter-interfaced renewable power plants are required to provide frequency and voltage support to the grid in a form of frequency droop and automatic voltage control or voltage droop functions [8-10]. There are two distinct operating modes for grid-following converters, namely the small disturbance mode and the large disturbance mode. Small disturbance mode is when the grid conditions are

within the continuous operating range of the power converter (small switching transients, load changes, power quality issues, etc.), while the large disturbance mode is activated when the voltage falls outside normal operating range. This mode is known as the fault-ride-through mode. The transition between the operating modes is automatic with a threshold setting in the controller, and serves the purpose of keeping the power plants online as well as providing the needed services to the grids during large disturbances [11].

Power converters with control design that does not require PLL for grid synchronisation are known as grid-forming power converters. The synchronisation methods are usually based on active power injection [12-13], and the voltage control is based on direct control of the d-axis voltage. The grid-forming converters are operated as voltage sources during normal operation, so they can to some extent emulate the response of a conventional synchronous machine. However, their performance is still affected by current limiter during large transients where research is ongoing in the field [10].

Power converters have multiple applications in power systems. They are used as an interface between the grid and renewable sources (wind and solar), in flexible ac transmission systems (FACTS) such as static voltage compensator (STATCOM), and high voltage direct current applications (HVDC). In recent years, battery energy storage system (BESS) is proven to be an appealing and key enabling technology for renewable energy based systems as it can provide different supporting functions to the system and contribute to a stable system operation [14]. Increasing need for flexibility in power delivery and reducing costs of battery technologies has resulted in many projects around the globe focusing on BESS integration in power systems. Besides providing flexibility in power system and enabling higher levels of renewable energy integration, BESS can offer multiple other functions to the system, such as peak shaving, oscillation damping, frequency support, black start etc [15]. Large BESS installations have been emerging across the globe.

1.1.2 Reinventing the Synchronous Condenser

The synchronous condenser (SC), which is essentially a synchronous generator without a prime mover attached, has been in the mix of power system composition for decades. The primary application for synchronous condenser was in reactive power support in the past. However, with the advent of semiconductor-based reactive power compensation such as static var compensators, capable of reactive power compensation at much lower cost and higher efficiency, new synchronous condenser installations declined steadily. However, the current scenario of declining short circuit ratio and reduced inertia due to decommissioning mostly coal-based power plants have resulted in a renewed interest in SC. The services from SC can, to an extent, compensate for the loss of inertia and other services from the retired power plants, thus ensuring sufficient system strength for stable system operation. In addition, it is also possible to convert the redundant, synchronous generators from the retired power plant to SCs with inertia enhancement with flywheel installations [11, 12].

Multiple European projects such as SCAPP [13] and the Phoenix project [3], have demonstrated the benefits of SC in ensuring system security and reliability. Some of the key benefits of SC which can improve the system performance are

- Provide Mvar and short circuit current/power
- Provide natural and instantaneous inertia
- Capable of short term overloading multiple times of the rated value for short duration
- Ensure voltage source characteristic of the system

Figur 1.4: 140 MVA H-SC installed as a field trial of Phoenix project at Neilston, Scotland [3]

1.2 The Phoenix Project

The Ph.D. is part of a Ofgem (Office of Gas and Electricity Market, Great Britain) funded project, under Network Innovation programme, titled "Phoenix - System Security and Synchronous Compensators". The project demonstrated and investigated the application of the concept of Hybrid Synchronous Compensators, consisting of an SC and STATCOM, to maintain the stability of the GB transmission grid. The Phoenix project demonstrated that the static and rotating components in the hybrid system are complementary and can compensate for the services being lost from conventional power plants that are being decommissioned. The project's partners are ABB, National Grid ESO, SP Transmission (SPT), the University of Strathclyde, and DTU. A 140 MVA field trial of the hybrid system is carried out in Scotland, where the H-SC installation at the Neilston substation at Scotland is shown in Fig. 1.4.

In addition, to the hybrid solution of SC and STATCOM, the project also investigated the advantages of hybrid solution based on SC and Battery Energy Storage System. To that end, the Ph.D. was mainly tasked with model development and studies of these hybrid solutions within the Phoenix project, focusing on the potential applicability of hybrid solutions on improving the power system stability and reliability.

1.3 Motivation and Objective

Several functions of the synchronous machines cannot be easily replaced by power converters. Synchronous machines have voltage source characteristic, meaning that they regulate and stabilize the terminal voltage and have significant overloading capability in terms of reactive power, while converters usually have limited current and voltage control capabilities.

Additionally, fast acting controllers of power converters can interact with each other and introduce control interaction stability concerns. Limited overloading capability means that the system short term capacity is reduced making it more sensitive to disturbances, and reduced short-circuit levels can compromise the operation of protective relays in the power system.

In order to ensure a safe transition from the conventional synchronous machine-based to a power converter-dominated power system, multiple projects across the world are being conducted

to address this growing problem. Among others, project "MIGRATE"funded by the European Union deals with grid stability, investigating 100% renewable based power system, and possible improvements on power converter controls [14]. Phoenix project is looking into combining a STATCOM and Synchronous Condenser in a single unit in order to provide a unique solution to some of the problems listed above [15]. The Stability Pathfinder project lead by National Grid UK ESO is investigating potential stability issues in the power system that is dominated by power converter interfaced renewable energy.

One of the interesting proposed solutions is a Hybrid Synchronous Condenser (HSC) system consisting of BESS and Synchronous Condenser (SC). The proposal is part of the Phoenix Project as one of the configurations of the HSC, where the SC in the hybrid solution has the same capacity as the power converter. Major advantage of SCs over power converters is their significant overloading capability and short-circuit current contribution. Additionally, SCs posses kinetic energy in their rotating mass and consequently have inherent feature of inertia support. On the other hand, power converters have physical limitations and can provide only a small level of overloading current for a short period of time. However, power converter control has a high bandwidth and can provide fast frequency and voltage control and provide the possibility of implementation various control strategies. One of the advantages of power converters is that they can provide full rated current in inductive and capacitive mode, while the SC can only absorb a portion of the full rated current due to the physical limitations. By combining these two technologies, the advantages of both can be utilized to form a new technology capable of providing various functions and services. A disadvantage of this solution over a standalone SC with the same rating would be the diminished contribution in terms of overloading capability, more complex installation and area and complex coordinated control.

1.3.1 Objectives

The objectives of the project can be summarised as follows:

- Implement a model of BESS in various simulation platforms to enable testing and investigation of different scenarios and various control functions.
- Design a control structure for SC, BESS and master controller for HSC and validate it in a power hardware in a loop setup.
- Implement a controller for grid-following and grid-forming control strategies.
- Draw a comparison between the technologies, namely standalone SC, standalone BESS (grid-following and grid forming) and a HSC solution.
- Design a controller for torsional oscillation damping and integrate it within the HSC master controller.
- Design a controller for maximizing the inertia support from the SC.

1.4 Contribution Summary

The summary of the main contributions of the PhD thesis is as follows:

- A detailed model of BESS was developed in PowerFactory, PSCAD, and RSCAD. The model was validated against a model in the literature. A model for converter control was also developed and validated in a power hardware-in-a-loop (PHiL) setup. The functions that the model can provide active and reactive power control, automatic voltage control, frequency and voltage droop control, fast frequency response based on RoCoF measurement, fault-ride-through strategy, and automatic seamless transition from normal operation to fault mode. The BESS model is combined with a synchronous condenser model that was modelled and validated against a blackbox model of the real installed SC provided by Hitachi ABB.
- Designed and implemented a master controller for HSC that combines the controllers for synchronous condenser and BESS. Implemented an equal reactive power sharing control strategy within the master controller which ensures that the synchronous condenser and BESS contribute an equal amount of reactive power during disturbances. A comprehensive studies were done in order to showcase the validity of the controller.
- Implemented a grid-forming control strategy based on power synchronization loop and provided a detailed comparison of the performance of standalone technologies as well as HSC. The results were summarised, providing a useful insight into all advantages and disadvantages of each technology.
- Developed a control strategy for mitigating torsional oscillation of generators. The controller consists of separate loops for each mode of oscillation. The input to the controller is the local voltage measurement, which is beneficial as it does not require access to the power plant where the affected generators are located. A particle swarm optimization method was used to tune the gain and phase of the oscillation damping signal. The solution was validated by utilizing a damping factor scanning method, where a small perturbation was added to the mechanical torque and measured speed and electrical torque deviation to obtain the damping scan. Finally, the controller was tested and validated in a PHIL setup for small and large disturbances and different operating conditions.
- Developed a controller that acts to maximize the inertial contribution from HSC by using BESS to compensate the active power oscillation of synchronous condenser during a frequency disturbance. SC provides oscillating active power to the system after large grid disturbances, where it periodically injects and absorbs active power following a frequency disturbance event. The power that is being absorbed by the SC is compensated by BESS through the control. A detailed analysis of energy storage requirements is provided as well as compared the performance with the case of a flywheel.

1.5 Methodology

The overview of the methodology applied to achieve the objectives of the project is given bellow.

- **Literature review.**

  A literature review was conducted in order to investigate possible gaps and identify the path to be taken within this project.

- **Modelling and Simulation.**

  Detailed models were developed in PowerFactory, PSCAD, and RSCAD in order to investigate and validate the behaviour of different technologies.

- **Validation.**

  Validation of the models was performed in a power-hardware-in-a-loop setup, which consists of a 150 kW converter stack, controller, and RTDS rack.

1.6 Thesis Overview

- In chapter 2, the battery model development and implementation is presented. The description of the battery model based on the Thevenin equivalent is provided. Additionally, in this chapter several functionalities of power converters are investigated and implemented.
- In chapter 3, an evaluation of the HSC master controller is presented. Detailed studies are provided to demonstrate the effectiveness of the HSC solution. A grid-forming control strategy was implemented and comparison between the standalone technologies and HSC are provided.
- In chapter 4, an oscillation damping controller was developed for mitigating torsional oscillations caused by a subsynchronous resonance. A modal analysis approach was used to identify the torsional oscillation modes and a detailed description of optimization methodology was provided. It is also described how the damping factor scan was implemented, and the results of simulation and PHIL validation are presented.
- In chapter 5, a control design for inertia maximization was described. An analysis of energy requirements is provided, as well as a demonstration and evaluation of performance in case of using a flywheel.
- Chapter 6 contains conclusion that can be drawn from the project and finally possible future work is described and given.

1.7 Assumptions and Limitations

- The battery model is a simplified representation of the battery chemistry. Detailed battery models require high computational power while the accuracy improves by only a few percentage points, which is not enough to justify the additional computing burden. Thermal models, ageing parameters, and self-discharge were neglected as those processes take time to have significant impact on the model performance, which makes their omission justified.
- The system used in all studies is a simple system and the assumption is that the results are scalable to larger systems, but this assumption needs to be validated. Additionally, only the impedance type loads are considered in all the studies for the sake of simplicity.
- The most commonly used control architectures for grid-following and grid-forming converters are considered in the work with the acknowledgement that there are many other possible implementations.
- For the PHIL validation, it was assumed that the scaling of the power converter stack does not influence the results in a significant way.

1.8 List of publications

The relevant publications which are the core of this thesis are listed as follows:

[**Pub. A**] Nuhic, M., Vatta Kkuni, K., Yang, G., (2022), SSR Damping Controller Integrated within Hybrid Synchronous Condenser System. *To be submitted*

[**Pub. B**] Nuhic, M., Vatta Kkuni, K., Yang, G., (2022), Inertia Maximization for Hybrid Synchronous Condenser System . *To be submitted*

[**Pub. C**] Nuhic, M., & Yang, G. (2019). A Hybrid System Consisting of Synchronous Condenser and Battery - Enhanced Services for Weak Systems. Proceedings of 2019 IEEE PES Innovative Smart Grid Technologies Europe, ISGT-Europe 2019, 8905459.https://doi.org/10.1109/ISGTEurope.2019.8905459

[**Pub. D**] Nuhic, M., Vatta Kkuni, K., Yang, G., & Ramachandran, J. (2019). Comparative study of hybrid synchronous condenser incorporating battery energy storage system for ancillary service provision. Proceedings of 19th Wind Integration Workshop, Wind Integraion Workshop 2019.

[**Pub. E**] Nuhic M., & Yang G. (2021) Battery Energy Storage System Modelling in DIgSILENT PowerFactory. Chapter 7 in: Gonzalez-Longatt F.M., Rueda Torres J.L. (eds) Modelling and Simulation of Power Electronic Converter Dominated Power Systems in PowerFactory. Power Systems. Springer, Cham. https://doi.org/10.1007/978-3-030-54124-8_7

Additionally, the following reports were submitted as deliverables for the Phoenix project.

[**Pub. F**] Nuhic, M., & Yang, G. (2018). "Report on Synchronous Condenser Model for Phasor Studies"Phoenix project deliverable report, June 2018

[**Pub. G**] Nuhic, M., & Yang, G. (2018). "Report on Battery Energy Storage for Phasor Studies - PowerFactory"Phoenix project deliverable report, October 2018

[**Pub. H**] Nuhic, M., & Yang, G. (2018). "Report on Battery Energy Storage System (BESS) Model for EMT studies PSCAD"Phoenix project deliverable report, June 2019

The following publications have also been prepared during the course of the Ph.D. study, but have been omitted from the thesis because they are not directly related to the primary objective, or they are partially covered by other presented papers.

[**Pub. I**] Kkuni, K. V., Nuhic, M., & Yang, G. (2021). Power System Stability Impact Assessment for the Current Limits of Grid Supporting Voltage-Source Converters. IEEE Power and Energy Society General Meeting, 1-5.https://doi.org/10.1109/PESGM46819.2021.9637902

KAPITEL 2

Battery

This chapter is based on **[Pub.E]**.

2.1 Introduction

The increasing presence of renewable sources in power systems is introducing a serious challenge for system operators due to a reduction in total inertia of the system, limitation in voltage support, reduced frequency support capabilities, general system weakening, etc. As more renewable sources is being installed, the number of large synchronous generators will steadily decrease, thus creating a significant strain on the power system operation, reliability, and security [16]. In that regard, the battery energy storage systems (BESS) are attracting major interest as a technology that can provide ancillary services required for stable system operation [17]. The fast response combined with various functions and capabilities of a battery system makes it a very viable solution that can address some of the issues that the future power systems face [18].

One of the best readily available battery chemistries are the lithium-based batteries. They are characterized by high energy density, long lifetime, excellent efficiency (>90%), wide temperature range, etc. The main drawback of this battery technology is that it is still relatively expensive [19]. There are three general types of battery models:

1. Chemical Models; the chemical models are used when the accuracy of the model is essential for investigation of internal chemical processes of the battery. The models are very detailed, complex, and computationally expensive [20].
2. Mathematical models; these models are used when only the simple and approximate battery models are required. They are usually easy to build and do not require significant computational power [21].
3. Electrical models; they are based on equivalent electrical circuits. The chemical processes within the battery are represented by electrical components. The models provide a decent trade-off between complexity/accuracy and computational burden [22].

For power system simulations, the models based on equivalent electrical circuits are widely used, as they provide reasonable accuracy (1-5%) and are easy to model. The model that can be found in use in most of the publications that is related to battery modelling in power systems is based on the so-called "Double Polarization Model". The model captures the two distinct phenomena within the lithium-based battery cells, namely the separating concentration polarization (short-term dynamics), and the electrochemical polarization (long-term dynamics). Two RC circuits represent the two processes [23]. The electrical performance of the battery is characterized by the capacity, internal impedance, open circuit voltage, and self-discharge. The parameters of the equivalent

circuit are dependent on SOC, temperature, charging/discharging current, and state of health of the battery cell [16]. A more precise method for impedance-based battery modelling is by using a so-called ZARC element to represent the two distinct processes. The ZARC element is a parallel connection of a constant phase element (CPE) and resistance, which is an arc shaped impedance [9]. The ZARC element can be expressed as:

$$Z_{ZARC} = \frac{1}{1/R + (j\omega^N \cdot Q)} \tag{2.1}$$

N is the depression factor and it can be between 0 and 1 (0-pure resistance, 1-pure-capacitance). The CPE element is used to represent a non-ideal capacitor. The method that is used to extract the battery parameter (dependent on SOC, temperature and C-rate) is called the "Electrochemical Impedance Spectroscopy". The impedance is measured for a frequency spectrum and usually represented by a Nyquist plot. Five RC circuits can approximate one ZARC element with very low approximation error. The model that uses CPE elements provides high accuracy, but the measurements can be time-consuming [24]. The control structure of the battery model can provide flexibility in terms of ancillary services and the speed of the response. If we consider the frequency support capabilities, the battery systems can provide a significant contribution with fast response and readily available stored energy. The three key parameters that characterize a frequency disturbance are: (1) rate of change of frequency (RoCoF), (2) frequency nadir, and (3) steady-state frequency. The reduced inertia in a system will result in an increased RoCoF and lower frequency nadir, while the steady-state frequency relies solely on the primary frequency response (PFR). The reactive power capability of a converter can provide support under severe voltage dips and stay connected to the grid in extreme conditions. The fault-ride-through capability of a power converter is becoming a requirement in most grid codes. One of the biggest challenges in renewable energy dominated power systems is the intermittent nature of the renewable sources (i.e. wind and solar power), which can lead to significant forecast errors. Battery systems can, to a large extent, address the issues mentioned here, and possibly provide additional services such as oscillation damping, harmonic filtering, etc [16]. In this chapter, we try to provide detailed instruction on how to build a model of a battery energy storage system, including several functions, which can serve as ancillary services and provide support to the grid during disturbance and transient operating conditions.

2.2 Battery model

The model that is widely used in the literature is the "Double Polarization Model". The equivalent electrical circuit is shown in Fig. 2.1. The model captures the two distinct chemical processes within the battery, namely separation polarization and electrochemical polarization (the short-term and the long-term dynamics, respectively). The element R_0 represents the internal resistance of the battery cell. The R_{Ts} and C_{Ts} represent the separation polarization process, while the R_{TL} and C_{TL} represent the electrochemical polarization process within the battery cell. V_{OC} is the open-circuit voltage, also referred to as the internal voltage of the battery cell. The $R_{self-discharge}$ characterizes the loss of charge over a longer period. This parameter is usually not relevant for short-term studies because the loss of charge is negligible (up to 5% per month) [23].

The parameters of the equivalent circuit are dependent on the state of charge (SOC), temperature, and the operating state of the battery cell (charging or discharging). The most influential factor is the state of charge, and for this reason, estimating the state of charge is of the primary concern

with respect to battery modelling. There are several methods for SOC estimation, and the two most widely used methods are Coulomb counting and OCV-based estimation [25]. The Coulomb counting method is a very accurate method and simple to implement. The main drawback is that it requires an accurate estimation of the initial state of charge. The OCV-based SOC estimation is a straightforward method, but the main disadvantages are that it requires sufficient relaxation time to enable accurate OCV measurement and it can be challenging to estimate the SOC for flat areas of the OCV curve. In practice, these two methods are combined in order to provide a simple and efficient approach for SOC estimation. Some of the other methods used in practice are an impedance-based estimation, model-based estimation, estimation using fuzzy logic and machine learning, etc [25]. The method that we implemented is the Coulomb counting method. This method represents the charge transfer measurement to and from the battery, and it requires a current measurement. The SOC estimation is based on the following equation:

$$SOC = SOC_0 - \frac{1}{C_{cell}} \int_0^t I_{cell} dt, \tag{2.2}$$

where SOC_0 represents the initial state of charge, C_{cell} is the capacity of the battery cell, and I_{cell} is the charging/discharging current. Once we know the state of charge, the other parameters can be estimated based on a lookup table or a parametrized function. The terminal voltage of the battery cell as per the circuit in Fig. 2.1 is:

$$U_{cell} = U_{OC} - I_{cell} \cdot R_0 - U_{Ts} - U_{TL} \tag{2.3}$$

The voltage drop across the RC circuits is determined by solving the following differential equations:

$$\begin{aligned} I_{cell} &= \frac{U_{Ts}}{R_{Ts}} + C_{Ts} \cdot \frac{dU_{Ts}}{dt} \rightarrow \frac{dU_{Ts}}{dt} = \frac{I_{cell}}{C_{Ts}} - \frac{U_{Ts}}{R_{Ts} \cdot C_{Ts}} \\ I_{cell} &= \frac{U_{TL}}{R_{TL}} + C_{TL} \cdot \frac{dU_{TL}}{dt} \rightarrow \frac{dU_{TL}}{dt} = \frac{I_{cell}}{C_{TL}} - \frac{U_{TL}}{R_{TL} \cdot C_{TL}} \end{aligned} \tag{2.4}$$

A complete battery pack is comprised of several battery cells stacked together to form a battery pack with a specific voltage, power, and energy rating. The number of cells in a single string

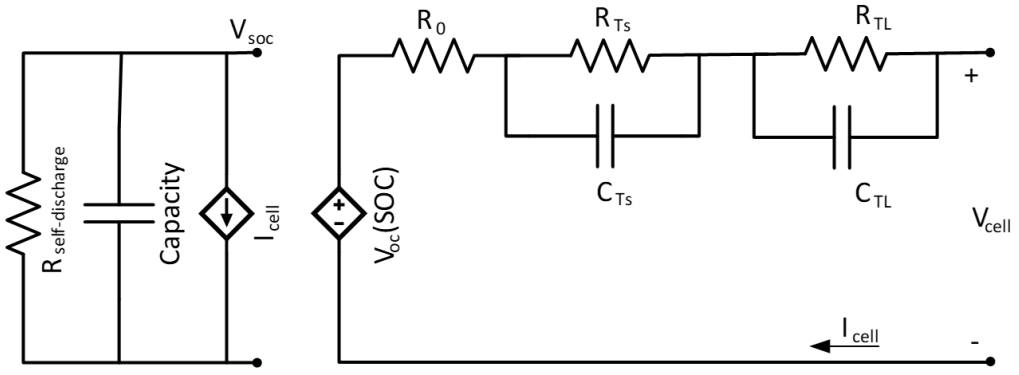

Figur 2.1: Equivalent Electrical Circuit of a Battery Cell.

determines the battery terminal voltage. Since the nominal voltage of a battery cell is known, we can calculate the number of cells in a string n_S based on the required DC voltage level:

$$n_s = \frac{U_{batt}}{U_{cell}} \tag{2.5}$$

If the power requirement for the battery is known, then we can calculate the rated current as:

$$I_{batt} = \frac{P_{batt}}{U_{batt}} \tag{2.6}$$

The number of strings that need to be connected in parallel in order to achieve the rated current can be calculated as:

$$n_p = \frac{I_{batt}}{I_{cell}} \tag{2.7}$$

I_{Cell} is the rated current of a single battery cell. The capacity of a single battery cell is usually expressed in Ah. C-rate represents the charging or discharging rate of a battery expressed in terms of the total battery capacity in Ah. 1C rate represents the current for which the battery is fully charged or discharged in one hour. The capacity of the battery pack is determined by the capacity of single-cell multiplied by the number of parallel-connected strings. Based on this, the total energy stored in a battery pack can be determined from:

$$E_{batt} = U_{batt} \cdot C_{batt} \tag{2.8}$$

The battery pack model can be extrapolated from a single battery cell model. The model in PowerFactory is represented as in Fig. 2.2.

The parameters of the equivalent circuit are updated for every new value of SOC by using a special DSL function in PowerFactory "*lapprox*"[26], which uses a linear approximation method to evaluate the parameter based on the state of charge, as shown in the following DSL code of the model.

```
1

3 !Estimating the open circuit voltage based on SOC
```

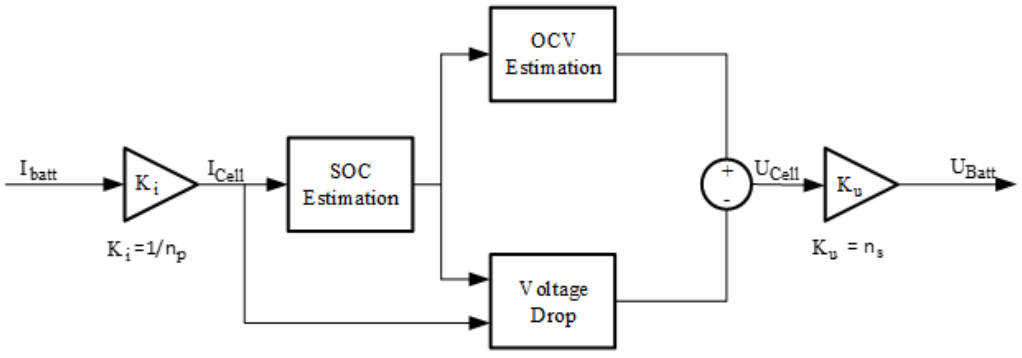

Figur 2.2: Block diagram of a single cell in PowerFactory.

```
OCV=lapprox(SOC,array_OCV)

!Estimating the parameters based on SOC
R_0=lapprox(SOC,array_R0)
R_Ts=lapprox(SOC,array_Rts)
R_TL=lapprox(SOC,array_Rtl)
C_Ts=lapprox(SOC,array_Cts)
C_TL=lapprox(SOC,array_Ctl)

!Calculating the voltage drop
U_0=Icell*R_0
U_Ts.=(Icell/C_Ts)-U_Ts/(R_Ts*C_Ts)
Uts=U_Ts
U_TL.=(Icell/C_TL)-U_TL/(R_TL*C_TL)
Utl=U_TL
U_drop=U_0+Uts+Utl
```

The values of the parameters are stored in an array under the tab "*Advanced 1*"of the DSL common model, as shown in Fig. 2.3. This model of the battery is based on the data provided in [27].

The parameters of the equivalent circuit can be given in the form of a function of SOC. The parameters of this model are based on the model that is given in [23]. The DSL code for this model is given below.

```
!Calculating the open-circuit voltage of the battery cell
OCV=-1.031*exp(-35*SOC)+3.685+0.2156*SOC-0.1178*sqr(SOC)+0.3201*pow(SOC,3)

!Calculating the parameters of the equivalent circuit
R_0=0.1562*exp(-24.37*SOC)+0.07446
R_Ts=0.3208*exp(-29.14*SOC)+0.04669
R_TL=6.603*exp(-155.20*SOC)+0.04984
C_Ts=-752.90*exp(-13.51*SOC)+703.60
C_TL=-6056*exp(-27.12*SOC)+4475

!Calculating the voltage drop
U_0=Icell*R_0
U_Ts.=(Icell/C_Ts)-U_Ts/(R_Ts*C_Ts)
U_TL.=(Icell/C_TL)-U_TL/(R_TL*C_TL)
U_drop=U_0+U_Ts+U_TL
```

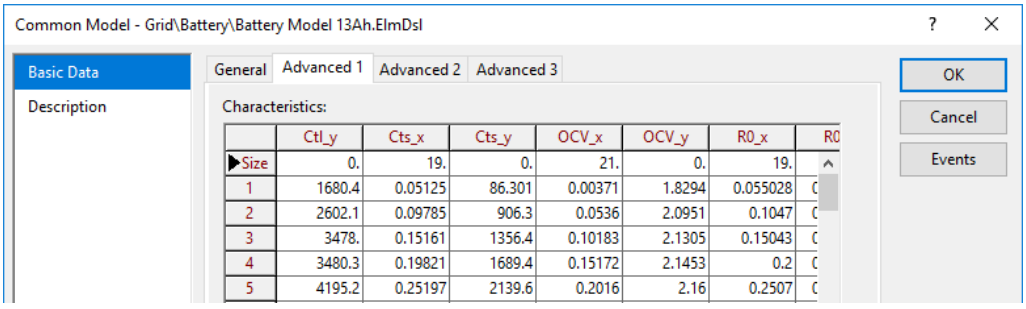

Figur 2.3: PowerFactory common model of a battery - Equivalent circuit parameters.

The battery in DigSilent PowerFactory is represented by a voltage-controlled DC voltage source. The battery model controls the voltage level of the DC voltage source. The voltage at the battery terminal is determined by following the procedure as described below:

1. The DC current is controlled by the power converter through which the battery is connected to the grid,
2. The DC current is measured by the DC Current Measurement block in PowerFactory,
3. Based on the current state of charge, the parameters of the equivalent circuit are evaluated, and by knowing the parameters of the circuit and the current, the actual voltage at the terminal of the battery is evaluated and used as a reference point of the DC voltage source.
4. The estimated state of charge is constantly updated, and information is provided to the power converter controller.

The complete system is placed within a composite frame in PowerFactory (*Battery.ElmComp*) with three slots included; slot for the battery (based on an equivalent circuit), DC Current Measurement slot, and the slot for the DC Voltage Source. The diagram of the model is shown in Fig. 2.4.

2.3 Power converter model

A standard two-level converter is responsible for controlling the battery pack. The block diagram of the control structure is given in Fig. 2.5. The block diagram shows the components of the complete battery system (converter, battery, and measurement components), as well as the main control blocks (frequency droop, active and reactive power control, and charging and discharging control). This structure is implemented in PowerFactory as a composite frame (*BESS.ElmComp*).

There are two main loops in the control structure, namely the active and reactive power loop. PLL is used to synchronize the power converter voltage angle with the grid and measure the system frequency. The delay block is used to represent the communication and response latency of the battery system. The "Charge and Discharge Control"block has three main functions:

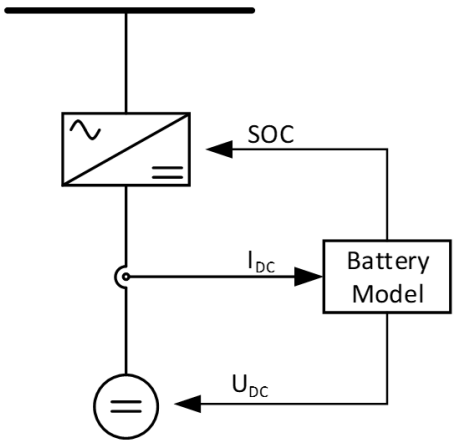

Figur 2.4: Representation of BESS in PowerFactory.

1. To control the charging and discharging mode of the battery (stopping the discharge at minimum SOC, or stopping the charge at maximum SOC),
2. To limit the charging current when the battery is at high SOC in order to prevent dangerous overvoltage at the battery terminal,
3. To limit the current of the power converter.
4. To switch to fault-ride-through operating mode under severe voltage dips (below 0.9 pu).

2.3.1 Active power control loop

In the active power control loop, there are three basic functions:

1. Frequency droop control,
2. ROCOF based control,
3. Active power set-point.

Combining the droop and RoCoF functions can be considered a fourth function of the active power control loop. The frequency control based on the rate of change of frequency (RoCoF) and the frequency droop is a part of the frequency control loop of the battery system, as shown in Fig. 2.6. The frequency droop co-efficient can be calculated as:

$$R_{droop} = \frac{1}{K_{droop}} = \frac{f_{ref} - f_{meas}}{P - P_{ref}} = \frac{\Delta f}{\Delta P} \tag{2.9}$$

The parameter R_{droop} determines the active power change of the battery system, ΔP, for a change in the frequency of Δf. In most cases, the grid code defines an insensitive region of the frequency change known as deadband, which is a tolerated deviation in system frequency (usually between 0.02 and 0.05 Hz). The low pass filter prevents the controller reaction to high-frequency transients. The output of this control loop is an active power change signal to the active power controller. For under-frequency disturbances, the output will be positive, and the battery system will switch to discharging mode, while for the over-frequency disturbances, the output will be negative, and the battery will start charging.

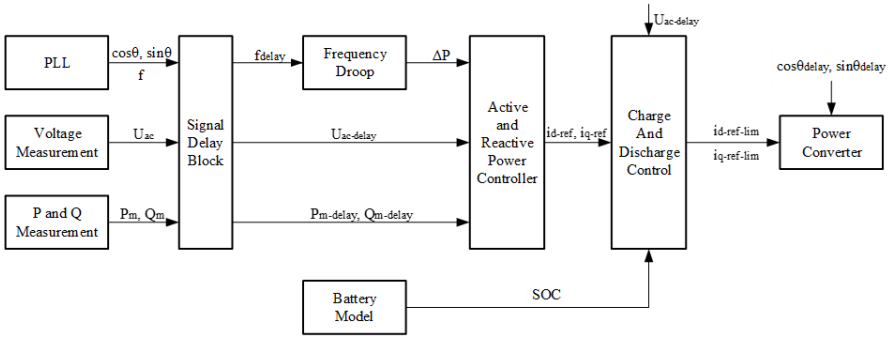

Figur 2.5: The block diagram of BESS in as modelled in PowerFactory.

The RoCoF function generates an active power reference, which is proportional to the rate of change of frequency. The rate of change of frequency or the slope of the frequency change is a derivative of frequency over time, and the relationship between RoCoF and the active power can be expressed as:

$$\Delta P = K_{rocof} \cdot \frac{df}{dt} \tag{2.10}$$

The time window of the RoCoF calculation will have a significant impact on the result, the smaller the time interval between the frequency measurements, the higher the response will be. If we want a larger time interval than the sampling time of the simulation, we can use the following expression:

$$\frac{df}{dt} = \frac{f(t) - f(t - \Delta t)}{\Delta t} \tag{2.11}$$

In PowerFactory, the RoCoF is calculated by using the "*delay*"function [26], which stores the value of a variable *x(t)* and returns the value $x(t - t_{delay})$, as shown in the following DSL code.

```
!Initial Conditions
inc(p0)=dpref
inc0(f0)=frq
inc(xf)=0
inc(xrc)=0
inc(df_dt)=0

vardef(db)='pu';'Deadband for frequency control'
vardef(droop)=;'Droop coefficient'
vardef(p_min)='pu';'Lower limit for droop control'
vardef(p_max)='pu';'Upper limit for droop control'
vardef(Tf)='s';'LPF time constant'
vardef(T_rocof)='s';'Derivation time step for RoCoF'
```

The active power control block (Fig. 2.7) generates the d-axis reference current. The inputs provided to the control block are the set-point active power control (P_{ref}), the frequency support reference (), as well as the $_d$. The $_d$ signal comes from the converter current limiter, and it prevents the PI controller integrator windup in cases where the reference current exceeds the limit. The low pass filter eliminates the measurement noise and limits the rate of change of active power. The d-axis

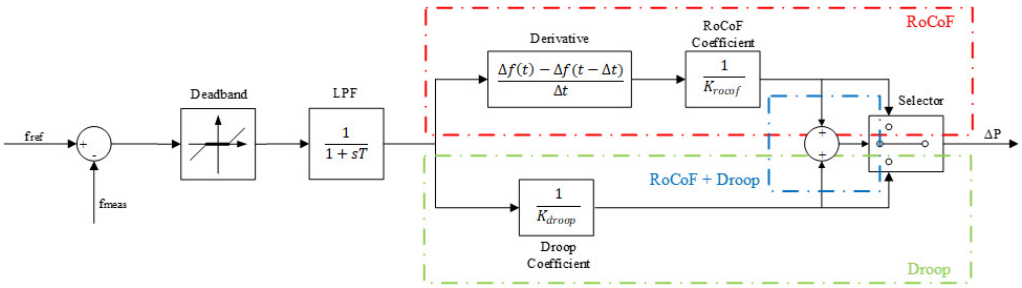

Figur 2.6: Frequency Droop/RoCoF Controller.

current i_{d-ref} is the reference current generated by the active power controller. The next step in the active power control loop is to limit the active power current according to the rating and determine the mode of the battery (charging, discharging or standby).

The block diagram of the PowerFactory common model (*Charge-Discharge.ElmDsl*) is shown in Fig. 2.8. Four functions characterize this control block:

1. Battery mode selector - determines the operation mode of the battery (charging, discharging, and standby).
2. Charging current limiter - keeping the battery voltage constant at high SOC (>80%) by reducing the charging current.
3. Dynamic limiter - the d-axis current limits are recalculated when the system is operating in fault-ride-through mode.
4. Anti-windup loop - generates the Δi_d signal to prevent the integrator windup of the active power block PI controller

The mode selector switches between the charging and discharging modes based on the sign of the input current of the block. The algorithm of the decision procedure is shown in Fig. 2.9. Two conditions need to be satisfied in order to initialize the charging or discharging mode. If the input current is positive, and the state of charge of the battery is larger than the minimum state of charge (minimum SOC represents the discharged state), the discharging mode will be activated. For a negative current and the SOC lower than maximum, the battery will be in the charging mode. The standby mode (no charging nor discharging) is initiated if the reference current is equal to zero. The charging and discharging of the battery will be blocked as long as the battery is fully charged ($SOC \geq SOC_{max}$) or fully discharged ($SOC \leq SOC_{min}$), respectively.

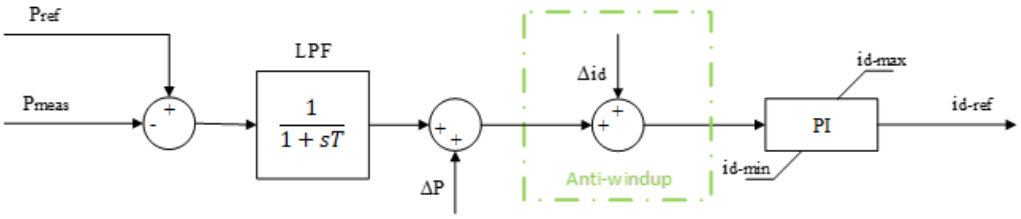

Figur 2.7: Active power control loop.

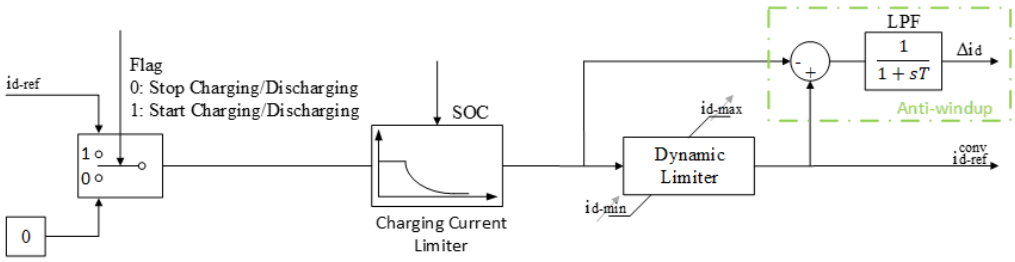

Figur 2.8: Charging/Discharging control and current limiter block diagram - d-axis cur-rent.

As previously said, the battery voltage needs to be kept below the maximum permissible level when the battery is charging because the voltage level tends to rise exponentially beyond the physical limits when the SOC is high (>80%), and it can cause a thermal runaway in the cell. Therefore, the charging current needs to be controlled in such a way that the battery voltage stays constant once it reaches the maximum level for continuous operation. This means that the charging current needs to be reduced at higher levels of SOC. The charging current can be expressed as:

$$I_{batt} = \frac{U_{OC} - U_{batt}}{R_0 + R_{Ts} \cdot (1 - e^{\frac{t}{\tau_{Ts}}}) + R_{TL} \cdot (1 - e^{\frac{t}{\tau_{TL}}})} \qquad \tau_{Ts} = R_{Ts} \cdot C_{Ts}, \quad \tau_{TL} = R_{TL} \cdot C_{TL} \tag{2.12}$$

U_{batt} is the voltage at the battery terminal, and it is kept constant during the whole process of charging. The other parameters in the equation will change depending on the SOC. Once we calculate the charging current for each value of SOC, we can implement a limiter in PowerFactory as a look-up table, where the current lim-it is a function of SOC. The process of battery cell charging is exemplified in Fig. 2.10. The battery cell was charged with a constant current of 0.5C, until the terminal voltage reached the maximum permissible value. After this point, the battery was charged in constant voltage mode until it was fully charged. In the literature, this process of battery charging is known as "*Constant Current â Constant Voltage*"(CCCV) charging method.

The current limit look-up table is stored under the "*Advanced 1*"tab of the *"Charge-Discharge.ElmDsl"* common model within the *"BESS.ElmComp"* composite frame, as shown in Fig. 2.11.

The dynamic limiter can operate in two modes. The first mode is the *normal operation mode*, where the priority is given to active power injection. The current limits are based on the battery ratings.

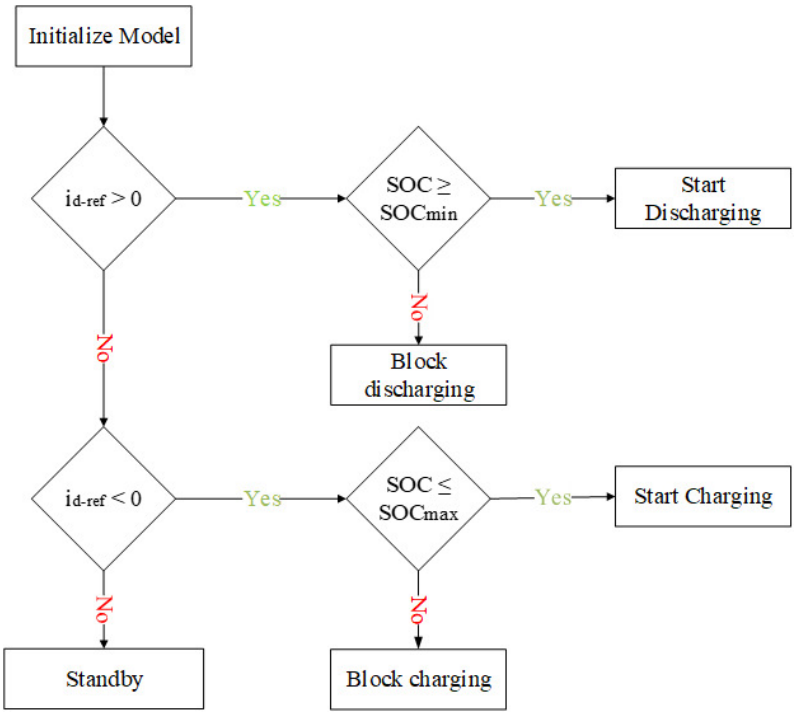

Figur 2.9: Flow chart of the charging/discharging algorithm.

The other mode of operation is the *fault-ride-through* mode (voltage drops below 0.9pu), where the priority is given to reactive power injection, and the d-axis current limits are given as:

$$i_{d-ref}^{conv} = \sqrt{i_{max}^2 - {i_{q-ref}^{conv}}^2} \tag{2.13}$$

The anti-windup effect is accomplished by subtracting the input of the limiter block from the output. The sum is passed through the low pass filter in order to avoid the forming of an algebraic loop. In PowerFactory, the charging algorithm is represented by a DSL block reference *"Charging.BlkRef"*. The flag variables for charging and discharging states (logic variables with values 0 or 1) are obtained by using a special DSL function, "*flipflop*"[26]. The variable state will change from 0 to 1 when the logical variable *"startc"* is 1 and the logical variable *"stopc"*is 0. The *"startc"* and *"stopc"* are also logical variables that indicate if the charging process has started or if it was stopped. The variables are obtained by using a special DSL function *"picdro"* [26].

```
!Initial conditions, charging variables
limits(Te)=[0.001,]
inc(charging)=flipflop(startc,stopc)
inc(startc)=picdro({SOC<lim(maxSOC,0.2,1) .and. idr<-0.0001},0,0)
inc(stopc)=picdro({SOC>lim(maxSOC,0.2,1)-0.001 .or. idr>-0.0001},0,0)
inc(xcharge)=max(idr,Ir)
!Initial conditions, discharging variables
inc(startdc)=picdro({SOC>lim(minSOC,0.1,0.9) .and. idr>0.0001},0,0)
inc(stopdc)=picdro({SOC<lim(minSOC,0.1,0.9) .or. idr<0.0001},0,0)
inc(discharging)=flipflop(startdc,stopdc)
inc(xdischarge)=lim(idr,0,1.5)

!Charging current limiter
Ir=select(BattSel<1.5,lapprox(SOC,array_Icharge085),lapprox(SOC,
    array_Icharge13))
```

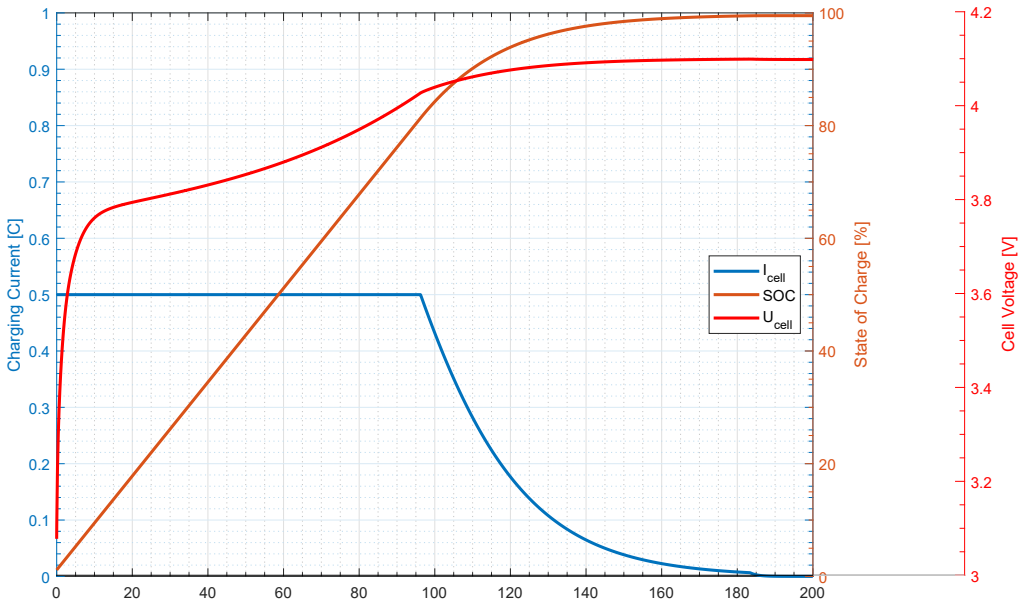

Figur 2.10: CCCV battery charging method.

```
15 !Charging current, low pass filter
   xcharge.=(select(charging=1,max(idr,Ir),0)-xcharge)/0.005
17 icharge=xcharge

19 !Limiting the rate of change of the battery current upon sudden interruption
   inc(Tc)=time()
21 inc(aux1)=0
   inc(aux2)=0
23 aux1=aflipflop(time(),stopc,startc)
   aux2=aflipflop(time(),stopdc,startdc)
25 Tc=select(charging<0.5 .and. stopc>0.5 .and. idr<0, aux1, select(discharging
       <0.5 .and. stopdc>0.5,aux2,delay(Tc,0.01)))
   idc=max(idr,Ir)*exp(-(1/Te)*(time()-Tc))
27
   !Conditions to begin charging
29 startc=picdro({SOC<lim(maxSOC,0.2,1) .and. idr<-0.0001},0.01,0)
   !Conditions to stop charging
31 stopc=picdro({SOC>lim(maxSOC,0.2,1)-0.001 .or. idr>-0.0001},0.01,0)
   !Charging flag variable, 0 or 1
33 charging=flipflop(startc,stopc)
   !Conditions to begin discharging
35 startdc=picdro({SOC>lim(minSOC,0.1,0.9) .and. idr>0.0001},0.01,0)
   !Conditions to stop discharging
37 stopdc=picdro({SOC<lim(minSOC,0.1,0.9) .or. idr<0.0001},0.01,0)
   !Discharging flag variable, 0 or 1
39 discharging=flipflop(startdc,stopdc)

41 !Discharging current, low pass filter
   xdischarge.=(select(discharging=1,lim(idr,0,1.5),0)-xdischarge)/0.005
43 idischarge=xdischarge

45 !The reference id current
   idref=select(charging,icharge,select(discharging,idischarge,idc))
```

This function evaluates the logical expression(s) (in our case those are the conditions for starting or stopping the charging state), and it pics up a logical state of 1 if the logical expression is *true* for the predefined pick-up time. A low pass filter with low time constant is implemented to prevent fast transients and eliminate noise.

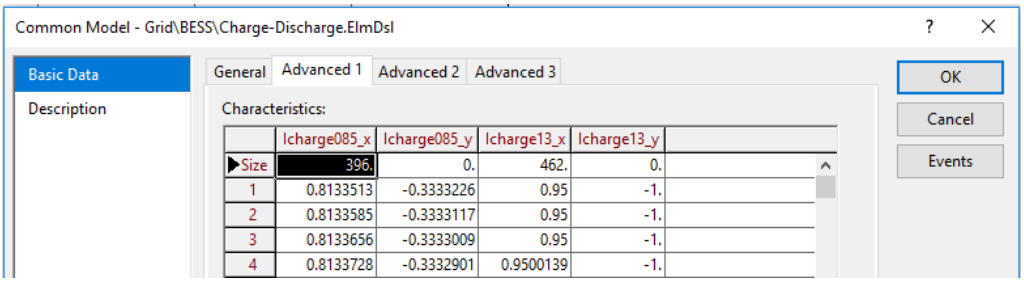

Figur 2.11: Battery charging current limiter characteristic.

2.3.2 Reactive power control loop

The reactive power control loop allows for three basic functions:

1. Reactive power set-point,
2. Automatic voltage control,
3. Fault-ride-through mode.

Under normal operating conditions ($V_{meas} > 0.9pu$), the reactive power control loop can provide voltage support with two basic functions. The block diagram is shown in Fig. 2.12. The reactive power set-point control adjusts the reactive power output as per user input. The automatic voltage control compares the reference voltage and the measured voltage and generates reactive power accordingly in order to reduce the voltage deviation. As the voltage is measured at the HV side of the connecting transformer, we must compensate for the transformer impedance with an additional signal $K_{slope}Q_{meas}$. The slope coefficient determines the allowed error between the measured voltage and the reference voltage.

The compensation block serves an additional function of ensuring an equal reactive power sharing between the BESS system and other voltage support components connected in parallel (synchronous machine, wind turbine, etc.). The resulting voltage error can be written as:

$$\Delta V = V_{ref} - V_{meas} - K_{slope} \cdot Q_{meas} \tag{2.14}$$

The user can choose which strategy should be employed for a simulation scenario. The resulting signal error is further forwarded to a PI controller, as shown in Fig. 2.13. The low pass filter is used to prevent fast transients an eliminate noise. The Δi_q signal serves the same purpose as in the active power control loop, to prevent the PI controller windup. The control block generates the q-axis reference current i_{q-ref} (*PQ Controller.ElmDsl*).

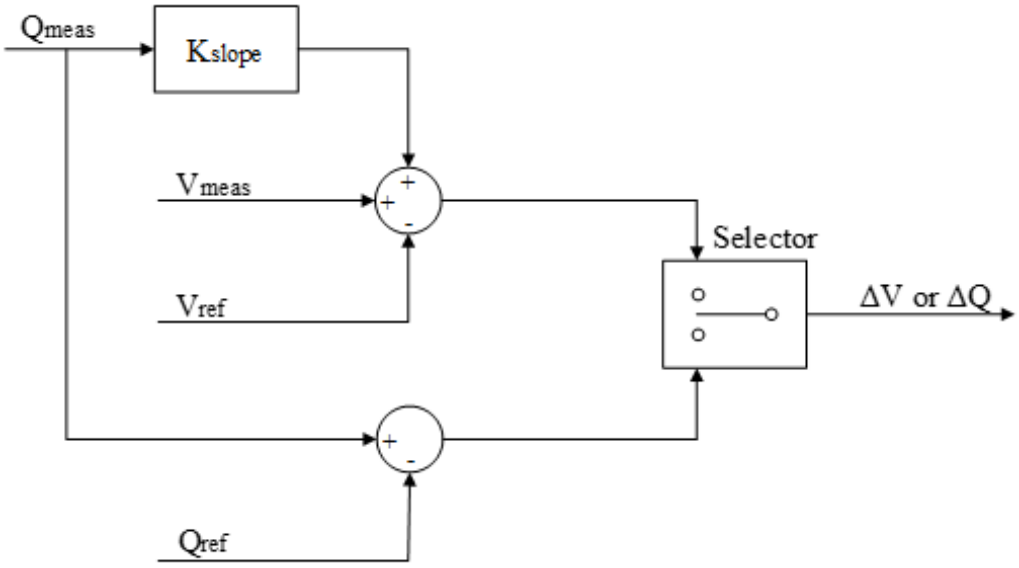

Figur 2.12: Reactive power controller.

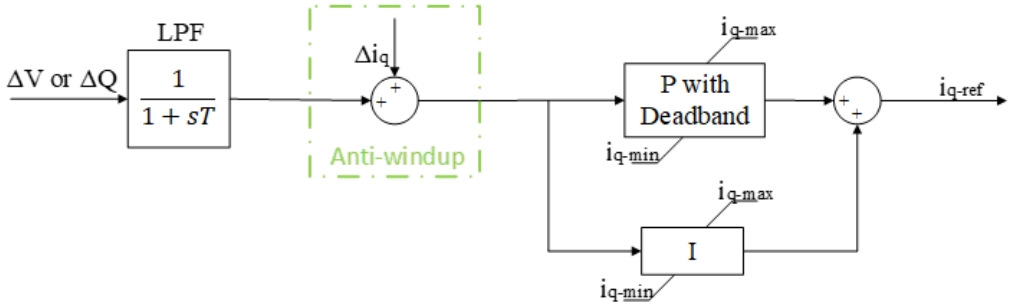

Figur 2.13: Reactive power control loop.

The q-axis current reference i_{q-ref} is the input to the current limitation and fault-ride-through mode selection block (*Charge-Discharge.ElmDsl*). This block includes three functions for the reactive power control loop:

1. Activating fault-ride-through mode for extreme voltage dips $(V_{meas} < 0.9pu)$.
2. Dynamic limiter - the q-axis current limit is recalculated if the system is operating under fault-ride-through mode.
3. Anti-windup loop - generates the Δi_q signal to prevent the integrator windup of the PI controller of the reactive power control block.

The block diagram is shown in Fig. 2.14.

The fault-ride-through mode is activated if the system voltage drops below 0.9 pu (the parameter is user adjustable). The flowchart of the fault-ride-through algorithm is given in Fig. 2.15. If the measured voltage dips below 0.9 pu, the controller will enter the fault-ride-through mode and give priority to the reactive power injection. As per the UK grid code <[28], the total reactive current injected by the converter is a sum of the pre-fault value of the reactive current and the current estimated based on an I-V fault characteristic modelled as per the grid code. In most European grid codes, the requirement is to inject 1.00 pu of reactive power once the voltage (V_{min}) drops to 0.5 pu. The current injected during the fault-ride-through operation mode can be expressed as:

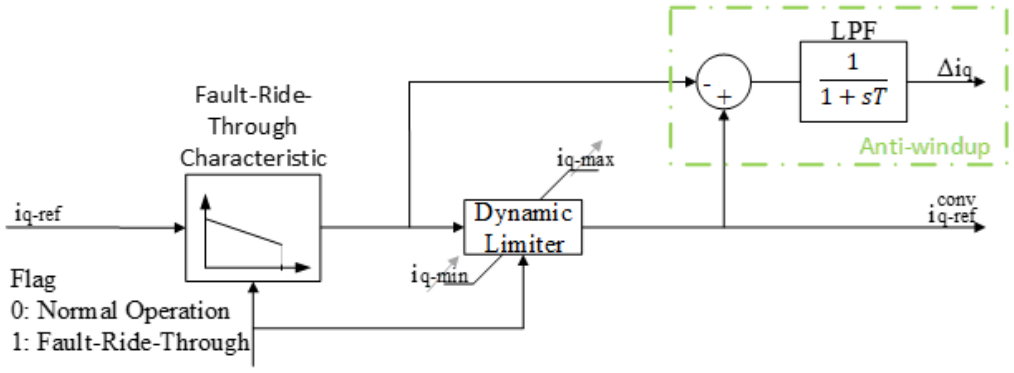

Figur 2.14: Fault-ride-through mode and current limiter.

$$i_{q-ref}^{conv} = i_{q-ref}^{pre-fault} + K_{frt} \cdot \Delta V \tag{2.15}$$

The slope of the characteristic is K_{frt}, which is determined by the following equation:

$$K_{frt} = \frac{i_r - i_{q-ind-r}}{V_{min} - V_{threshold}} \tag{2.16}$$

The i_r current is the rated current of the converter (1.00 pu), $i_{q-ind-r}$ is the rated inductive current of the converter operating in normal mode, V_{min} is the voltage limit beyond which the reactive current injection requirement is 1.00 pu, and $V_{threshold}$ is the voltage at which the fault-ride-through mode is activated. For voltage dip to 0.50 pu, we have chosen the reactive current injection to be equal to the maximum rated current of the converter (1.10 pu), and this current represents the maximum overcurrent that the converter can provide continuously.

In PowerFactory, the fault-ride-through algorithm is implemented by using the "*picdro*"special DSL function. The mode will activate once the voltage drops below the threshold (logical expression in the "*picdro*"function switches to true). The limits are updated depending on the mode of operation. For normal operation, the d- and q-axis current limits are set according to the active and reactive power rating of the battery system, while for the fault ride through mode the priority is given to the reactive power injection.

```
!Initial conditions
inc(uref)=uac
inc(frt)=0
```

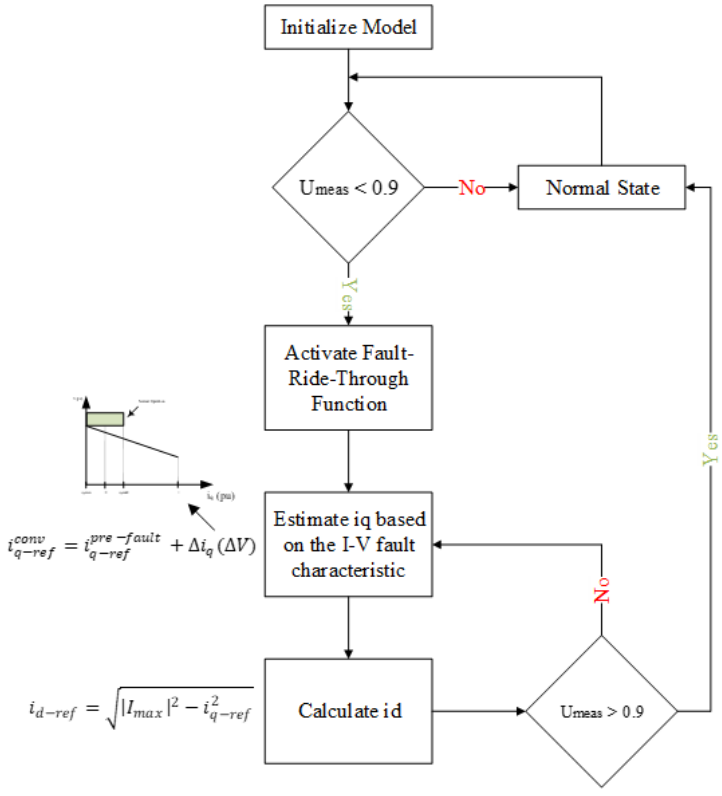

Figur 2.15: Flow chart of the FRT function.

```
inc(i_pre)=iqout
inc(iq_state)=iq_lim
inc(iq_ref_limit)= maxAbsCur*maxAbsCur-idin*idin
inc(id_ref_limit)= maxAbsCur*maxAbsCur-iqin*iqin

!Fault-ride-through flag variable
frt = picdro(abs(uac-uref)>=dU,0.001,0.01)

!Fault-ride-through current characteristic as per grid code
iq_lim=select(frt,lim(i_pre-3.625*((1-dU)-uac),-maxAbsCur,i_pre),i_pre)

!Current limit calculation
var_d=select(idin>idmax,idmax,select(idin<idmin,idmin,idin))
var_q=select(iqin>iqmax,iqmax,select(iqin<iqmin,select(frt,-iq_lim, iqmin),
    iqin))
lim_d=select(idin>0,idmax,idmin)
lim_q=select(iqin>0,iqmax,-lim(iq_lim,-iqmin,maxAbsCur))
!normal operation iq limit
iq_ref_limit=abs(lim(maxAbsCur*maxAbsCur-var_d*var_d,0,lim_q*lim_q))
!frt operation id limit
id_ref_limit=abs(lim(maxAbsCur*maxAbsCur-var_q*var_q,0,lim_d*lim_d))
!selecting limits based on operation mode
lim_sel=sqrt(select(frt,id_ref_limit,iq_ref_limit))

!Fault-Ride-Through current reference with low pass filter
iq_state.=(iq_lim-iq_state)/0.02

!Generating id and iq reference currents
idout=select(frt,lim(idin,-lim_sel,lim_sel),lim(idin,idmin,idmax))
iqout=select(frt,lim(iq_state,-maxAbsCur,maxAbsCur),lim(iqin,-lim_sel,lim_sel)
    )
```

The output of the "*Charge-Discharge.ElmDsl*"common model blocks are the d-axis and q-axis currents, which serve as a reference for the power converter block. In PowerFactory, the power converter block has a built-in inner current controller, so it requires only the reference d- and q-axis currents, as well as the voltage phase angle in order to generate the reference voltage signal for the PWM.

2.4 Case Study: Testing the Battery Model and Control

In order to test the battery model and the implemented control strategies, we have used a simple network consisting of the battery system and a large synchronous machine rated at 2.55 GVA, 19 kV, 4 seconds inertia constant. This setup is used for the frequency support test, while for the voltage support test we have used a Thevenin equivalent to represent the grid (2800 MVA short circuit power, 33 kV voltage level, and 18.85 X/R ratio). The rated parameters of the battery system are given in Table 2.1.

2.4.1 Frequency control functions

As we previously discussed, there are three possible frequency support functions within the battery model. The droop control is based on the frequency deviation, where the controller injects active

Single Cell Capacity	13 Ah
Nominal Cell Voltage (50% SOC)	2.228
Number of Cells in a Single String	585
Number of Strings Connected in Parallel	197
Nominal Voltage of a Battery Pack (50% SOC)	1.3 kV
Maximum Charging and Discharging Current	3C
End of Discharge Voltage ($\approx$ 0% SOC)	1.07 kV
Minimum SOC	10 %
Maximum SOC	100 %
Rated Power (Charging and Discharging)	10 MW
Stored Energy	3.34 MW

Tabel 2.1: Rated parameters of the battery pack.

power in proportion to the level of frequency change. The second function is based on the rate of change of frequency (RoCoF). The controller acts in proportion to the rate of frequency deviation. The third function consists of using both control strategy to address the frequency disturbance at different time scales. The RoCoF function acts very fast following a disturbance and tries to counter the frequency change in a similar way to the inertial response of a synchronous machine.

The RoCoF function has an influence on the slope of frequency change and the resulting nadir. The frequency droop control has an impact on the frequency nadir and the steady-state. We have performed the simulation with four different cases in order to capture the effect of the function implementation, as well as the proportional coefficient (droop and RoCoF). For the base case, the battery system does not provide any frequency support, while for the other three cases, we changed the droop and RoCoF parameter within the range of 0.01-0.05 (0.5-2.5 Hz frequency deviation). The results of the simulations are shown in Fig. 2.16.

At 1.0 seconds a load of 200 MW is connected to the same bus as BESS. The frequency response of the system clearly demonstrates the effect of the control strategies. The RoCoF function acts fast to arrest the frequency drop, while the droop function response is slower, affecting the frequency nadir and especially the new steady state value of the frequency. The effect of both strategies can be observed in the bottom-right plot where we compare the different strategies with the base case (no frequency support) at the same droop/RoCoF coefficient.

2.4.2 Fault-ride-through capability

The fault-ride-through algorithm is a requirement for most grid-connected generating units. The reactive current vs. voltage characteristics are included in most grid codes, and the requirement is to inject a certain level of reactive current during severe voltage drops (grid faults). In this example,

we have tested the BESS response to a three-phase fault at the PCC. The results of the simulation are shown in Fig. 2.17. The fault is applied at 0.1 seconds, which results in a voltage drop to 0.5 pu. At the instance of the fault inception, the BESS was delivering full rated active power of 70 MW. Following the fault, the controller activates the fault-ride-through mode and injects the maximum permissible reactive current (1.1 pu, which includes 10% overcurrent) into the grid. The limiter acts to limit the active current so that the total injected current does not exceed the maximum overcurrent of the power converter.

The bottom left and right plots show the reference currents before and after the limiter. The $i_{d-ref-out}$ and $i_{q-ref-out}$ are the reference currents that are sent to the converter model. As the injected reactive current matches the maximum overcurrent of the converter (in fault-ride-through mode priority given to the reactive current), the active current must be limited to zero.

2.4.3 Charging and discharging control

The active power control function is a simple control algorithm, where the system operator (or higher-level automatic control) sets the active power reference. This function is used for scheduled charging and discharging of the battery. The top left and top right plots in Fig. 2.18 show the voltage and current of a single battery cell during 1.0 second of charging and 1.0 second of discharging. The rated charging and discharging currents for this battery cell are 3C or 39 A, which corresponds to the rated active power output of the entire battery system. The voltage of the battery cell exhibits a typical behaviour of a lithium-ion cell under load. It can be distinguished the immediate voltage drop due to the R_0 resistance (Fig. 2.1), and the fast and slow dynamics exemplifying the two RC circuits. The bottom left plot shows that the battery is being charged and discharged under

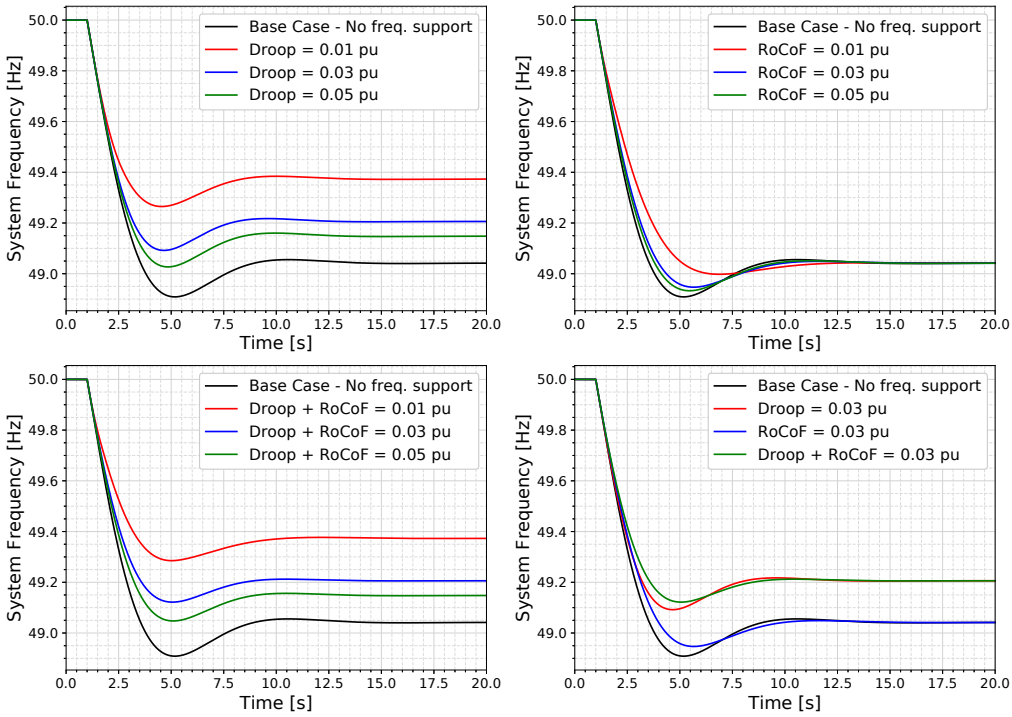

Figur 2.16: Frequency response of BESS. Top left: Droop controller active; Top right: RoCoF controller active; Bottom left: Droop + RoCof controllers active; Bot-tom right: Comparison between the functions.

equal power. However, the state of charge is not the same at the end of the simulation as it was at the beginning. The reason for this is that the discharging current will cause a voltage drop at the battery terminals (due to the internal resistances of the battery) and consequently the discharging current will increase in order to have a rated power output of 1.00 pu at the battery terminal. Similarly, the charging current will cause the voltage to rise and to cause a lower than nominal charging current for the rated power input. This phenomenon is the cause of the SOC mismatch.

The charging/discharging controller of the battery system is constantly updated with the information about the state of charge. Most battery technologies have the longest lifetime if the state of charge is kept between 20% and 80%, which we have set as the minimum and maximum SOC for this example. Once the battery is fully charged or discharged, it is important not to interrupt the charging/discharging current instantaneously because this can cause unwanted transients and potential instability in the grid. The user can set the time constant of the battery switching from charging/discharging mode to the standby mode (parameter T_e within the "*Charge-Discharge.ElmDsl*"common model). Fig. 2.19 shows the battery response once the fully charged state has been reached.

Once the SOC reaches 80%, the charging current starts to drop. After approximately 5.0 seconds, the current is reduced to zero and the battery is in the standby mode. The top- and bottom-left plot show that the active power and the current reference remain at 1.00 pu, while the actual measured power and current are zero. This indicates that the charging has stopped because the battery was fully charged. The top-right plot shows that SOC is slightly above 80%, and the reason behind this is that the battery was still charging after the standby mode was initiated. The charging current of a single battery cell (bottom-right plot) is not equal to 3C (even though the power reference was 1.00 pu). The reason for this is that when the battery is charging, the terminal voltage will be higher than in the case when the battery is discharging (even though the power exchange is the same). The other significant reason is that for higher SOC, the open-circuit voltage (OCV) of the battery will be high, and consequently the terminal voltage.

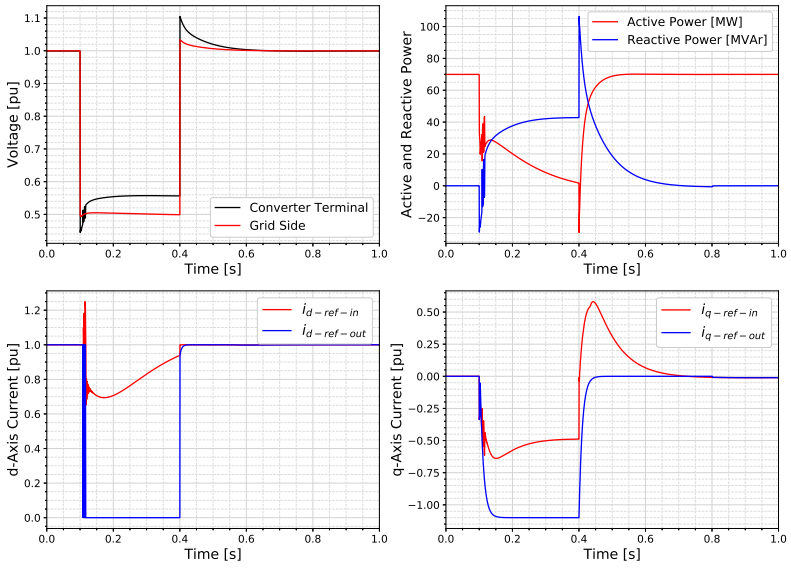

Figur 2.17: BESS response in FRT mode of operation.

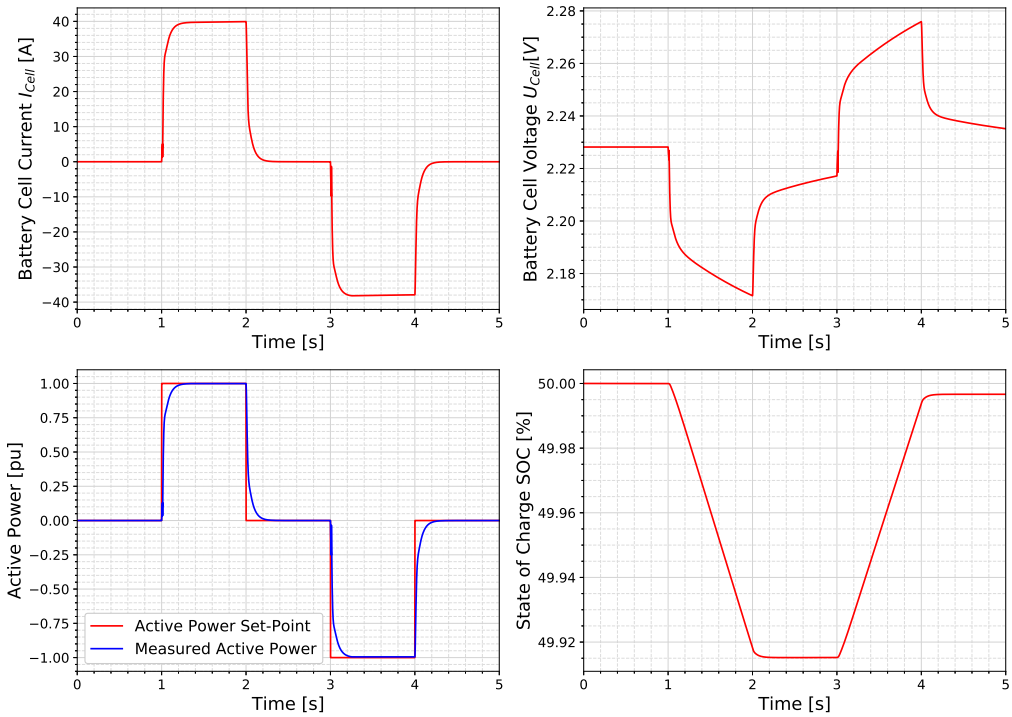

Figur 2.18: Scheduled charging/discharging of BESS.

2.5 Conclusion

This chapter presented a procedure about the modelling of battery systems in DIgSILENT PowerFactory simulation software. The battery model is based on an equivalent electrical circuit, which captures the internal chemical processes that characterize the electrical performance of a battery cell. It has included two types of parameter representation, namely the approach based on a look-up table and the parametrized function approach. We have dedicated a significant space to control design, and control strategies implementation. The main features of the model include frequency and voltage support, as well as the fault-ride-through function. The frequency control block includes two functions for frequency sup-port, RoCoF and frequency droop, and the third function is the hybrid function, which combines the two into a singular frequency control function providing the frequency support at two different time scales. The voltage support consists of automatic voltage control for steady-state operation (voltages above 0.90 pu), and the fault-ride-through mode for operation under severe voltage dips. All the functions were tested under different scenarios in order to verify the validity of the model. The BESS model can be easily expanded to include the thermal model of the battery, as well as other ancillary services, such as oscillation damping, harmonic attenuation, etc.

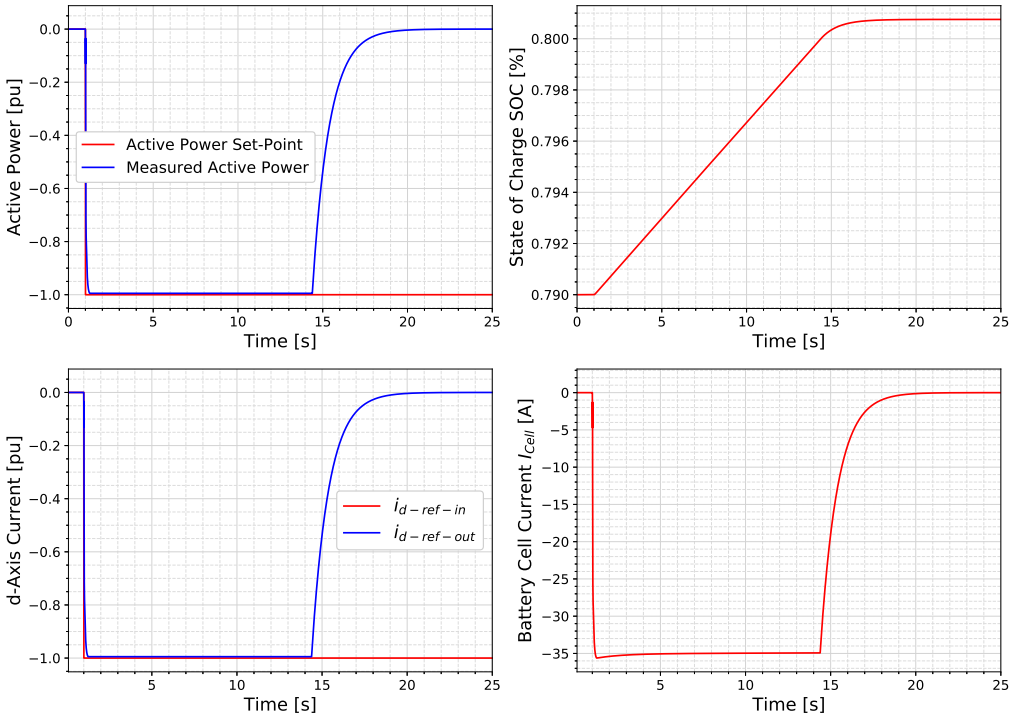

Figur 2.19: Fully charged battery state

KAPITEL 3

Hybrid Synchronous Condenser System

The chapter is based on **[Pub. C]** and **[Pub. D]**.

3.1 Introduction

In recent years, we have seen an increase in synchronous condenser installation in order to address the issues related to decrease of synchronous machine-based generation [29]. Synchronous condensers have been used in the power systems since the 1950's, but mainly to provide reactive power and contribute in voltage control. In recent years, synchronous condensers have been considered for inertial support because they retain the inherent capabilities of a synchronous machines [30]. The effect is naturally less than that of a conventional synchronous generator since the mechanical input torque and the electric output torque are zero at the moment of disturbance inception [31]. Furthermore, a significant advantage of synchronous condensers is their overloading capability under various conditions in the system in terms of voltage (e.g. voltage dips, short circuits) [32]. The authors in [33] present a case for using synchronous condenser to improve the short circuit ratio (SCR) of the system, and they demonstrate the improvement in fault-ride-through performance in terms of higher retained voltage and faster voltage recovery.

The implementation of battery energy storage systems in power grids is becoming a major interest in terms of ancillary services provision [17]. A frequency response service as a part of the control structure of BESS can provide full rated active power within a second of the frequency disturbance inception [18]. In [34], the authors discuss the use of battery system for secondary frequency control and reducing the area control error (ACE) to zero. Utilising BESS for power system oscillation damping have been demonstrated in [35]. The intermittent nature of renewable sources such as wind and solar power and inevitable error in forecast make the battery systems a viable solution for those issues, as exemplified in [36] and [37].

An attractive solution for industry is a hybrid synchronous condenser system consisting of a synchronous condenser and static compensator (STATCOM). Scottish Power and Energy Network initiated a pilot project where a hybrid SC is installed at Neilston substation in Scotland, UK [38], and commissioned in 2020. The system is connected to the 275 kV transmission network with a rating of 140 MVA. It is characterized by a coordinated control of the two technologies by the master controller, which includes voltage control and reactive power sharing, improved fast transient response, power loss minimization, among others [39]. The frequency support is very limited as STATCOM cannot provide active power, so the systemâs active power contribution relies solely on the inertia of the synchronous condenser. In [40], a similar hybrid system from the Phoenix project is proposed consisting of a synchronous condenser and a battery energy storage system (BESS).

The converter is controlled in grid support mode to provide conventional droop control for the active and reactive power. The control consists of cascaded outer and inner loop, as well as a basic phase-locked loop (PLL) for grid synchronization. Multiple control loops and the PLL dynamics can possibly have a negative impact on the response and stability of the converter. A significant improvement on this type of control strategy is a power-synchronization based control where the need for PLL and additional control loops is avoided by implementing a simple control concept using the phase angle and voltage magnitude to directly control the active and reactive power [41]. Main disadvantage of this control strategy is that it requires an additional control at current limit in case of severe grid disturbances. Once the current limit of the converter is reached, the control must switch to current control mode and additionally, a PLL is required. Power-synchronization control can be categorized as virtual synchronous machine (VSM) type of control and converters equipped with this control strategy are known as grid-forming converters (GFC). In [42], the authors investigate the capability of the GFC connected at the onshore PCC of the offshore wind farm as opposed to synchronous condenser and STATCOM.

There has not been study in literature that provides detailed assessment of the characteristics of different hybrid solutions in terms of technologies and controls. Therefore, the focus of this paper is to investigate and compare the capabilities of the different technologies and control strategies and attempt to quantify the contribution in terms of voltage and frequency support. The criteria for comparison are based on the speed of the response, overloading capability, and performance in weak and strong grids. The idea is to test each technology and control strategy against voltage and frequency disturbance, voltage angle jump, and short circuit.

3.2 Model of a Hybrid Synchronous Condenser System

3.2.1 Component Modelling

The model of the battery cell is based on an equivalent electrical circuit shown in Fig. 3.1.

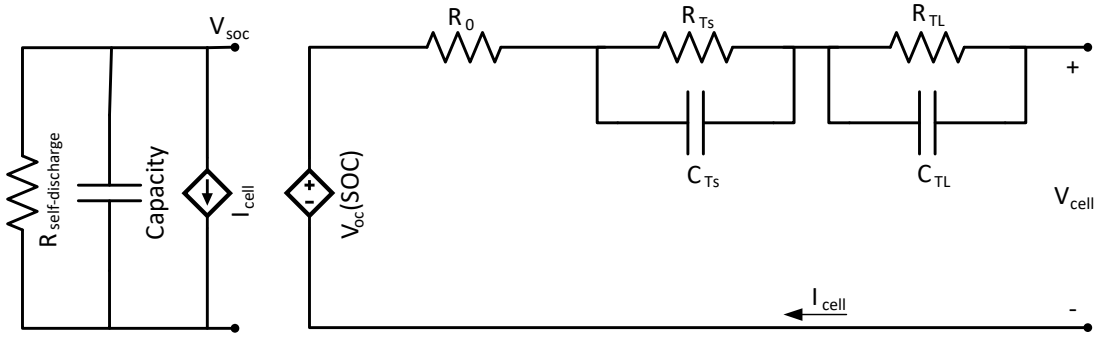

Figur 3.1: Equivalent Circuit of a Battery Cell

The given model is based on the standard representation of a battery as described in [23]. The elements of the model represent different chemical phenomena within the battery. R0 is the internal resistance of the battery, and it represents the immediate voltage drop at the battery terminal when the battery is loaded. The RC circuits simulate two distinct processes: R_{TS} and C_{TS} are the resistance due to the charge transfer and polarisation and double layer capacitance existing on the interface between an electrode and the surrounding electrolyte (in the literature, this process is referred to as the short-term dynamics); R_{TL} and C_{TL} are the concentration polarisation resistance

and capacitance (referred to as the long term dynamics). V_{OC} is the internal voltage of the battery, and it represents the open circuit voltage at the battery terminal. $R_{self-discharge}$ characterises the loss of charge over time. This parameter is not relevant for short-term studies, because the loss of charge is negligible (usually up to 5% per month [43, 44]).

All the parameters are dependant on the state of charge, temperature, and to some extent on the rate of charge/discharge of the battery. The model that we used considers only the dependence on state of charge, since the assumption is that the battery is enclosed in temperature-controlled environment, and because of the short time scale of the simulation. The state of charge of the battery can be estimated by the following equation (Coulomb counting method):

$$SOC = SOC_0 - \frac{1}{Cap} \int_0^t I_{cell}\, dt. \tag{3.1}$$

SOC_0 is the initial state of charge, Cap is the capacity of the cell, and I_{cell} is the cell current. As per Eq. 3.1, the state of charge is calculated based on the initial state of charge and the extracted/acquired charge with respect to the actual discharge/charge current. Once the state of charge is known, other parameters can be estimated from a lookup table by reading the value of the parameter for certain state of charge. The values of the parameters are given in [27]. The battery cells are stacked in series and in parallel in order to increase the voltage and power to a desired level.

Tabel 3.1: The ratings of the battery system

Parameter	Value
Single Cell Capacity	13 Ah
Nominal Cell Voltage (∼50% SOC)	2.228 V
Nominal Voltage of a Battery Pack (∼50% SOC)	24 kV
Maximum Charging and Discharging Current	3C
SOC Range	10 % - 90 %
Rated Power	70 MW
Stored Energy	23.34 MWh

The voltage, current, and power of the battery pack can be calculated as:

$$U_{batt} = n_s \cdot U_{cell};\ I_{batt} = n_p \cdot I_{cell};\ P_{batt} = U_{batt} \cdot I_{batt}. \tag{3.2}$$

The ratings of the battery pack used in this paper are given in Tab. 3.1.

The rated stored energy of the battery pack does not reflect an economically viable solution, as the power to energy ratio is relatively low, but that aspect is not significant for this study as it only addresses the short-term behaviour. The battery pack is modelled in PowerFactory simulation software, and the single line diagram is shown in Fig. 3.2. The battery is represented by the voltage-controlled voltage source. The charging and discharging currents are controlled by the power converter, which is an input to the battery model. Based on the charging/discharging current, the battery voltage and SOC are calculated and forwarded to the voltage source and the power converter, respectively.

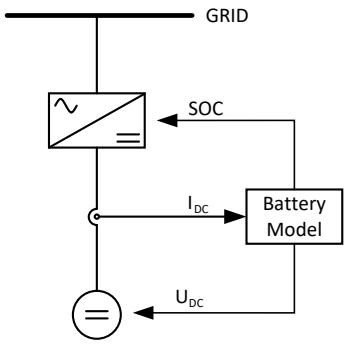

Figur 3.2: Battery System Equivalent

3.2.2 Synchronous Condenser Model

The synchronous condenser is modelled as a synchronous motor without the mechanical load. The voltage of the synchronous condenser is controlled by the AVR, which is based on the standard IEEE AC8B model given in [45]. The control also includes overexcitation limiter (OEL), based on an inverse time characteristic modelled with a leaky integrator, as presented in [46]. The underexcitation limiter (UEL) is not included in the model because there is no active load on the machine shaft, which means that the risk that the machine falls out of synchronism is low. Consequently, it is possible to reduce the excitation current to zero, so that the machine can consume as much reactive power as possible. The specification data of the synchronous condenser are given in Table II.

Tabel 3.2: The ratings of the synchronous condenser

Parameter	Value
Rated Voltage	13.8 kV
Rated Power	70 MVA
Inertia Constant (H)	1.34 s
Frequency	50 Hz
Rated Reactive Power Capability	-33 MVAr ÷ 70 MVAr
Overcurrent Capability (for 10 s)	180 %

3.2.3 Control System

The control diagram of the battery energy storage system is shown in Fig. 3.3. The control consists of two loops: frequency and voltage control loops (P- and Q-loop). The frequency control is based on the droop control described by the following equation (ΔP_{droop}):

$$K_{droop} = \frac{f_{ref} - f_{meas}}{P - P_{set}}. \tag{3.3}$$

The voltage control loop controls the voltage at the HV side of the transformer that connects the system to the grid, so in order to allow an error between the desired voltage reference and the measured voltage and to ensure equal reactive power sharing between the synchronous condenser and BESS, we must introduce the compensation block. The voltage error can be expressed as:

$$\Delta V = V_{ref} - V_{meas} - K_{slope} \cdot Q_{meas}. \tag{3.4}$$

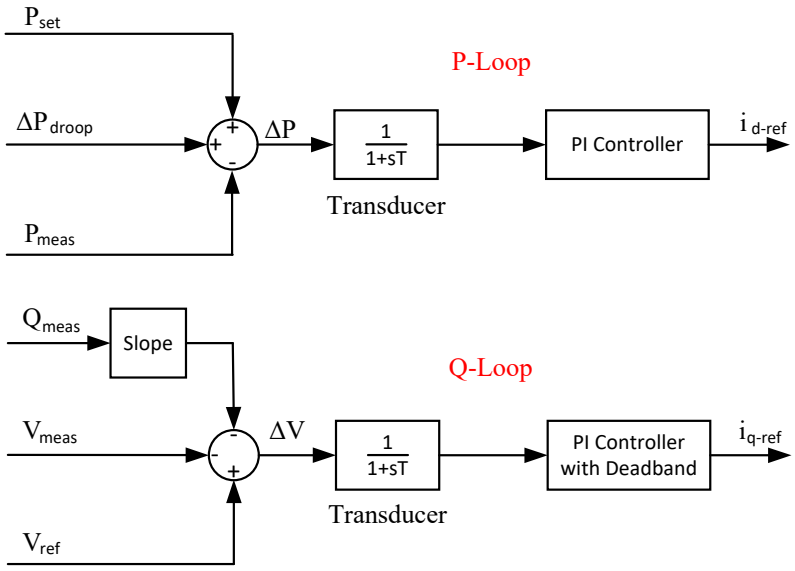

Figur 3.3: BESS Control Block Diagram

The charge control block controls the charging and discharging current of the battery pack (charging possible if $SOC < SOC_{max}$; discharging possible if $SOC > SOC_{min}$), as well as limiting the current output of the converter. The absolute maximum current output of the converter is specified by the ratings of the converter, and can be expressed as:

$$i_{max} = \sqrt{i_{d-ref}^2 + i_{q-ref}^2}. \tag{3.5}$$

Under normal operating conditions, the preference is usually given to the active power injection (i_d). When the voltage drops below the predefined limit, the control system will enter the fault-ride-through mode, and in that case the preference is given to the reactive power injection. The maximum i_d current can then be calculated from:

$$i_{d-max} = \sqrt{i_{max}^2 - i_{q-ref}^2}, \quad i_{q-ref}^2 \leq i_{max}^2. \tag{3.6}$$

3.2.4 Simulation Results

The grid used for testing the hybrid system response to different disturbances is represented by a large synchronous machine (rated at $24kV$ and 2.2 GVA) connected to the hybrid system through a transformer and a single transmission line. The single line diagram of the grid is shown in Fig. 3.4.

The frequency droop parameter K_{droop} is set to 0.03, which means that the battery system will inject full rated power for frequency drop of 1.5 hertz. The reactive power sharing parameter K_{slope} is set to 5%, which means that the allowed voltage error is 5%.

The first scenario includes a load event, or to be precise, the load of 200 megawatts will be switched on at 5 seconds mark in order to test the response of the system to frequency deviation.

Fig. 3.5 shows the system frequency response when a load of 200 MW is connected. We considered 3 separate cases: hybrid system (BESS and synchronous condenser), only synchronous condenser, and the case with only BESS connected. We can observe that the cases with the battery system

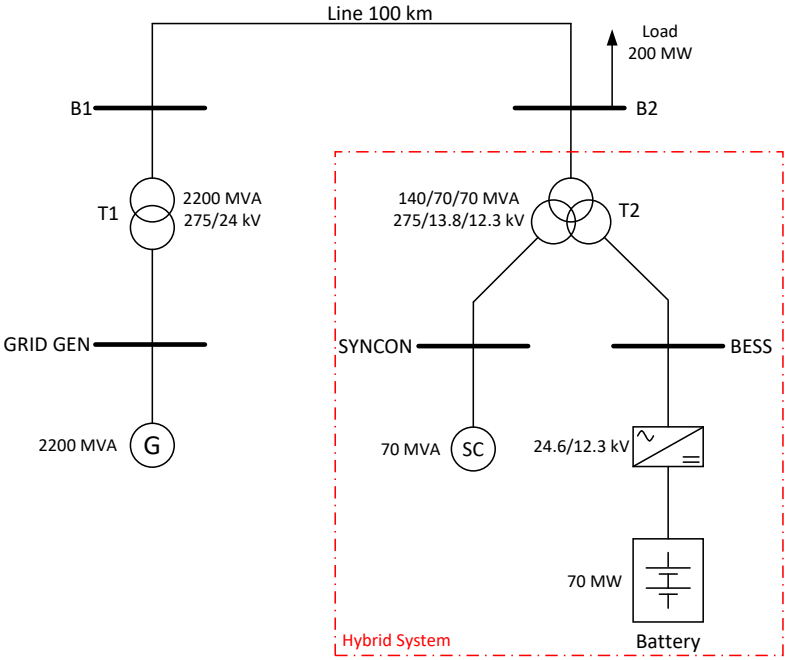

Figur 3.4: Simple Test Grid Used for the Simulation

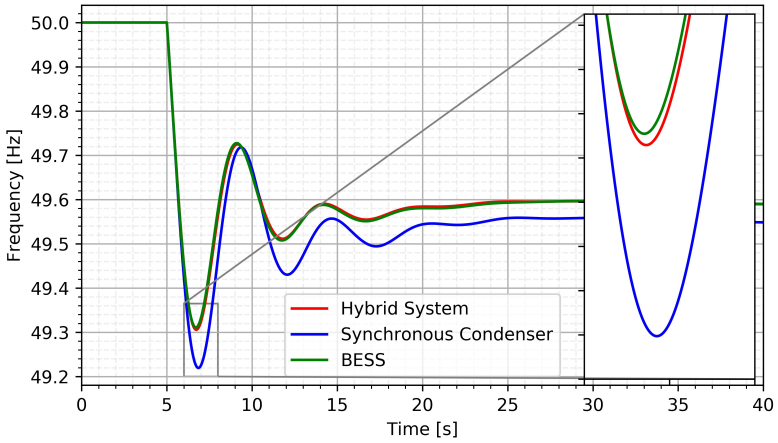

Figur 3.5: System Frequency Response Following a Disturbance

connected show significant improvements in comparison with the one with the synchronous condenser.

The fast response of the battery system ensures that the frequency nadir does not go below 49.3 hertz. In this case, the frequency settles at 49.58 hertz.The synchronous condenser does not influence the frequency response in a significant way, because the inertia constant of the condenser is relatively low (1.34 s). The main advantage of the synchronous condenser is that it provides almost instantaneous response to a disturbance, so it can contribute to frequency containment before the battery system reacts. Fig. 3.6 shows the frequency of the grid when we change the response delay of the battery system. It can be noticed that the fast response of BESS can improve the frequency support of the hybrid system.

Fig. 3.7 shows the DC voltage level at the battery terminal and state of charge. The frequency drop means that the active power has to be injected from the battery to the grid, so the battery starts to

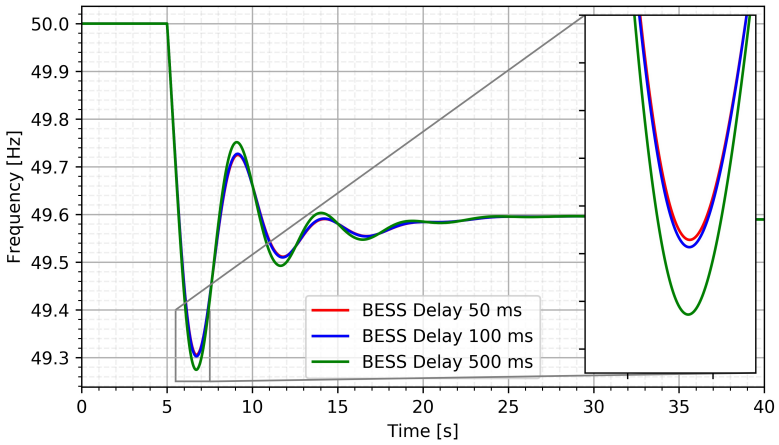

Figur 3.6: Influence of BESS Response Delay on Frequency

discharge following the load increase disturbance. The voltage at the terminal drops, as described by the Eq. 3.4. The rate of discharge of the battery is reflected in the decrease of the state of charge.

The second scenario represents the voltage regulation capability of the hybrid system and it demonstrates the equal reactive power sharing between the synchronous condenser and the BESS. There are two voltage reference setpoints for the hybrid system: 0.97 per unit, and 1.03 per unit. Fig. 3.8 shows the response of the hybrid system when the reference voltage is set to 0.97 per unit. We can see that BESS has significantly faster response in comparison to the synchronous condenser. Both components reach an equilibrium of approximately 29 megavars of reactive power injection. Fig. 3.9 shows the response of the system when the reference voltage is set to 1.03 pu. The total reactive power injected to the system is close to 30 megavars, which is eventually equally shared between the two components.

The main differences between the synchronous condenser and BESS is that the battery system has faster response, while the synchronous condenser has high overloading capability, which can go up to 2 per unit of reactive power, albeit for a limited amount of time. The limiting factor is the overheating of the excitation circuit. Fig. 3.10 shows the hybrid system response to a voltage drop of 0.1 per unit. The figure indicates that the synchronous condenser is providing $\sim$66% more reactive power ($\sim$50 megavars) than BESS.

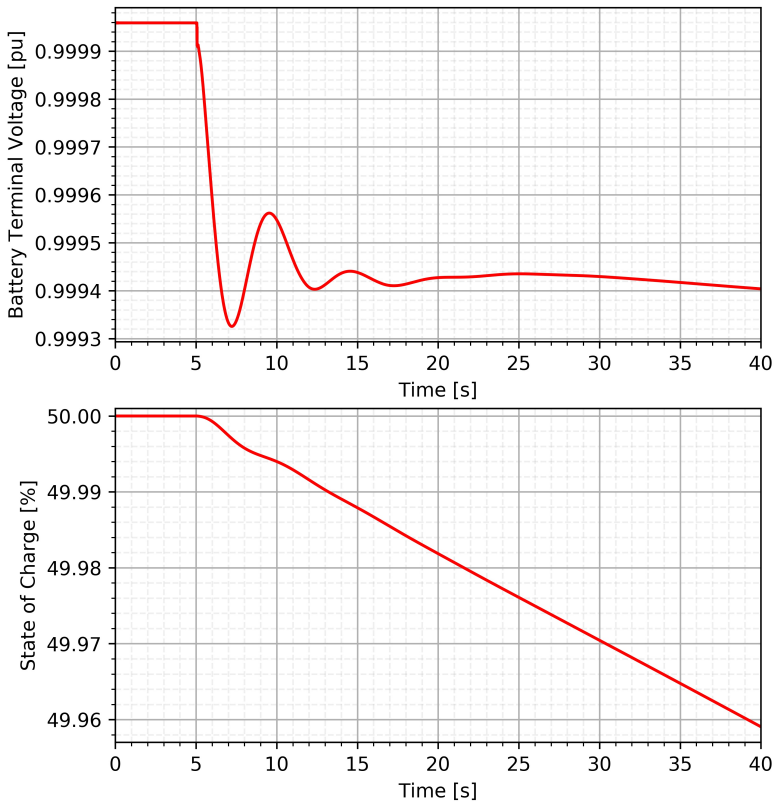

Figur 3.7: Battery Voltage and State of Charge

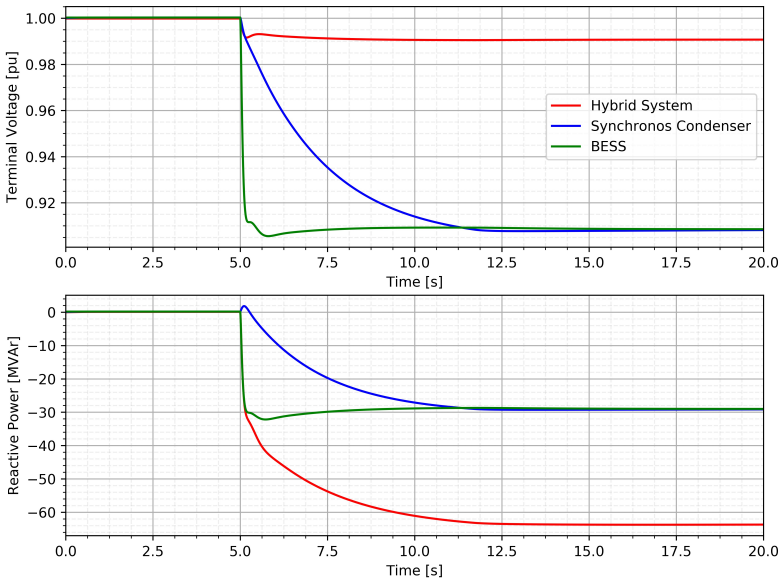

Figur 3.8: Reactive Power and Voltage Level of the Hybrid System: 0.97 pu Voltage Setpoint

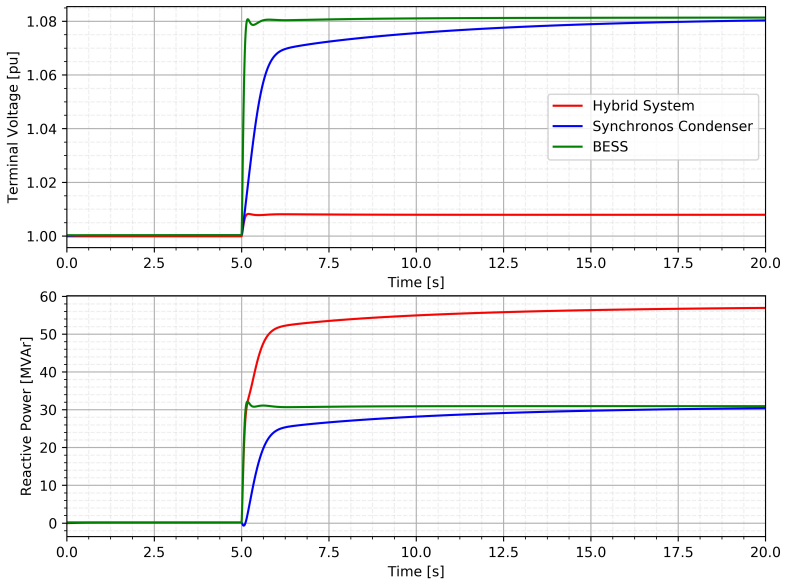

Figur 3.9: Reactive Power and Voltage Level of the Hybrid System: 1.03 pu Voltage Setpoint

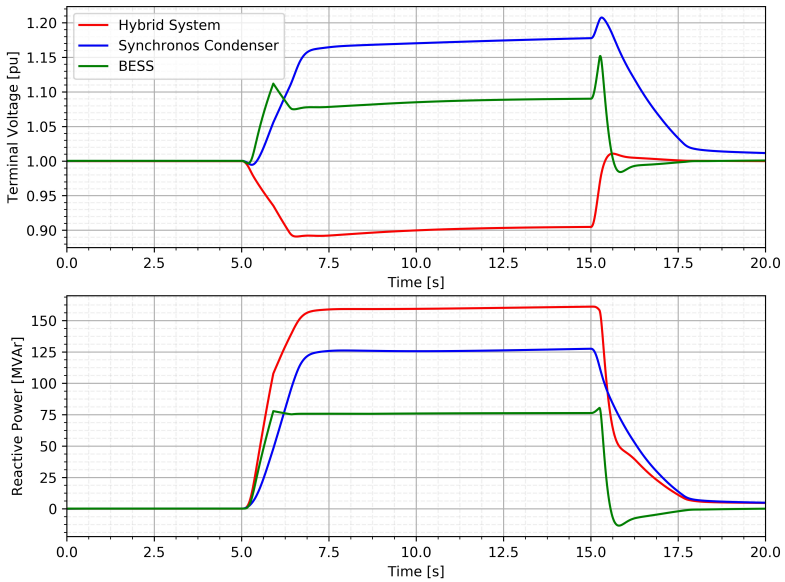

Figur 3.10: Overloading Capability of a Synchronous Condenser

TABLE I
TECHNOLOGY COMPARISON

Technology	Inertia/Fast Freq. Response	Volt./Curr. Characteristic	Short-Circuit Current	Response Time
SynCon	1.3 - 3.5 s typical values for the inertia constant* Instantaneous Response	High overloading capability Physical limitations for the inductive mode, close to 0.5 pu of rated current	3 - 3.5 pu of the rated current at subtransient time scale**	Seconds for post-fault settling time and reference voltage change
BESS Grid Following	No inertia Droop control Possibility of so-called synthetic inertia	Full rated reactive current for cap. and ind. mode Possible instability due to cascaded control loops and PLL	Constrained by the overcurrent limiter, typical values 1.1 - 1.3 pu	1 - 3 cycles
BESS Grid Forming	No inertia Fast freq. response, similar to SM Possibility of so-called synthetic inertia	Full rated reactive current for cap. and ind. mode	Constrained by the overcurrent limiter, typical values 1.1 - 1.3 pu Requires current control once the current exceeds max. value	0.5 - 2 cycles
SynCon + BESS Grid Following	1.3 - 3.5 s inertia constant* Instantaneous Response + droop control Possibility of so-called synthetic inertia	High overloading capability Less than 1 pu of inductive current due to the SynCon limitations (close to 0.75 pu) Possible instability due to cascaded control loops and PLL for BESS	2.05 - 2.4 pu of the rated current at subtransient time scale**	Improved response for post-fault settling time and reference voltage change due to the compensation of SynCon by BESS
SynCon + BESS Grid Forming	1.3 - 3.5 s inertia constant* Instantaneous Response + fast freq. response, similar to SM Possibility of so-called synthetic inertia	High overloading capability Less than 1 pu of inductive current due to the SynCon's limitations (close to 0.75 pu)	2.05 - 2.4 pu of the rated current at subtransient time scale** BESS requires current control once the current exceeds max. value	Improved response for post-fault settling time and reference voltage change due to the compensation of SynCon by BESS

*Depends on the design of the machine, can be higher, **Depends on the design of the machine, can be higher

Figur 3.11: Technology Comparison

3.3 Comparison of Hybrid System, Synchronous Condenser and Power Converter Based Technologies

3.3.1 Components and Control Models

There is a notable difference in how the synchronous machine and power converter operate, both in terms of control and in terms of their capabilities. One of the main advantages of synchronous condensers over power converters is the significant overloading capability and short-circuit contribution. Synchronous condenser can provide up to 3.5 pu of rated current during faults, while the power converters are limited by design for up to 1.3 pu of rated current. The short circuit level of the system has a significant influence on voltage levels and protection operation during faults. Furthermore, synchronous machine have rotating masses and this means that the inertia is an inherent feature of synchronous condenser, which is an especially important factor for future systems with high penetration of renewable energy. Power converters, on the other hand, provide fast frequency support (if coupled with active power source), fast voltage control, and the possibility of a number of different control strategy implementations. Synchronous condenser has much slower response to voltage reference change and voltage dips in comparison with power converters and since there is no prime mover the only contribution in terms of active power is inertia. Additional advantage for power converters is the capability to provide full rated current in inductive and capacitive mode. In terms of control strategies, power converters can be divided in grid-following and grid-forming converters. The two main advantages of grid-forming converters are the save of the otherwise used cascaded control loops and PLL and provides faster voltage and frequency support, while the main drawback is switching to current control in case of current exceeding the maximum limits.

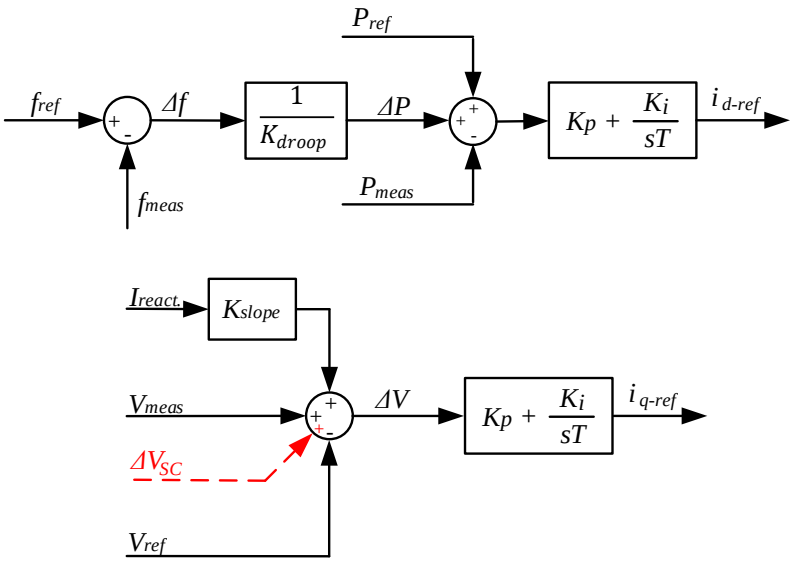

Figur 3.12: Grid-Following Control

Based on the characteristics of the individual technologies, some general assumptions on the performance of the combined effect of the individual technologies considered as a single hybrid system can be made as shown in Fig. 3.11. The hybrid system is assumed to be of the same total rating as the individual components. This will effect some of the characteristics of the SC and the power converter response. The main advantages of a hybrid system over a synchronous condenser are the extended range of frequency support, increased rating of reactive current, storing electric energy, compensating for slower voltage regulation of the SC, and maximization of the inertia support to the system by compensating for the SC oscillations. The advantages of the hybrid system over BESS are: inertia support, increased overloading capability, and increased short-circuit current contribution. The obvious drawback of the hybrid system is that we are effectively reducing the contribution from the SC as the rating of the machine is two times lower. The study in this paper compares the benefits and limitations between different technologies and try to draw conclusions on the design and application in different situations.

3.3.2 Control Modelling

BESS model is based on the work done in [40], where the battery is modelled as equivalent circuit of two RC networks and voltage controlled voltage source. Synchronous condenser is a standard synchronous machine operating without a prime mover. SC is controlled by the AVR model based on the standard IEEE AC8B AVR model. The grid-following converter control is based on the standard *dq* domain control with outer and inner control loops. The inner (current) control is a well known standard model with *dq* decoupling and feed-forward voltage. The reference currents are generated in the outer loop as shown in figure 3.12. The d axis current-control loop controls the active power and consequently provides frequency support in a form of droop control, while the q axis-control loop controls the reactive power and provides voltage support and ensures equal reactive power sharing between the SC and BESS (they have the same K_{slope} parameter). The grid-forming converter control is based on the power synchronization control as demonstrated in [41]. As can be seen in figure 3.13, the error between the measured and reference active power is transformed to a frequency deviation, By integrating the frequency, the voltage angle reference is

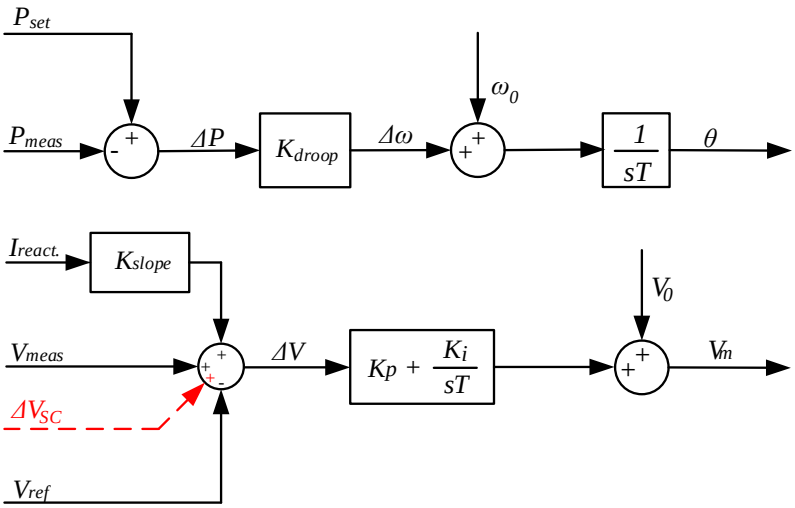

Figur 3.13: Grid-Forming Control

obtained and the use of PLL is unnecessary. The power synchronization control implemented here is equivalent in structure to the inertia less virtual synchronous machine control termed VSM0H [42]. The reactive power loop is very similar to the grid-following control and the difference is that the output of the loop is the voltage magnitude. The signal marked with red (ΔV_{SC}) is the voltage feedback signal from the SC. The response of the SC for sudden changes in the voltage, and post fault recovery is relatively slow, so by adding the SC voltage error (this is the same voltage delta ΔV as in the converter control) we can compensate that lag by providing more reactive power from the converter, as described in [39].

3.3.3 Analysis of the Hybrid system

Frequency response of the hybrid system

Hybrid system with grid following has the active power response to the change in frequency of the supply given by

$$\Delta P = \frac{2HS}{\omega_n} * \frac{d\omega_{sc}}{dt} + \frac{f_{ref} - f_{POC}}{f_n} * \frac{1}{K_{droop}} \tag{3.7}$$

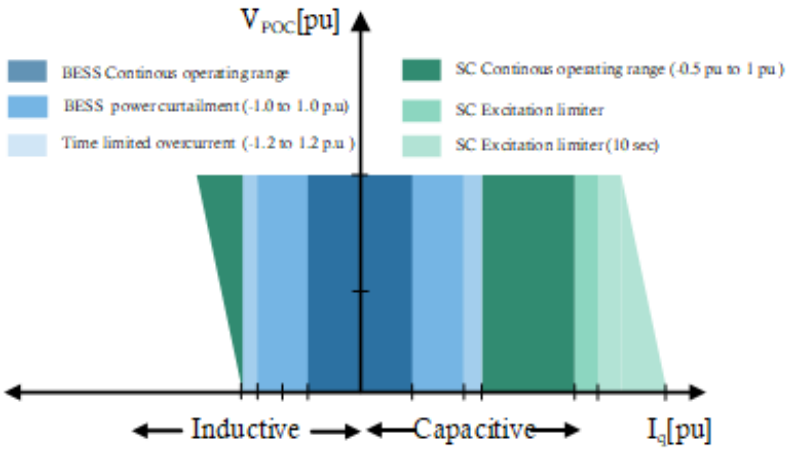

Figur 3.14: Reactive current injection capability of the hybrid system with respect to the POC voltage

Where H is the inertia constant of the SC in seconds, ω_n,f_n are the nominal frequency in radian/sec and in hertz, ω_{sc} is the rotor speed of the SC in rad/sec and f_{POC} is the measured frequency of the POC. The inertial response consists of two terms, the first term is the inertial power exchanged by the SC and the grid while the second one is the fast frequency response from the grid following converter. The fast frequency response speed is slower than the inertial response but is faster than a primary frequency controller. Where as for Hybrid system with grid forming, the response is given as

$$\Delta P = \frac{2HS_n}{\omega_n} * \frac{d\omega_{sc}}{dt} + \frac{f_{ref} - f_{GFC}}{f_n} * \frac{1}{K_{droop}} \tag{3.8}$$

Where f_{GFC} is the frequency of the GFC set by the active power loop as shown in Fig. 3.13. The frequency response of the hybrid system with grid forming converter has both inertial response from the SC and a fast frequency response from GFC. Having a voltage source characteristics enables the grid forming frequency response to be instantaneous and faster compared to the fast frequency response of grid following converter.

Steady State Voltage Support Characteristics

The steady-state reactive droop voltage control ensures the steady-state reactive power-sharing between the BESS and SC. In this study, the behaviour of BESS control for both grid forming and following in steady-state operation is configured to be the same. Further, all the three components in steady state have characteristics of a voltage source of magnitude V_{ref} behind a per-unit reactance corresponding to K_{slope} connected at the POC bus provided the limits are not triggered. As a for the active power case, the SC provides no support during the steady-state after the grid phase or frequency is settled. Both the Grid following and grid forming converter injects active power as shown in eqn (3.9)

$$P = \frac{f_{ref} - f_{POC}}{f_{nom}} * \frac{1}{K_{droop}} \tag{3.9}$$

Where the f_{POC} and f_n are the steady state frequency of the POC and the nominal frequency respectively.

Transient operation

A sub-transient time scale is used to explain the behaviour of the components considered in this paper. It is assumed that no control or excitation system is fast enough to respond in this time frame, for the sake of understanding, it is also assumed that the converter does not enter current limit. It is well known that the SC can be approximated by sub transient internal voltage ($E_g^{''}$) and connected behind a sub transient internal impedance ($X_d^{''}$). The grid following converter has a voltage source characteristics. Therefore, the grid following converter can be assumed to be a constant voltage source with voltage equal to pre-transient level ($V_m^{''}$) behind the filter impedance. The transient equivalent circuit of the hybrid system with grid following converter is shown in Fig. 3.15.

Where $X_p^{tf}, X_s^{tf}, X_t^{tf}$ are the reluctance's of primary secondary and tertiary winding respectively.

Assuming that both the converter and SC are unloaded before the transient event, the sub-transient SC voltage and converter voltages are equal. Therefore, the thevenin circuit of Fig. 3.15 can be represented as in Fig. 3.16

Where, the thevenin impedance can be written as

$$X_{th}^{GFC-SC} = \frac{(jX_d^{''} + jX_s^{tf})(jx_{vsc} + jX_t^{tf})}{jx_{vsc} + jX_t^{tf} + jX_d^{''} + jX_s^{tf}} + jX_p^{tf} \tag{3.10}$$

Thus, the transient active power (P_{tr}^{GFC-SC}) and reactive current(Iq_{tr}^{GFC-SC}) provided by the the Hybrid combination of SC and grid forming converter for interfacing BESS can be derived as

$$P_{tr}^{GFC-SC} = \frac{E_g^{''}.V_{poc}.\sin(\theta_{poc})}{X_{th}^{GFC-SC}} \tag{3.11}$$

$$Iq_{tr}^{GFC-SC} = \frac{E_g^{''} - V_{poc}}{X_{th}^{GFC-SC}} \tag{3.12}$$

The grid following converter, which has a measurement based response, acts approximately as open circuit in the sub transient time period, therefore a hybrid system composed of grid following will only have response from the SC during sub-transient time period.

$$Iq_{tr}^{GFol-SC} = \frac{E_g^{''} - V_{poc}}{jXd'' + jX_s^{tf} + jX_p^{tf}} \tag{3.13}$$

Since X_{th}^{GFC-sc} is smaller than the denominator of eqn (3.13), the fault current from hybrid system in subtransient time period is higher for grid following control. Even if the converters enters current limit mode in grid forming control during large disturbance, this would happen at a very fast rate when compared to grid following solution.

3.3.4 Simulation and Results

The test system used for simulating the different technologies is a simple system where the grid is represented by an equivalent generator for frequency response scenario (as shown in Fig. 3.17),

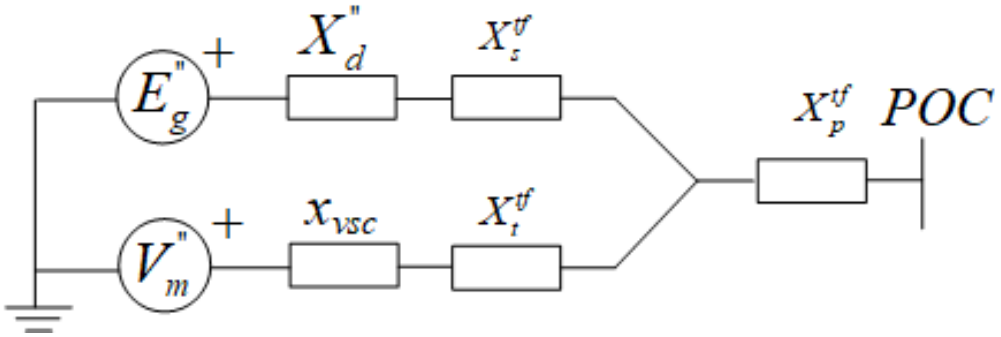

Figur 3.15: Equivalent circuit of hybrid system with grid forming converter during transient operation

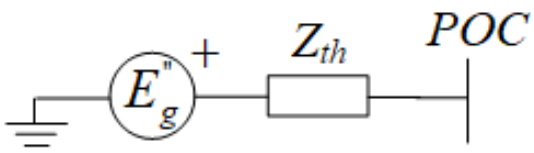

Figur 3.16: Thevenin equivalent circuit of hybrid system with grid forming converter during transient operation

while for the other scenarios, we used a Thevenin equivalent. The generator is rated at 24 kV / 2.2 GVA connected to the grid through a transformer, while the Thevenin voltage source is connected directly to the 275 kV rated grid. The hybrid system is connected to the grid through a three-winding transformer. The rating of the synchronous condenser and the power converer is the same at 70 MVA in the case of the hybrid system, while the individual technologies are rated at 140 MVA in order to ensure consistent capacity and comparable results. The droop settings for both the voltage and the frequency control are set to 5%. The inertia constant of the synchronous condenser is 1.35 seconds.

3.3.5 Frequency Event Scenario

The performance level in terms of frequency support is evaluated in a system as shown in Fig. 3.17 where a load of 330MW is switched on at 1 second. Two scenarios have been evaluated where the inertia constant of the grid equivalent generator was 3 seconds for the first test, and 4 seconds for the second test. The frequency of the system for the two scenarios is shown in Fig. 3.18 and Fig. 3.19. As expected, the response of BESS operating as grid-following and grid-forming is very similar after the first 200-300 milliseconds. The grid-following converter is slower to respond to the frequency change because of the additional control loops and mainly because of the PLL. The contribution of SC is limited to inertial support, so the only differentiating factor between the hybrid system and the individual BESS technology in terms of frequency nadir and steady-state frequency is the rating of the component. A notable difference in the response of each technology is within the first 200-300 milliseconds as can be seen in Fig. 3.20 and Fig. 3.21. The peak active power injection instantly following the load step from the grid-forming BESS is 85MW, while for the grid-forming hybrid system the peak power is 75MW. The synchronous condenser peak contribution is 50MW. The grid-following hybrid system peak active power injection is 30MW, which is a contribution from the synchronous condenser, while grid-following BESS does not provide a notable contribution initially as the controller is based on the droop control.

3.3.6 Voltage Phase Jump Scenario

For this scenario, we have a grid represented by a Thevenin equivalent with two levels of short circuit power representing the weak and strong grid at 500 MVA and 2800 MVA, respectively. The voltage phase change of +30 degrees is applied at 1 second. The voltage phase tracking by each of the technology is shown in Fig. 3.22. The grid-following BESS provides no significant active power contribution for weak and strong grid scenario as seen in Fig. 3.23. The grid-following hybrid system contribution is mostly from the synchronous condenser. The grid-forming BESS provides

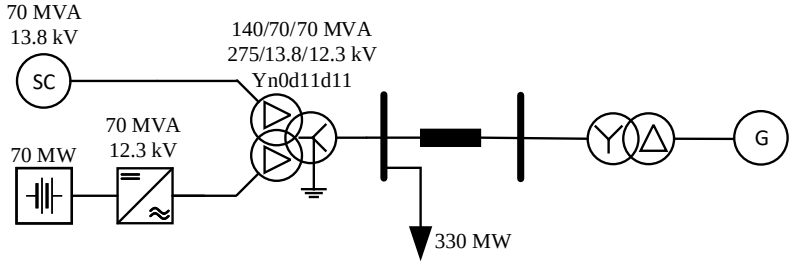

Figur 3.17: Test System Including the Grid Equivalent

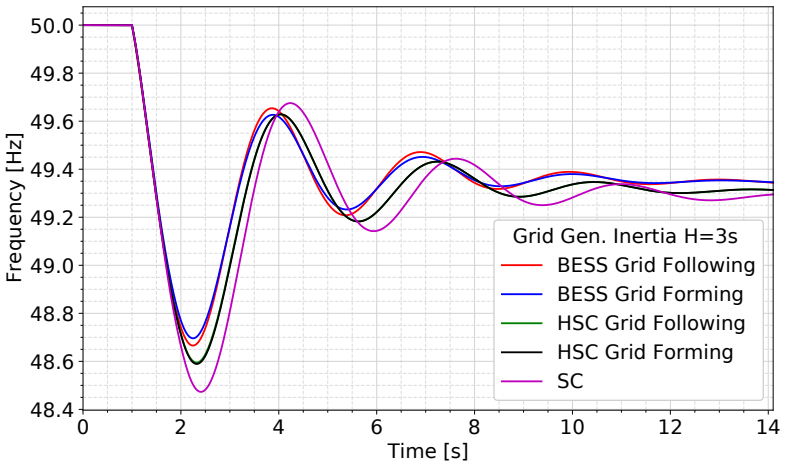

Figur 3.18: Frequency Response - 3s inertia constant

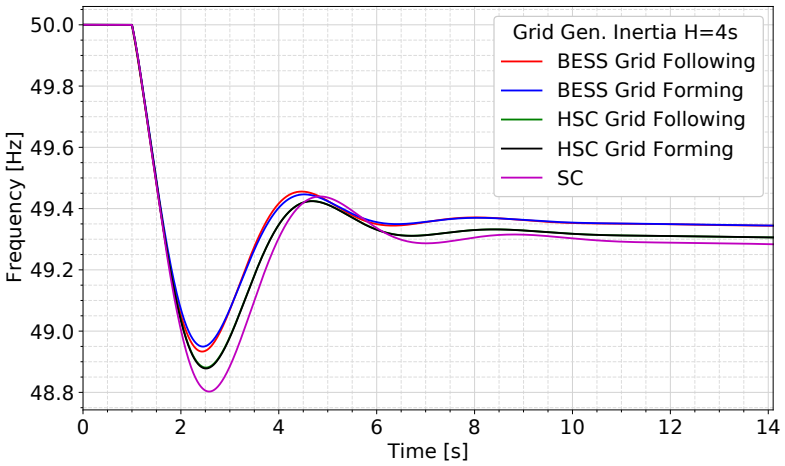

Figur 3.19: Frequency Response - 4s inertia constant

the response superior to other systems as it provides the highest level of response to the voltage phase disturbance. In the case of a strong grid, the grid-forming BESS and hybrid system hit the current limitation and switch to current control mode for a short period, resulting in a prolonged settling time. This efect is due to the reduced impedance between the Thevenin source and the system under investigation.

3.3.7 System Voltage Drop

As in the previous scenario, the grid is represented by a Thevenin equivalent. At 1 second, the system voltage instantaneously changes to 0.5 pu. For a weak system (SCL = 500 MVA), the reactive current injection from the converter and the synchronous condenser results in a significant voltage retention as the Thevenin impedance is relatively high, as shown in Fig. 3.24, left. The grid-following and grid-forming BESS are current limited to 1.2 pu, so the contribution from the converter is the same pu value in all cases (Fig. 3.25). For the weak grid case, the voltage settles at 0.84 pu with the converter solution, while for the hybrid system and synchonous condenser solution the voltage is approximately 0.9 pu following the disturbance. The retained voltage is

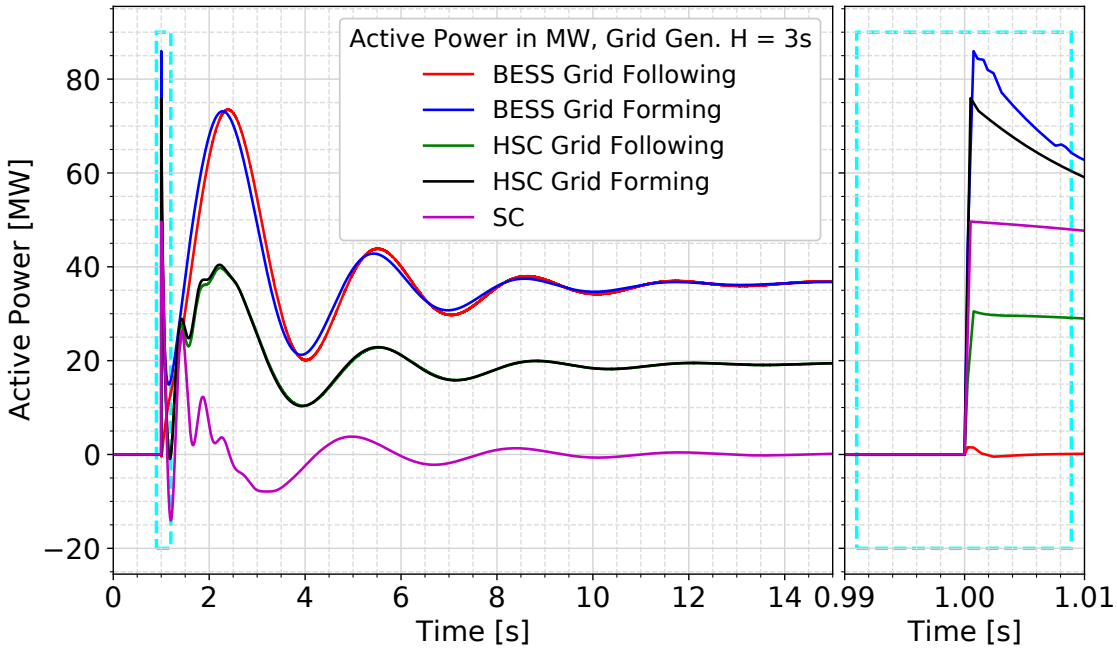

Figur 3.20: Active Power Contribution - 3s inertia constant

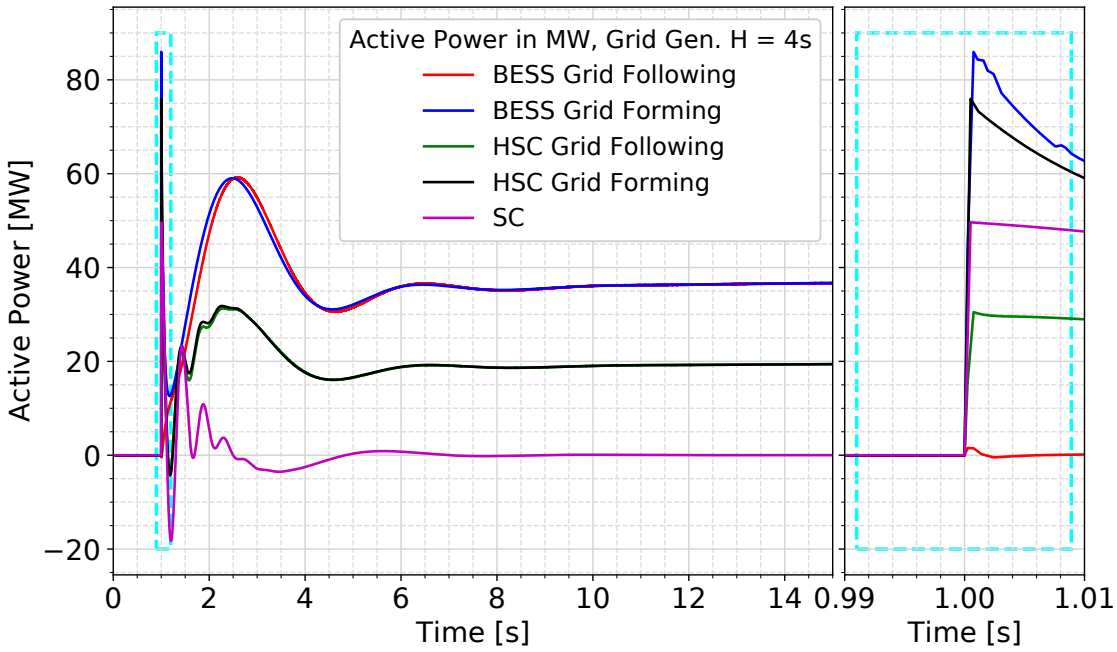

Figur 3.21: Active Power Contribution - 4s inertia constant

higher in the latter case due to the overloading capability of the synchronous condenser. The same disturbance in a strong grid (Fig. 3.24, right) results in a lower voltage as the Thevenin impedance is significantly lower than in the previous case. The voltage is at approximately 0.56 pu for grid-forming and grid-following BESS, 0.59 pu for the HSC solutions, and 0.61 pu for the synchronous condenser system. The difference between the HSC and SC solutions is due to the fact that the SC has a rating of 140 MVA, while the SC in the hybrid system is rated at 70 MVA and

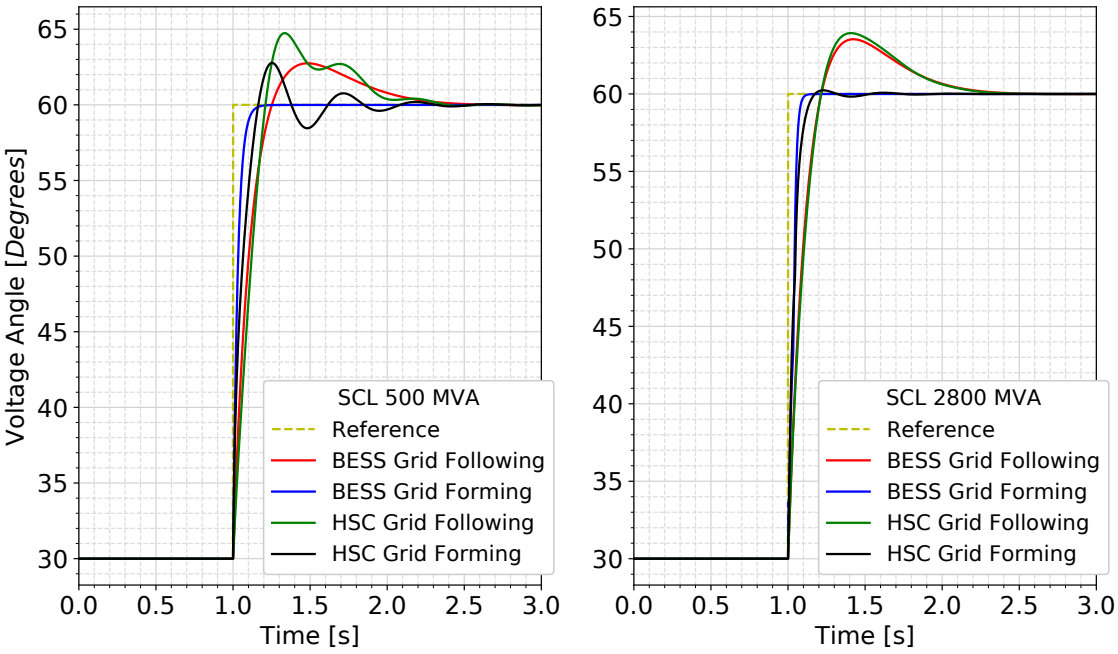

Figur 3.22: Grid Voltage Phase Jump by 30 Degrees: Left - 500MVA SCL, Right - 2800MVA SCL

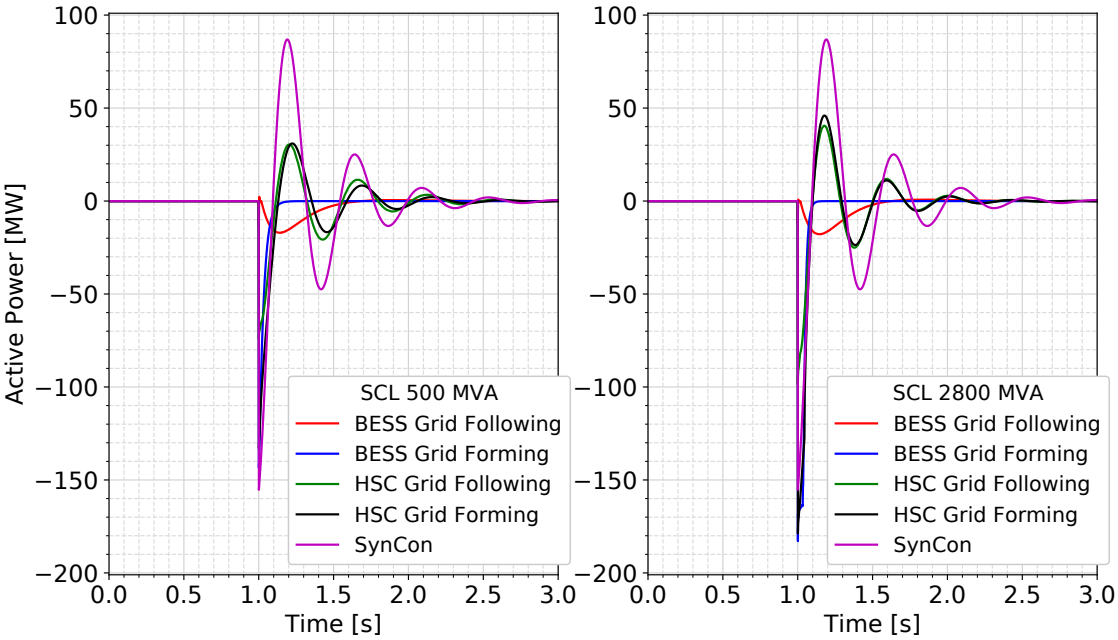

Figur 3.23: Active Power During Voltage Phase Jump: Left - 500MVA SCL, Right - 2800MVA SCL

consequently the hybrid system provides less reactive current as the converter is current limited to 1.2 pu, as shown in Fig. 3.25. The grid-forming based solution provides the faster response in comparison to the grid-following solution as the grid-forming converter control does not contain the current control loop and the PLL.

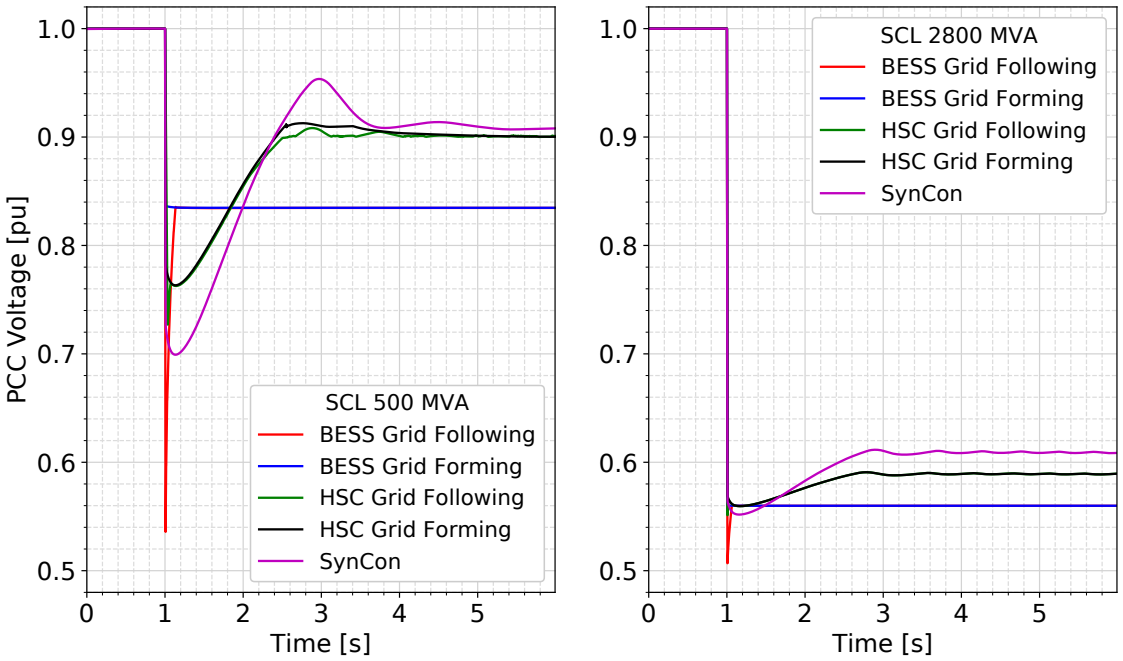

Figur 3.24: Voltage at PCC for 0.5pu System Voltage Drop: Left - 500MVA SCL, Right - 2800MVA

3.3.8 Short-Circuit Scenario

The three-phase short circuit is applied at 1 seconds at the PCC bus of the system. The short-circuit is a three-phase to ground fault with a fault resistance of 5Ω and a duration of 200 milliseconds. The voltage at the PCC for the weak grid is close to 0.045pu as the contribution from the grid is limited due to high impedance (500MVA SCL), and 0.18pu for the stronger grid, as shown in Fig. 3.26. SC shows the typical synchronous machine response during short circuits with current peak being at the initialisation stage of the fault when the subtransient reactance is dominant. The SC contributes with a current of 3 pu for the weak grid scenario (Fig. 3.27, left), and 2.9 pu for the stronger grid (Fig. 3.27, right). The difference in current contribution is due to the voltage at PCC being lower for the weak grid scenario. Contribution from the converter is predictably flat, reaching the current limit of 1.2pu and staying constant. The total contribution from the HSC solution is 2.41 pu for the weak grid, and 2.36 pu for the strong grid. The difference between the grid-forming and the grid-following solution is not significant during the fault, the grid-forming converter being slightly faster to reach the peak value. Post-fault, the synchronous condenser introduces active power oscillations and significant reactive power swing. By using the voltage compensation technique described previously, this reactive power injection from the SC can be significantly reduced in the case of the hybrid system, where most of the power can be absorbed by the converter, and thus reduce reactive power exchange with the grid.

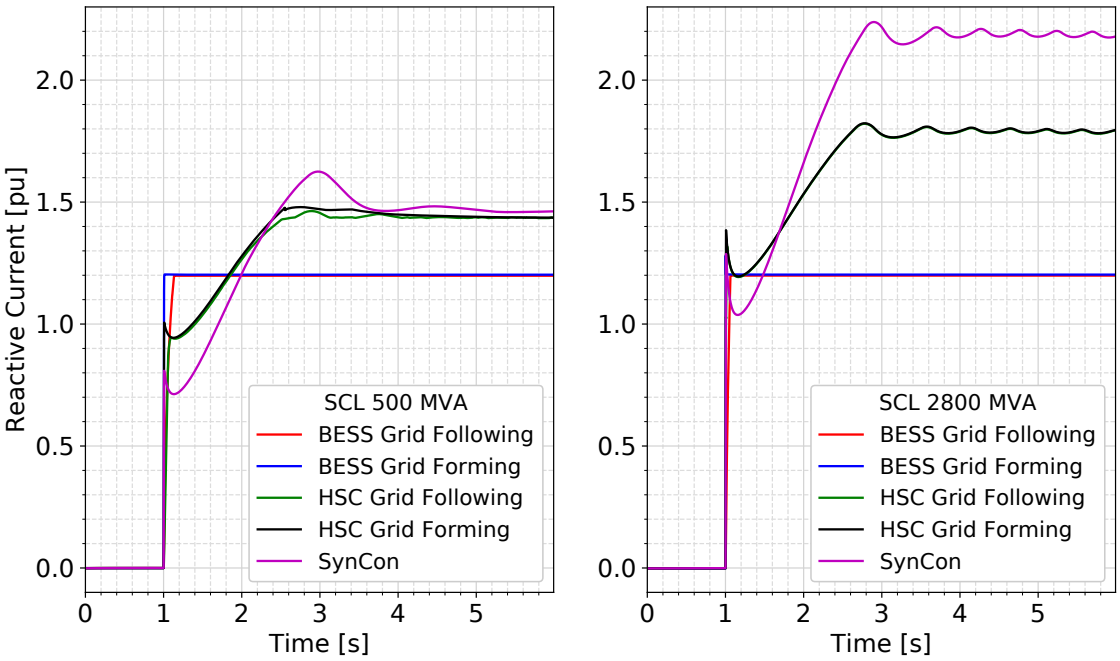

Figur 3.25: Reactive Current Injected at PCC for 0.5pu System Voltage Drop: Left - 500MVA SCL, Right - 2800MVA

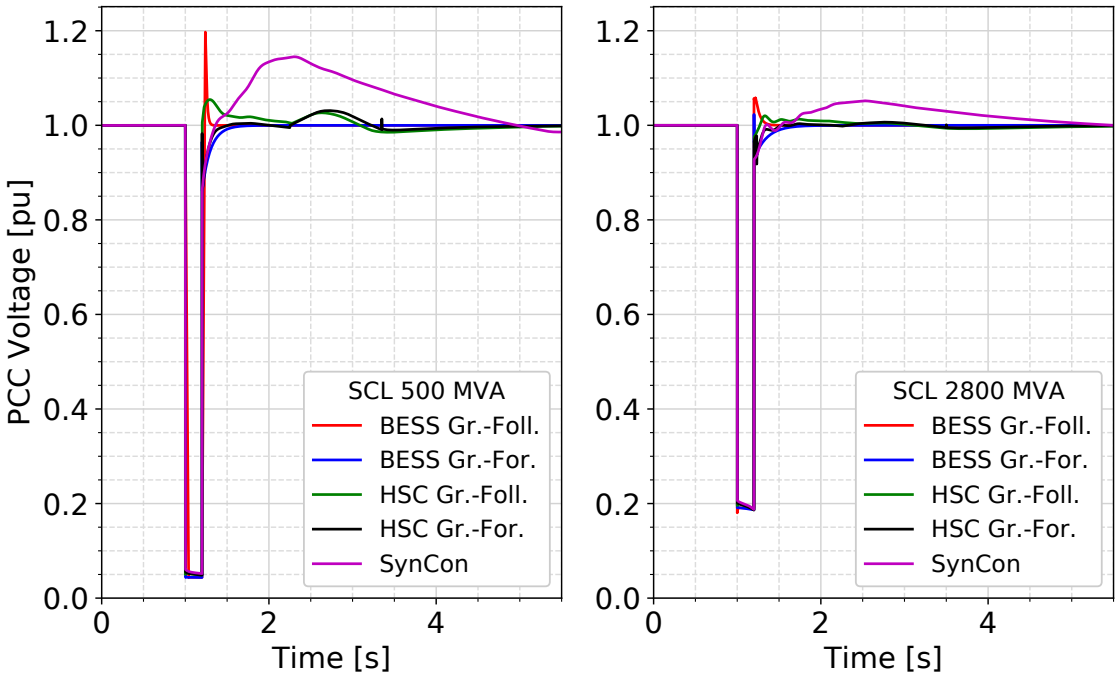

Figur 3.26: Voltage at PCC During Short-Circuit: Left - 500MVA SCL, Right - 2800MVA SCL

3.4 Conclusion

This paper proposes a hybrid system design consisting of a synchronous condenser and BESS as a way to address some of the issues that the future power systems face. The inertial response of the synchronous machine coupled with the fast frequency response of the battery system make

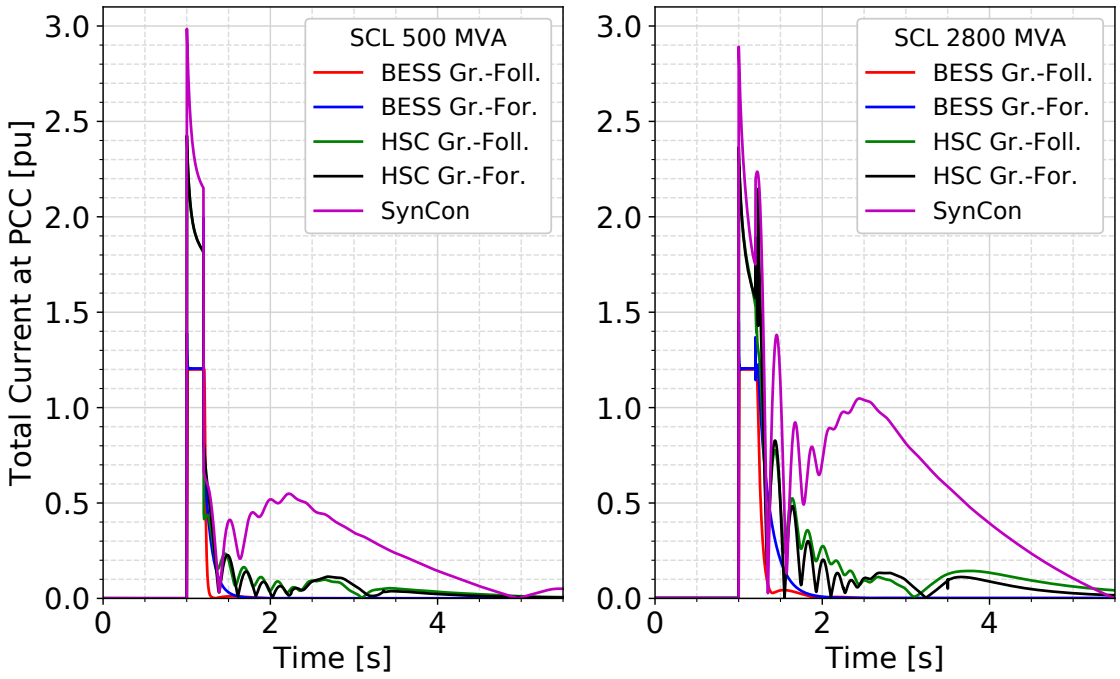

Figur 3.27: Current Magnitude Injected at PCC During Short-Circuit: Left - 500MVA SCL, Right - 2800MVA SCL

TABLE II
SUMMARY OF THE TEST CASE WITH PERFORMANCE OF EACH TECHNOLOGY RANKED FROM BEST TO WORST (1-5)

Technology	Frequency Event		Voltage Phase Jump		System Voltage Drop		Short-Circuit Event	
	Instantaneous	Dynamic	Instantaneous	Dynamic	Instantaneous	Dynamic	Instantaneous	Dynamic
SynCon	3	5	1	3	4	1	1	2
BESS Grid Following	5	4	5	5	5	5	5	5
BESS Grid Forming	1	1	3	1	1	4	4	4
SynCon + BESS Grid Following	4	3	4	4	3	3	3	3
SynCon + BESS Grid Forming	2	2	2	2	2	2	2	1

Figur 3.28: Summary of the Test Cases

it possible to emulate the response of synchronous generator to a frequency event. Additionally, the overloading capability of the synchronous condenser and the fast response of BESS in terms of reactive power, can provide a significant improvement for voltage control in weak systems. It is also possible to implement various other functions into the hybrid system, such as harmonic damping, low frequency power oscillation damping, wind power forecast accuracy improvement, and others, which were not considered for this paper, but can be implemented as a part of a more complex control system.

A summary of the performance of the technologies considered in the paper against the test cases is shown in 3.28. The instantaneous response measured at the half-cycle period, and the dynamic response, which is assessed based on the technology's response quality, are ranked from best to worst. The Syncon adds more robustness due to its notable overload capability, whereas the converter's current limiters can introduce a discrete response to large transients. The grid-forming converter based solutions provide the most balanced response in terms of frequency support as

they provide very fast response and in many ways are similar to the synchronous machine. In terms of voltage support, the solutions with synchronous condenser are dominant due to the significant overloading capability of the SC. The slower SC response can be compensated by faster converter control, which gives an advantage to the hybrid solution. Similarly, for short-circuit events, the solutions with synchronous condenser provide the best solution in terms of short-circuit current contribution, while the converter based solutions provide balanced post-fault response. Based on the findings in this work, we can conclude that the hybrid concept with grid-forming control brings the most balanced performance overall for grid support.

KAPITEL 4

SSR Damping Controller Integrated within a Hybrid Synchronous Condenser System

The chapter is based on **[Pub. A]**.

4.1 Introduction

One of the major challenges for current power systems to accommodate more renewable energy is due to the decommissioning of synchronous machine-based generation which results in reduced system inertia as well as the short circuit power levels [47], making the system prone to frequency and voltage collapse. To ensure the operational security, other technologies have to provide and replicate the characteristics and capabilities of synchronous machines in terms of voltage and frequency control, short-circuit power, inertia, oscillation damping etc. In this regard, power converter interfaced generation and transmission assets are required to provide the services needed by the system [48–50].

Flexibility of power converter control is one of the major advantages of this technology in bringing the necessary functions to the system and provide similar characteristics as a conventional generation. However, there are some obstacles that cannot be overcome by only power converters due to the physical and economical aspects of the technology [47]. Namely, power converters have a very limited overloading capability , which limits their ability during transients. This can of course be addressed by over-sizing the equipment however induces increased cost for normal operation, but economically is prohibitive.

Synchronous condensers have been identified as a technology that can contribute with high levels of short-circuit power and provide intrinsic inertia to the power system [13, 51]. However, SC has limited energy storaged in its shaft therefore its inertial contribution is less pronounced after the first couple of cycles. One of the more innovative solutions that has been proposed in recent years is a Hybrid Synchronous Condenser (HSC) that consists of a synchronous condenser and STATCOM [3], with possible integration of Battery Energy Storage System (BESS) replacing STATCOM to achieve higher energy storage [20]. Since 2016, Scottish Power and Energy Network started project called Phoenix, partnered with ABB, National Grid, University of Strathclyde and Technical University of Denmark, where two HSC concepts are investigated, SC+STATCOM and SC+BESS respectively, with the first concept being demonstrated at the substation Neilston in Scotland, UK [52]. The system was designed by ABB and commissioned in 2020. The system is rated at 140 MVA, with equal MVA of SC and STATCOM, and connected with the 275 kV transmission network through a three winding transformer.

The TSO is planning to start another project which will result in a larger HSC system at a location where two large synchronous generators are connected nearby. The transmission lines that link the generators to the local grid of are series compensated, which creates a problem of sub-synchronous resonance relating to the torsional modes of the generators [53]. Torsional oscillations can cause increased shaft fatigue and decreased lifetime of generators, and they appear due to the resonance in the system impedance in the sub-synchronous range, where most critically damped torsional modes can be found.

A grid side oscillation damping controllers can be dedicated to that specific function, such as passive filters. The solutions proposed in [54–56] provide a simple solution to the SSR problem, where a passive filter is connected in parallel to the capacitor used for series compensation. The filter is tuned to rectify the resonance created by the capacitor in sub-synchronous range by increasing the impedance and thus limiting the oscillating power between the grid and the generators. One of the disadvantages of such solutions is that they provide a very limited increase in damping ratio, so the oscillations will take a relatively long period of time to decrease. They also drive up costs and introduce losses. For example, in Scotland the TSO installed shunt reactors as damping device to suppress the resonance, however, the shunt reactors are the only device that can provide the damping in the system, where the generators need to be offline when it is under maintenance.

Another grid side torsional oscillation damping technology is thyristor-controlled series capacitor (TCSC), which is connected in parallel to the series capacitor and acts as a variable impedance to specifically affect the impedance in the sub-synchronous range. In [57], the authors propose a controller for TCSC with speed deviation as feedback to identify the torsional oscillations, and adjust the series compensation in sub-synchronous range. The proposed solution in [58] introduce multimodal oscillation damping, where several oscillating modes are considered.

On the other category, Static VAR Compensator (SVC) based solutions, and power converter based solutions (STATCOM, HVDC, renewable generation, etc.) can be equipped with supplementary control loop to provide passive (to known oscillations) or active (to unknown oscillations) damping to SSR issue. For example, generator can include a supplementary excitation damping controller [59] with an additional loop added to the AVR controller to damp all torsional modes. The effectiveness of the controller is largely limited by the rating of the excitation system and the bandwidth of the AVR controller. Additionally, if there is a group of generators affected by SSR, we would need to equip each of them with an additional controller targeting the specific torsional modes, and that would raise the costs. A dedicated equipment for damping of SSR oscillations connected at the generator terminal (low voltage side) is possible and has been implemented in practice **[24]**, but is also inefficient and costly as each generator would require a component, which would serve only one purpose.

In [30], the authors propose a active wide band SSR damping controller implemented on an HVDC link. The controller acts on a wider range of sub-synchronous frequencies without tuning for a specific mode. The controller is a simple band-pass filter with a centre frequency in between the modes of interest. However, the bandwidth of the controller is very wide, which could possible result in interacting with different components in the grid at frequencies sub-synchronous frequencies and other torsional modes. Additionally, the HVDC link needs to be in close proximity to the generators of interest. Another example of SSR oscillation damping controller is proposed in [31], where the authors use the current as a feedback for the oscillation controller loop. The authors assume that the HVDC link is in close proximity to the generator, and the damping torque within

the low frequency range (0-15 Hz) is negative, which can result in interaction with other torsional modes and low-frequency inter-area oscillations. In [32], an adaptive sub-synchronous frequency damping controller is proposed, which identifies the oscillation frequency in the measured current and injects 180° shifted suppressing current. However, the controller can respond only to one oscillating mode at a time.

STATCOM based solutions for torsional oscillation damping are quite common in the literature [33-34], with most of them using generator speed deviation as a feedback for the damping loop, while others use either local current or voltage measurement [35]. The authors in [33] propose a simple controller as is employed in traditional PSS control, with a wide range of frequencies. The controller is not tuned for specific frequencies, so it can interact with other components at wide range of frequencies and possibly result in unstable oscillations. Additionally, the paper does not include a scenario with multimodal oscillations and the authors assume availability of rotor speed measurement. In [34], it is proposed to use a multimodal SSR damping controller, where the authors isolate each individual torsional modes by using "mode filters". The gain and phase margin of the damping controller is not provided, so the stability margins are not known, which is significant for this number of cascaded filters. Moreover, the authors propose that the sole purpose of the component is to provide torsional oscillation damping, which is costly. Furthermore, it is assumed that the generator's rotor speed is available as a feedback for the controller, which is also challenging in reality, since speed measurement has high time constant therefore cannot be used as control input for this frequency range. A Kalman filter based detection and mitigation of SSR is proposed in [35]. The authors use local current measurement as a feedback for the controller loop. The damping torque at low frequency (0-15 Hz) is negative, and can interact with the system in presence of low frequency oscillations.

In this paper, we propose a VSC based damping controller for SSR torsional oscillations with support for multiple generator and multiple mode oscillation damping. The solution is integrated within an HSC system combining SC and BESS. The proposed controller acts as a supplement to the HSC control system, which means that the HSC can provide all other functions defined previously with only a small capacity margin reserved for the SSR oscillation damping. The controller uses local voltage measurement as a feedback for torsional oscillation identification and suppression. It is also capable to distinguish between oscillating modes with less then 2 Hz frequency difference. The tuning method for the controller is based on the exponential curve fitting of peaks of decaying oscillation signal. Finally, an experimental demonstration of controller operation is performed in RTDS (hardware-in-the-loop test), where we used a converter stack and a designated controller, while the rest of the system is modelled in RTDS. By this design, significant cost reduction and reliability enhancement can be achieved from the industrial point of view.

The rest of the paper is organised as follows. In section II we analyse and identify the oscillating modes of two generators and provide a damping and impedance profile of the system without HSC. In section III we describe the proposed solution and provide damping and impedance analysis of the system with included controller. The implementation and case studies are presented in section IV, and finally, conclusions about the work are summarised in section V.

4.2 System Configuration and Identification of Natural Frequencies

4.2.1 System Topology

The system chosen for the demonstration of effectiveness of the proposed oscillation damping control is a system consisting of two generators and two series compensated transmission lines

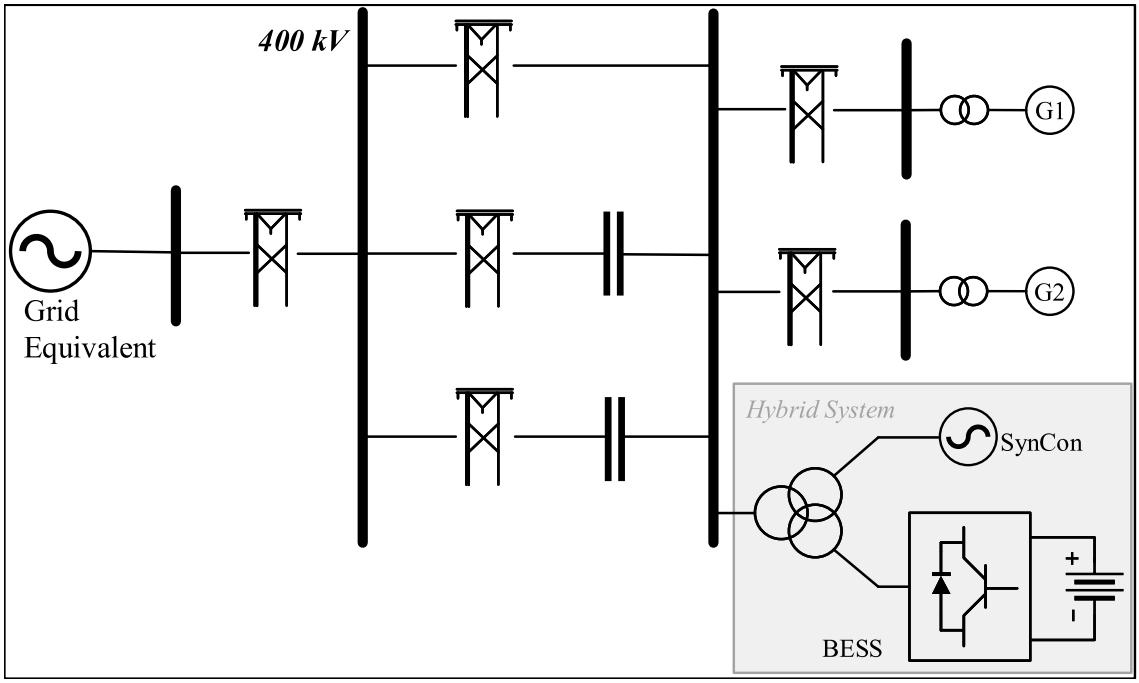

Figur 4.1: System Configuration

connecting Scotland and England, as shown in Fig. 4.1. The series compensation was introduced due to required increase of transmission capacity as a consequence of rising volumes of wind generation in Scotland [**?**]. The two generators are rated at 800 MW, and connected to the grid through the 400 kV series compensated transmission lines, with a compensation degree of 30%. Each generator system is modelled as a 7 multi-mass system as shown in Fig. 4.2. The system consists of a high pressure turbine (HP), intermediate pressure turbine (IP), two low pressure turbines (LPA and LPB), rotor of the generator, and two exciter rotors (ExcA and ExcB). the rotating masses are connected by shafts that are characterised by spring constants or torsional stiffness k_{ij}. Each mass is also defined by the inertia constant H_i and damping coefficient D_i. However, in this case we will only consider a worse case scenario where the damping is neglected.

The equations describing the dynamic behaviour of individual turbines is given as:

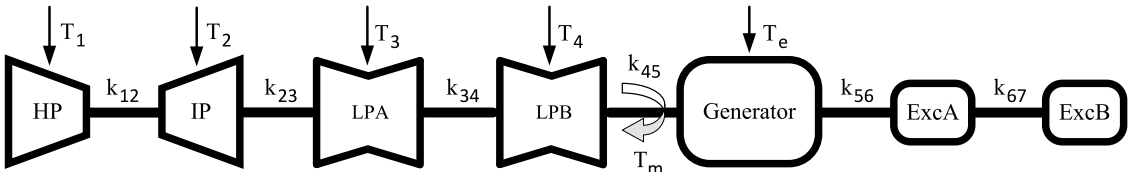

Figur 4.2: Multi-Mass System

$$
\begin{aligned}
2H_1\frac{d\Delta\omega_1}{dt} &= T_1 - K_{12}(\delta_1 - \delta_2) - D_1(\Delta\omega_1)\\
2H_2\frac{d\Delta\omega_2}{dt} &= T_2 + K_{12}(\delta_1 - \delta_2) - K_{23}(\delta_2 - \delta_3) - D_2(\Delta\omega_2)\\
2H_3\frac{d\Delta\omega_3}{dt} &= T_3 + K_{23}(\delta_2 - \delta_3) - K_{34}(\delta_3 - \delta_4) - D_3(\Delta\omega_3)\\
2H_4\frac{d\Delta\omega_4}{dt} &= T_4 + K_{34}(\delta_3 - \delta_4) - K_{45}(\delta_4 - \delta_5) - D_4(\Delta\omega_4)\\
2H_G\frac{d\Delta\omega_G}{dt} &= K_{45}(\delta_4 - \delta_G) - T_e - K_{56}(\delta_G - \delta_6) - D_G(\Delta\omega_G)\\
2H_6\frac{d\Delta\omega_6}{dt} &= K_{56}(\delta_5 - \delta_6) - K_{67}(\delta_6 - \delta_7) - D_6(\Delta\omega_6)\\
2H_7\frac{d\Delta\omega_7}{dt} &= K_{67}(\delta_6 - \delta_7) - D_7(\Delta\omega_7)
\end{aligned}
\tag{4.1}
$$

Notation T_i represents the mechanical torque developed by turbine sections, T_e is the generator's air-gap torque, K_{ij} is the shaft spring constant, D_i is the damping coefficient, H_i is the inertia constant, δ_i is the angle of the rotor section relative to the reference, and $\Delta\omega_i$ is the speed deviation of the respective rotor section.

4.2.2 Sub-synchronous Resonance Analysis

Since we are considering a seven mass system, there are seven oscillatory modes associated with them. In order to identify the frequency and damping of the oscillatory modes, we modelled the entire system in Matlab. The eigenvalues of the two generators are identical as the machine data is the same, and they are given in Table 4.1. There are three modes not shown in Table 4.1. The first mode represents the oscillation of the entire rotor against the power system (0.89 Hz) and this mode is usually associated with stability studies, but as it is not considered as a torsional mode of oscillation, it is out of the scope of the paper. The two super-synchronous modes are well damped and therefore not included in the analysis (63.32 Hz and 173.72 Hz). Figure 4.3 shows the system impedance profile as seen from the generator with and without the series compensation. The capacitors in the two transmission lines formed a resonance around the 38 Hz mark, and resulted in impedance reduction across the frequency range. This sequence of events contributed to torsional mode at 36.38 Hz becoming unstable.

In order to demonstrate the effect of the line compensation on the impedance of the system as seen from the affected generators, we performed a simplified impedance scan over a range of frequencies. A voltage source was connected in series with the generator, and consequently a voltage of 2% of nominal was injected at each frequency over the defined range. The voltage at the HV side and current injected into the system were measured, the voltage and current at the injected frequency were extracted from the base signal, and finally the impedance is calculated based on the measured and extracted values, as shown in Eq. 4.2, where the notation *p* represents the positive sequence, and *h* represents the frequency of interest (at resolution of 1 Hz).

$$
|Z_p^h(j\omega_h)| = \frac{|V_p^h(j\omega_h)|}{|I_p^h(j\omega_h)|} \tag{4.2}
$$

The resulting impedance curve is shown in Fig. 4.3. Without series compensation, the impedance is of inductive character, and it increases with the rise of frequency. Once we introduce the series capacitance, the impedance drops to a lower level across the frequency range, and a resonance occurs at $\sim$40 Hz.

Tabel 4.1: Eigenvalues of the generator

Mode Frequency	$\sigma \pm j\omega$
16.12 Hz	
27.04 Hz	
36.38 Hz	
38.09 Hz	

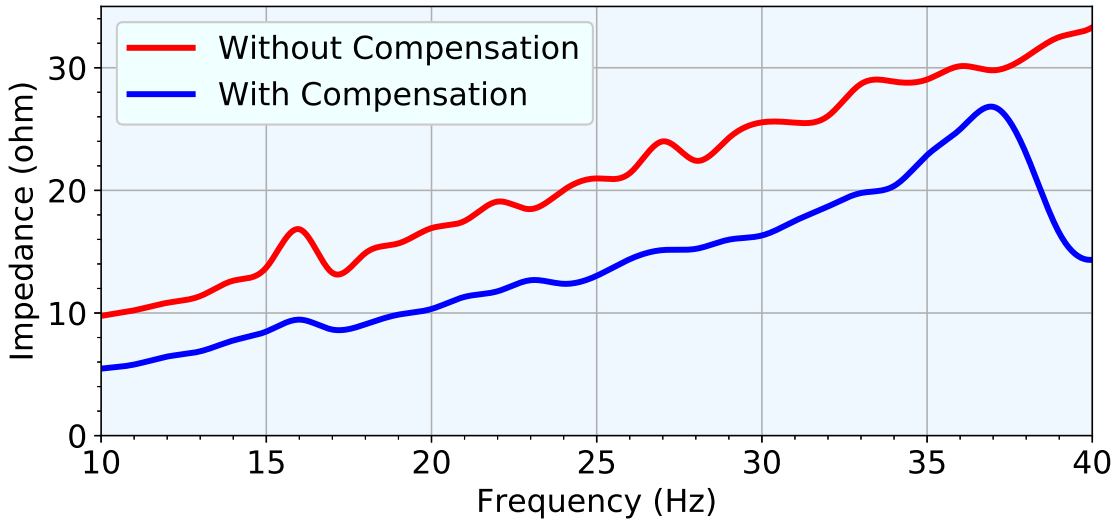

Figur 4.3: Impedance of the System as seen from the Generator

4.3 Proposed VSC Based SSR Damping Control

The diagram of the HSC system is shown in Fig. 4.4. The system consists of a synchronous condenser, battery system interfaced through a VSC, and they are both connected to the 400 kV transmission system through a three winding transformer. Each individual technology is equipped with their own controller, which are consequently controlled by the HSC master controller at a higher level of control. The master controller sets the active power output, voltage or reactive power reference, and it also determines the mode of operation of the HSC (voltage or reactive power control, enables the various functions of the technologies, etc.). As the AVR controller of the synchronous condenser has a low bandwidth that goes up to 10 Hz, it does not contribute directly to damping of torsional oscillations.

The inner control structure of BESS is a standard PI-based current controller as shown in Fig. 4.5, while the outer loop includes the damping controller and all other functions (voltage and reactive power control, fault-ride-through, frequency droop control, etc., represented by the i_{d-ref}) and i_{q-ref}. The dynamic behaviour of the VSC is described by the following equations:

$$\begin{aligned} L_f \frac{di_d}{dt} &= (v_{td} - v_{d-vsc}) + \omega L_f i_q \\ L_f \frac{di_q}{dt} &= (v_{tq} - v_{q-vsc}) + \omega L_f i_d, \end{aligned} \tag{4.3}$$

where the v_{td} and v_{tq} represent the terminal voltage of the VSC in dq frame. The ratings of SC and BESS are given in Table 4.2.

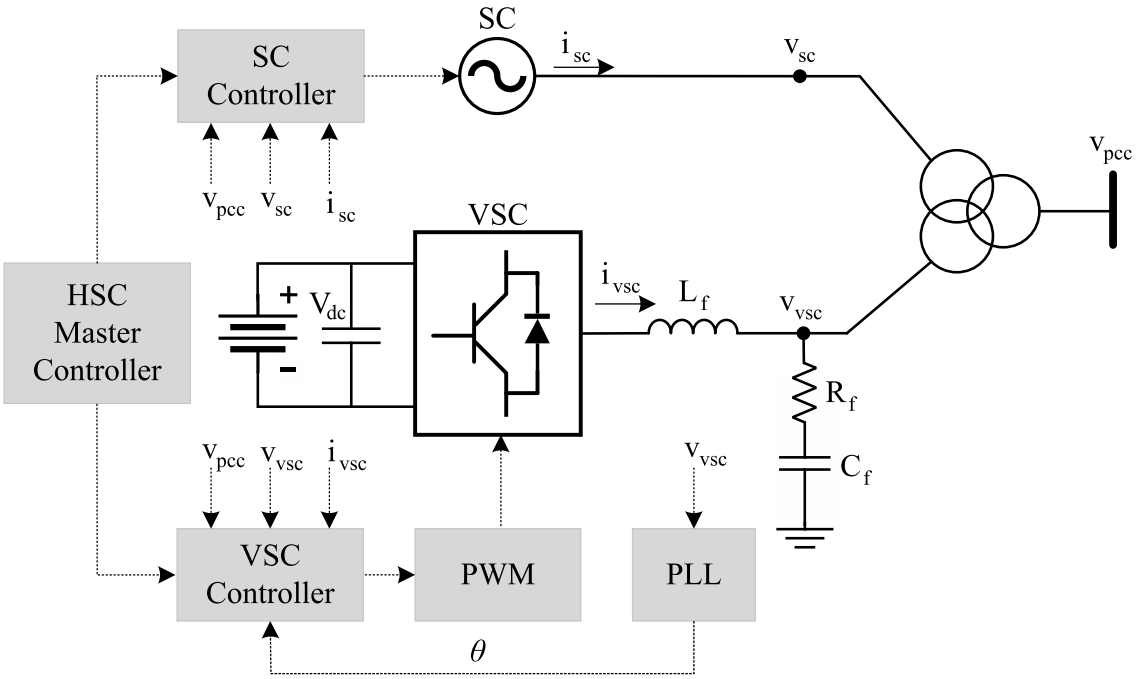

Figur 4.4: Impedance of the System as seen from the Generator

Tabel 4.2: SC and BESS Ratings

	BESS	SC
Voltage	12.3 kV	13.8 kV
Power	70 MVA	70 MVA
Reactive Power Capabilities	± 70 MVAr	-33.5/+70 MVAr
Active Power Capabilities	± 10 MW	-
BESS Reactor	2.1 mH	-
BESS DC Voltage	25 kV	-

4.3.1 Damping Controller Design

The two generators in the system shown in Fig. 4.1 are of the same rating and parameters, so the the torsional modes are also the same. in light of this fact, we have chosen a single measurement for the feedback of the damping controller loop, namely the PCC voltage of the VSC. By using a local measurement, we can avoid larger delays in signal acquisition, and more importantly we do not need access to the power plant in order to obtain the torque or speed deviation measurement signal. Additionally, the speed or torque measurement resolution does not become a factor in designing a damping controller.

The basic structure of the controller is shown in Fig. 4.5. As there are four oscillating modes, each of the modes will have a designated control loop, from where the outputs of each are added together to form a single additional input to the VSC current controller, namely i_{q-POD}. Each loop consists of three blocks: filter, gain, and phase compensator. The filter block isolates the signal with the targeted frequency and with a very narrow bandwidth and additionally attenuates the other three signals at their respective frequencies. The goal is to minimize the influence of one loop on other loops targeting different oscillating modes. The transfer functions of the filter blocks are given as:

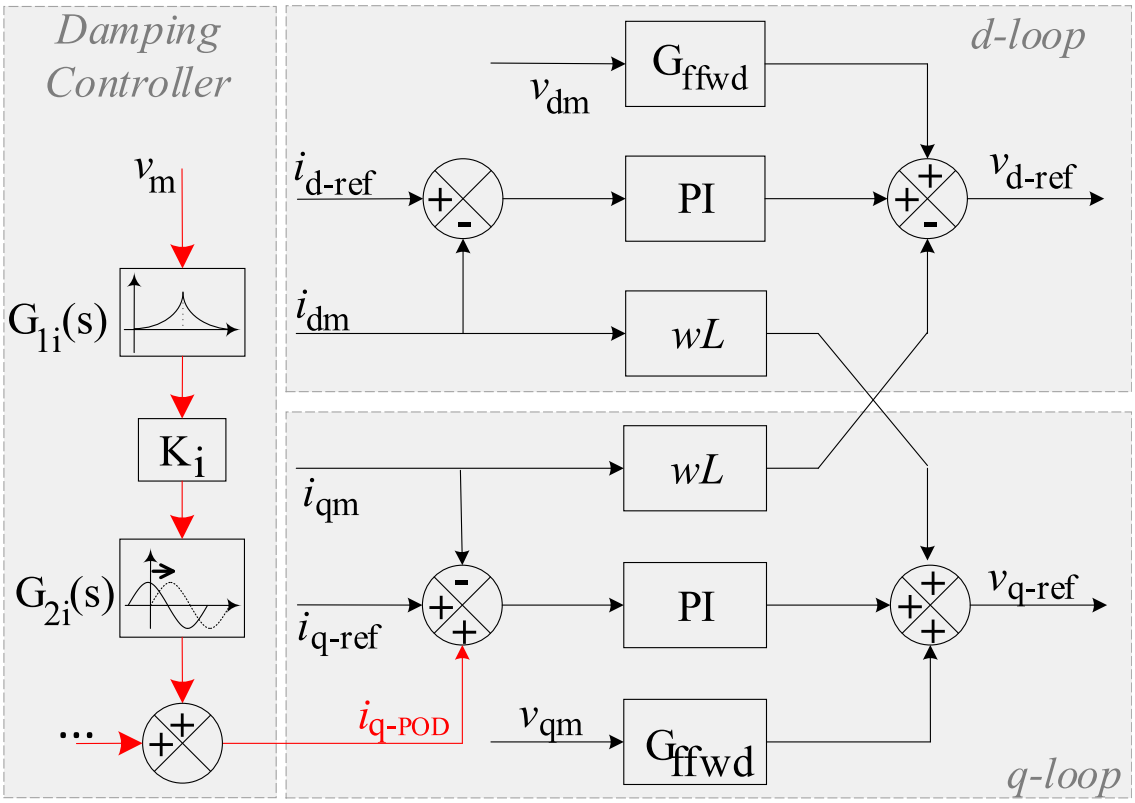

Figur 4.5: VSC Current Controller

$$G_{i-L} = \frac{1}{s^2 + \omega_{i-L}s + \omega_{i-L}^2} \tag{4.4}$$

$$G_{i-b1} = \frac{s^2 + \omega_{i-A1}}{s^2 + \omega_{bw}s + \omega_{i-A1}^2} \tag{4.5}$$

$$G_{i-b2} = \frac{s^2 + \omega_{i-A2}}{s^2 + \omega_{bw}s + \omega_{i-A2}^2} \tag{4.6}$$

$$G_{i-b3} = \frac{s^2 + \omega_{i-A3}}{s^2 + \omega_{bw}s + \omega_{i-A3}^2} \tag{4.7}$$

$$G_{i-G} = \frac{s}{s^2 + \omega_{bw}s + \omega_i^2} \tag{4.8}$$

$$G_{1i}(s) = G_{i-L} \cdot G_{i-b1} \cdot G_{i-b2} \cdot G_{i-b3} \cdot G_{i-G} \tag{4.9}$$

G_{i-L} (Eq. 4.4) is a transfer function of the low-pass filter, which ensures that the higher frequency signals are attenuated, while it provides a gain of 1 at all other frequencies. The cutoff frequency is set to 40 Hz, because all the oscillating modes are below that threshold. $G_{i-b(1-3)}$ (Eq. 4.5-4.7) are the attenuation filters, and their purpose is to eliminate the signal with specific frequency ($\omega_{i-A(1-3)}$). In our case, as we have four oscillating modes, each damping loop will have three of these filters, in order to isolate only the signal with the frequency of interest (ω_i). The bandwidth of the filter is influenced by the parameter ω_{bw}, and we used two different values because the modes at frequencies 36.38 Hz and 38.09 Hz are in close proximity, so the bandwidth needs to be as narrow as possible in order to eliminate possible overlap and at the same time ensure stable

operation. For the first two modes a bandwidth of 3 Hz was chosen, while for the two modes that are close in terms of frequency, we set the bandwidth to 1 Hz. The G_{i-G} (Eq. 4.8) represents the transfer function that serves to amplify the signal at frequency ω_i. The bandwidth of the filter ω_{bw} depends on which mode is the loop being designed for, as the last two oscillating modes require very narrow bandwidth (1 Hz). The total transfer function of the filter blocks is given by Eq. 4.9.

The remaining two blocks represent the gain (K_i) and phase compensation (G_{2i}). The transfer function of the phase compensator is given as:

$$G_{2i}(s) = \left(\frac{1 + a_i T_i s}{1 + T_i s}\right)^2 \tag{4.10}$$

The phase compensator adds a positive phase to the loop over the frequency range $1/a_i T_i$ and $1/T_i$. The parameters a_i and T_i are determined by the phase compensation that is needed ϕ_i and the frequency at which we are applying the compensation, as given by Eq.

$$a_i = \frac{1 + sin\phi_i}{1 - sin\phi_i} \tag{4.11}$$

$$T_i = \frac{1}{\omega_i \sqrt{a_i}} \tag{4.12}$$

In other words, the compensator will add phase lead of ϕ_i at frequency ω_i. This type of phase compensator can provide a maximum of $180°$ compensation, and for a full $360°$ compensation range we can use the gain (positive for up to $180°$, and negative beyond). In order to determine the necessary level of gain and phase compensation, we need to tune two parameters in each of the four loops, ϕ_i from which we can calculate parameters a_i and T_i (ω_i is known from the small signal analysis), and the gain K_i. The total damping current is given as the following:

$$i_{q-POD} = \sum_{i=1}^{4} (V_i K_{G1i} K_i K_{G2i} \cdot cos(\omega_i t + \delta_i + \theta_i + \phi_i)) \tag{4.13}$$

V_i is the voltage magnitude of mode i, K_{G1i} is the gain of the mode filter, K_i is the tuned loop gain, K_{G2i} is the gain of the phase compensator, δ_i is the phase of the voltage component v_i, θ_i is the phase shift added by the filter, and finally ϕ_i is the phase shift added by the phase compensator.

4.3.2 Tunning the Parameters of the Damping Controller

In order to tune the performance of the damping controller, or in other words find the optimal damping effect of the HSC system, we need to determine the parameters given by Eq. 4.11 and Eq. 4.12. In this paper we used a simulation-based approach, where we run simulations for each set of parameters and evaluate the fitness function. The fitness function used for the optimization procedure is based on the damping ratio of each oscillating mode, and is given as:

$$f = \sum_{i=1}^{N} \sum_{j=1}^{M} (1 - \zeta_{ij})^2 \tag{4.14}$$

subject to

$$\zeta_{ij} > 0 \tag{4.15}$$

$$i_{qmin} < i_{q-POD} < i_{qmax} \tag{4.16}$$

where N is the number of operating states, while *M* is the number of oscillation modes. We chose five operating states (N), namely 20, 40, 60, 80, 100 % generation from the two generators, and there are 4 oscillating modes (M). The limits are given by Eq. 4.15 and Eq. 4.16. The optimization algorithm used is the Particle Swarm Optimization (PSO), and it is run in MATLAB. The system is modelled in RTDS and controlled from MATLAB. The sequence is shown in Fig. 4.6. The feedback from RTDS is sent to MATLAB, from where the damping ratios are calculated from exponential curve fitting. The rotor speed deviation is fed to four different filters, which extract the waveforms with frequencies corresponding to the four oscillating modes. The four waveforms are then processed in MATLAB to determine the damping ratio of each oscillating mode. For damping estimation, we used a curve fitting algorithm based on the peaks of the waveform, as shown in Fig. 4.7.

The equation of the waveform, which is basically an exponentially damped sinusoid, can be written as:

$$f_i = A_i \cdot e^{-b_i t} \cdot cos(\omega_i t + \phi_i) \tag{4.17}$$

where b represents the damping factor. The algorithm extracts the peaks and performs exponential curve fitting from which the damping factor b is determined.

The bode plot of the resulting transfer function with tuned parameters is shown in Fig. 4.9. It can be noticed that the interaction between the individual loops can be considered non-existent or minimal, as the gain is significant only around the targeted frequency due to the narrow bandwidth of each control loop.

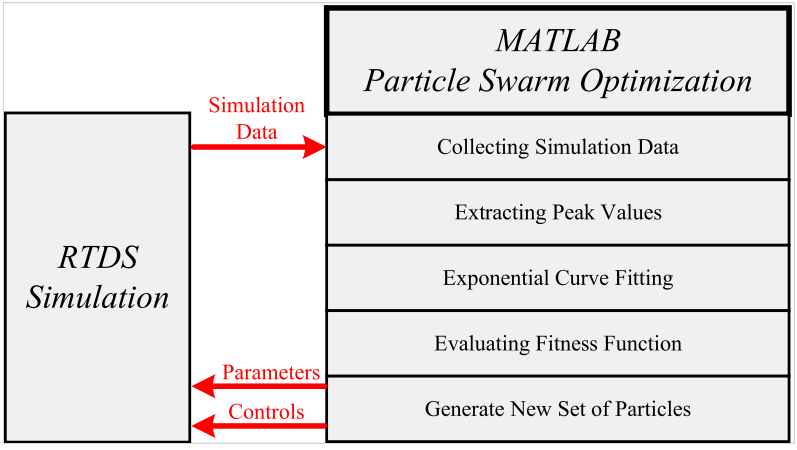

Figur 4.6: Impedance of the System as seen from the Generator

4.3.3 Small Perturbance Evaluation of the Damping Controller

In order to evaluate the performance of the damping controller, we performed an eignevalue analysis on a linearized model of the system and the relevant modes are shown in Table 4.3. We can notice the improvement in all four modes once the controller is activated.The analysis was performed for the most critical case, when the power generation of the two generators is at 20%. Fig. 4.8 shows the change in the impedance of the system as seen from the generator's side once the HSC with damping controller connected.

In order to validate the results obtained from the small signal analysis, we used a simulation based method to evaluate the damping profile of the system. A small perturbation was added to the mechanical torque input of the multi-mass model, while the measurements were taken for the electrical torque deviation and the rotor speed deviation. The transfer function can be written as:

$$G_e(s) = \frac{\Delta T_e(s)}{\Delta \omega(s)}. \tag{4.18}$$

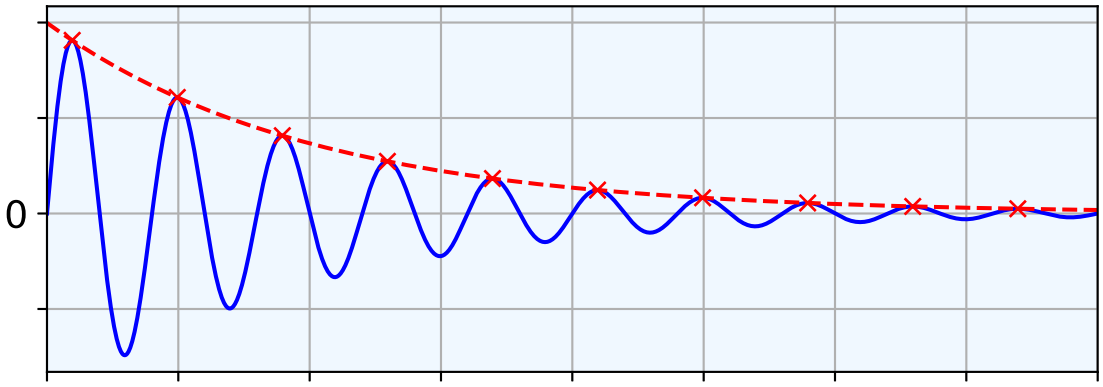

Figur 4.7: Exponential Curve Fitting

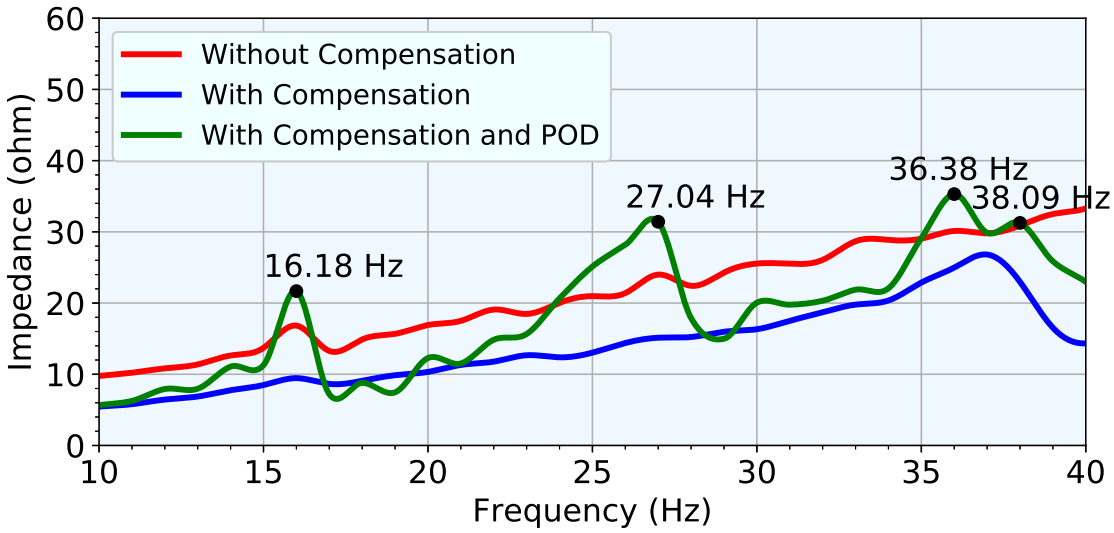

Figur 4.8: Impedance of the System as seen from the Generator

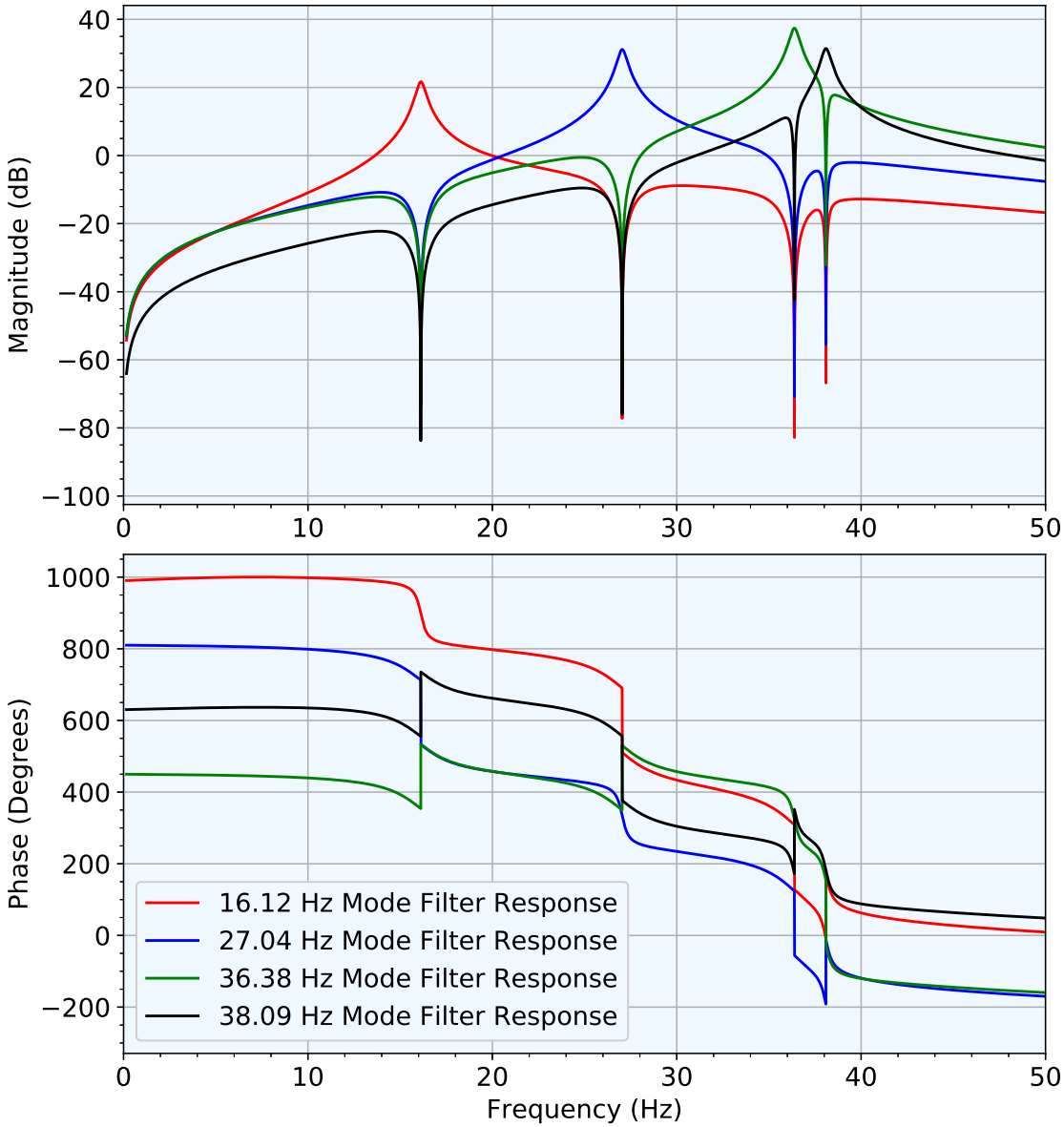

Figur 4.9: Transfer Function

Tabel 4.3: Eigenvalues of the generator

	Without HSC	With HSC
Mode Frequency	$\sigma \pm j\omega$	$\sigma \pm j\omega$
16.12 Hz	$-0.0245 \pm j101.2849$	$-0.0645 \pm j101.2913$
27.04 Hz	$-0.0069 \pm j169.8973$	$-0.0920 \pm j169.9321$
36.38 Hz	$+0.0026 \pm j228.5823$	$-0.0844 \pm j228.5823$
38.09 Hz	$-0.0024 \pm j239.3265$	$-0.0670 \pm j239.3265$

Once the gain and phase of the transfer function given in 4.18 are obtained, the damping factor can be easily determined from:

$$D_e(\omega) = R_e\{G_e(j\omega)\}. \tag{4.19}$$

Fig. 4.10 shows the resulting damping profile of the system for three different scenarios. It can be observed that the damping around the critical oscillating mode is negative, which results in an unstable system with undamped oscillations at 36.38 Hz frequency. A system with added passive filter to the compensating capacitors increases the damping around the critical mode and brings it back to the positive region. However, the damping factor is still relatively low, which means that the oscillation might last for a longer period and potentially cause stress on the generator's shaft, influencing the life-cycle of the machine. With the HSC connected, the damping profile is significantly improved, most notably close to the oscillating modes frequency.

4.4 Case Studies and Simulation Results

In order to demonstrate the validity and effectiveness of the proposed torsional oscillation damping controller, a time-domain simulation was performed in RSCAD. The model of the system is shown in Fig. 4.1. The performance of the system was evaluated for three different scenarios. Namely, a simulation was performed for a case where there is no additional damping in the system, to demonstrate the base case scenario. Second scenario includes a passive filter added in parallel to the compensating capacitor. And finally, a third case involves the implementation of oscillation damping controller as an integral function of the Hybrid Synchronous Condenser system. The performance was evaluated for the more critical case, when the generated power of the synchronous machines is low (100 MW per generator).

4.4.1 Simulation-Based Performance Evaluation of the Oscillation Damping Controller During Large Disturbance

A large disturbance in this case is a three-phase short circuit that occurs at PCC of the HSC. The duration of the fault is 140 ms, and is followed by a significant voltage dip. The three scenarios considered are the same as in the case with small disturbance performance evaluation, namely, a

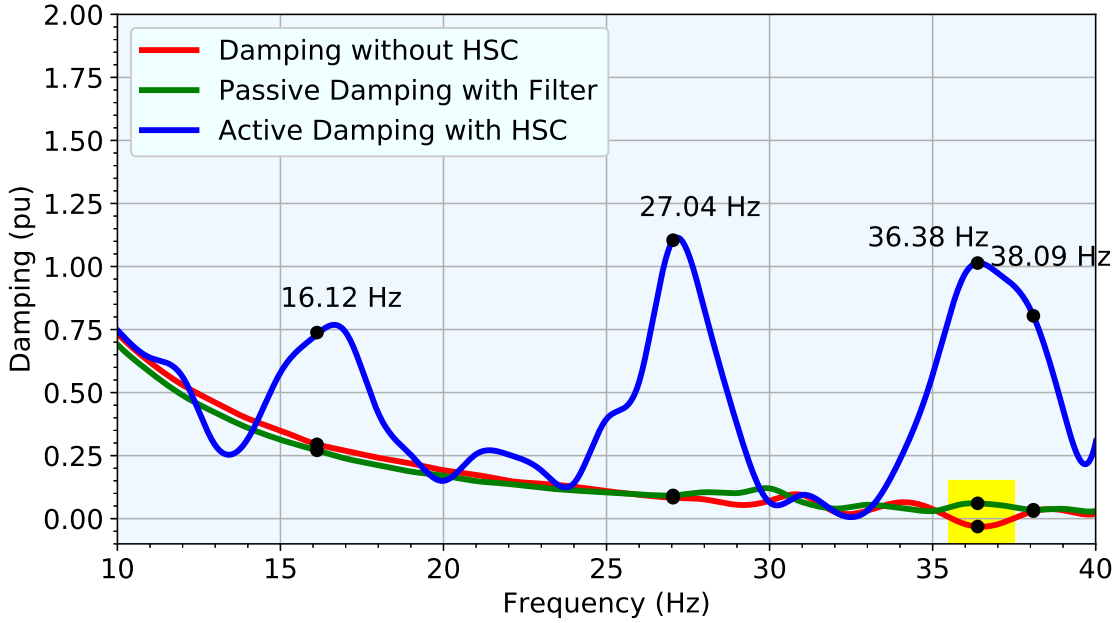

Figur 4.10: Damping Profile of the System without HSC

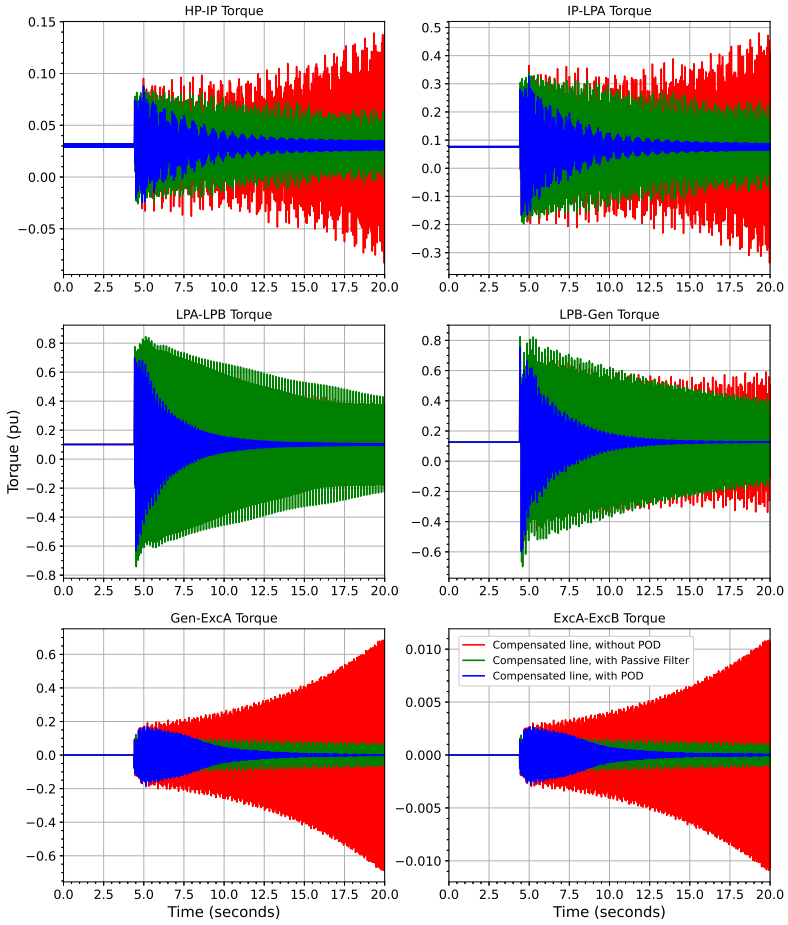

Figur 4.11: Multi-Mass Torques

case without any damping controller, a case with the passive filter, and the case with damping controller of HSC. The parameters of the damping controller are the same tuned parameters as in the previous section.

The fault occurs at 5s of simulation and the dynamic response of the shaft torques for the three scenarios is shown in Fig. 4.11. It can be seen that if there is no damping applied to the system, the oscillation continue to increase, meaning that the mode is an unstable mode. Once the passive filters were added in parallel to the compensating capacitors, the damping increased for the critical mode, and the oscillation subsided, resulting in a stable system. However, the duration and the amplitude of the oscillation can cause significant stress on the shafts of the synchronous machines degrading their performance and life-cycle. With the HSC connected to the system, and enabled oscillation damping controller, the damping of the critical mode is improved significantly. The controller starts injecting the damping current as soon as the fault-ride-through mode deactivates, which is in the order of 100 ms. Fig. 4.13 shows the rotor speed deviation of the synchronous machine. We can observe that the initial large magnitude oscillation is caused by the fault and significant voltage dip, resulting in high oscillation of the rotating masses.

4.4.2 Validation of the Results in Power Hardware-in-a-loop (PHIL) Setup

In order to validate the obtained results on the performance of the damping controller, a power hardware-in-a-loop platform was used. The platform consists of RTDS rack, I/O cards, 10kVA linear

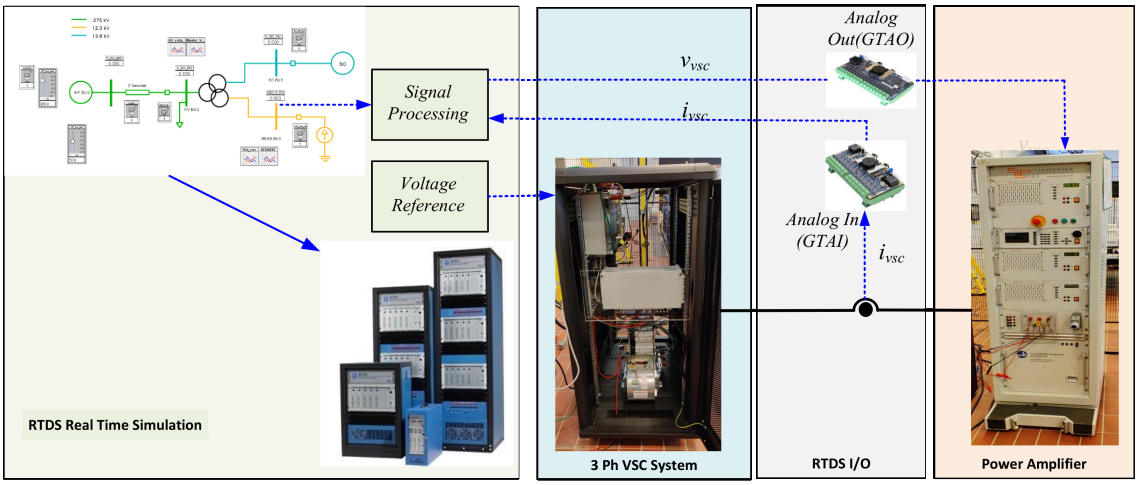

Figur 4.12: Power Hardware-in-a-loop Platform for Validation of Damping Converter Performance [4]

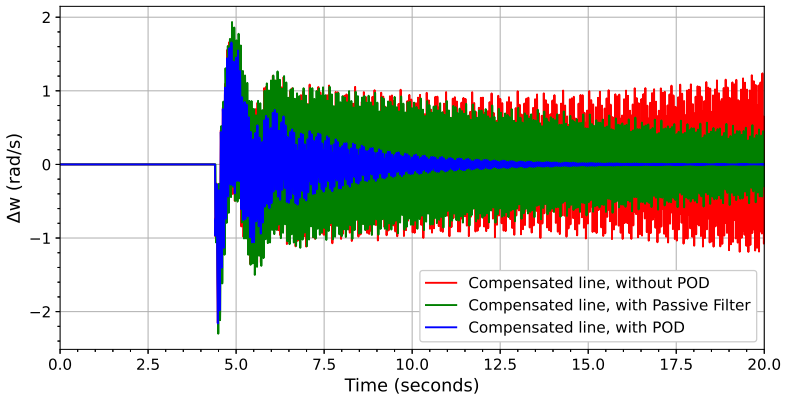

Figur 4.13: Rotor Speed Deviation of the Synchronous Machine - Simulation

amplifier and a Semicron based converter stack. The controller for the converter that was used is a National Instruments' General Purpose Inverter Controller (GPIC). Graphical interface was developed in LabView. The scaling factors were chosen based on the rating of the converter stack. Voltage measurement at PCC is sent to the controlled amplifier, while the current measured at the terminal of the converter stack was sent back to RTDS rack and used as a controlling input for the current source. Due to the delay in communication of 200ms, a correction of 1.8° was added to the phase angle parameter of each damping loop. The converter control loop for oscillation damping was programmed into the existing control structure using LabView. Fig. 4.14 shows the result of the test and it can be seen that the controller acts in the same way to damp the oscillations. This demonstration clearly shows the effectiveness of the proposed damping controller in providing sufficient damping current for two large synchronous machines. One of the major advantages of such a controller is that it does not require access to the power plant (speed or torque measurement), as it can use the measured voltage at PCC as an input.

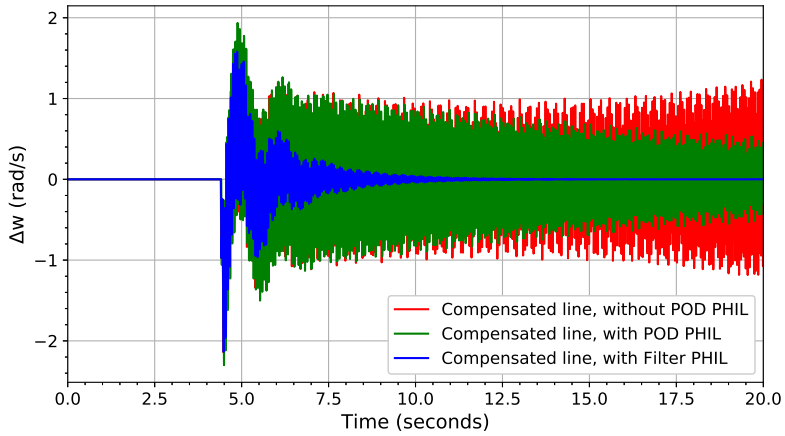

Figur 4.14: Rotor Speed Deviation of the Synchronous Machine - PHIL

4.5 Conclusion

In this paper, the authors propose a torsional oscillation damping controller as a part of the Hybrid Synchronous Condenser system. The controller is an additional function for the HSC and requires only a small proportion of the rated power to operate effectively. The major components of the control loop are the filter, gain and the phase compensator. The optimization method that was used for parameter tuning is Particle Swarm optimization, and the method can be used to optimize the controller for applications at different power plants.Small signal analysis of the system showed that the two synchronous machines have four torsional modes and that one of the modes had negative damping. Upon implementing the control design, damping for the critical mode significantly improved, and also for the other three torsional modes. The small signal analysis was validated in a simulation where was shown that the controller can effectively damp the critical torsional oscillation mode excited by a large disturbance (short circuit). Furthermore, it was shown that the controller can be implemented on an actual hardware. The power hardware-in-the-loop test has confirmed the results seen in both small signal analysis and the nonlinear EMT simulation. Finally, it was shown that the damping controller can be an integral part of the HSC without compromising the effectiveness of other implemented functions.

KAPITEL 5

Inertia Maximization

The chapter is based on **[Pub. B]**.

5.1 Introduction

The inertial support function is one of the key services a synchronous condenser system can provide. In addition, due to the voltage source characteristics, SC can support the system with instantaneous phase jump power during system contingencies allowing the system to ride through the events safely [60]. Inertial support provision from an SC is in the process of being monetized. For instance, the Stability Pathfinder project by National grid UK, seeking to procure inertial services for the GB-wide inertia solutions, selected options consisting of SC with inertia boosted with flywheels [11]. However, one challenge with the inertial power from an SC is that the damping power provided by the damper windings are quite low and the response can be oscillatory similar to conventional synchronous machine[53].

There is inertia boosted SCs with flywheels connected to the rotor available in the market [12]. And such solutions can also be a choice in being a part of a hybrid solution together with a converter-based resource. In this regard, the possibility of compensating oscillatory inertial active power from the SC using a converter-based solution in the hybrid system is intriguing. The hybrid solutions of SC and STATCOM have been shown to operate in several modes, such as loss minimization and inertia maximization [3]. But the low energy storage in the DC capacitance of the STATCOM results in the constrained application of inertia maximization. To this end, the chapter investigates the application of converter resources with energy storage as a part of the hybrid system in maximizing the inertia of the combined solution.

This chapter proposes a control method applicable to hybrid solutions in reducing peak oscillations in the inertial active power output of the hybrid solution. The proposed solution can eliminate the negative-going oscillations on the output power from the hybrid system and thus improve the inertia response. In addition, the estimated energy required from the converter resources for effective inertia maximization under various system conditions is compared and quantified to investigate the applicability of ultracapacitor, flywheel-based power converter for the hybrid system.

5.2 Inertia Maximisation Principle

The inertial response from the synchronous condenser is preferred for the system's stability. However, one major drawback for the SC output inertia is that it could be highly oscillatory due to a lightly damped electromechanical mode. When subjected to a constant rate of change of frequency, ideally, the inertial power output from a component installed for inertia should remain nonoscillatory. However, due to large oscillations, for a certain period after the frequency event, the SC inertial output power can be opposite of what is required from the component. This

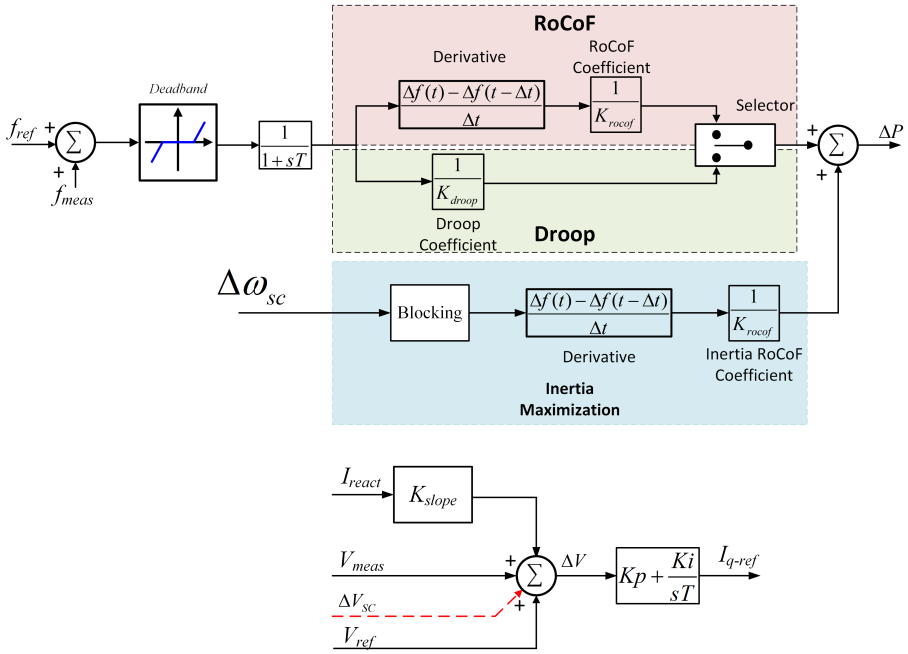

Figur 5.1: Inertia maximisation control implemented in the outer loops of the BESS, the reactive control remains the same as in previous chapters

section details a controller implemented in the BESS control, which can eliminate the out-of-phase oscillation inactive power in response to a constant rate of frequency change.

The previous chapters has demonstrated methods for implementing an emulated synthetic inertia in the BESS. One approach in emulated inertia implementation for the BESS is to measure the frequency change rate by estimating the frequency slope and regulating the BESS's active power output in proportion to this estimated rate of change of frequency.

$$\Delta P = \frac{\Delta f(t) - \Delta f(t - \Delta t)}{\Delta t} \cdot \frac{1}{K_{rocof}} \tag{5.1}$$

Where, $\Delta f(t)$ is the difference between the measured frequency using PLL (f_{meas}) and nominal frequency (f_{ref}), and K_{rocof} is the coefficient of RoCoF active power. However, although such a method can augment the inertial active power output from a hybrid system composed of SC and BESS, it cannot still eliminate the out-of-phase oscillation in the inertial active power output from the SC in a hybrid system. To that end, this work proposes utilising the rate of change of speed of the SC rotor ($\Delta\omega_{SC}$) to derive active power setpoint for the BESS. The change in active power reference of the BESS (ΔP) the sum of frequency droop control block and inertia maximization block given by

$$\Delta P = \begin{cases} 0 \;\; if \;\; \frac{d(\omega_{sc})}{dt} \leq 0 \\ \frac{1}{K_{rocof}} \frac{d(\omega_{sc})}{dt} \;\; if \;\; \frac{d(\omega_{sc})}{dt} > 0 \end{cases} \tag{5.2}$$

By selecting parameter K_{rocof} such that the out of phase oscilation to RoCoF response from SC can be eliminated in the total response of the hybrid system. The full control diagram of the outer loops including frequency and reactive power droop control and inertia maximisation block is demonstrated in Fig. 5.1.

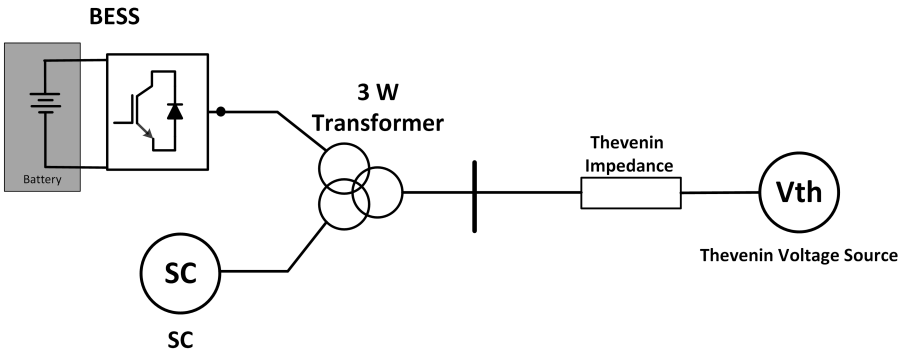

Figur 5.2: The hybrid system setup implemented in PowerFactory for simulation study

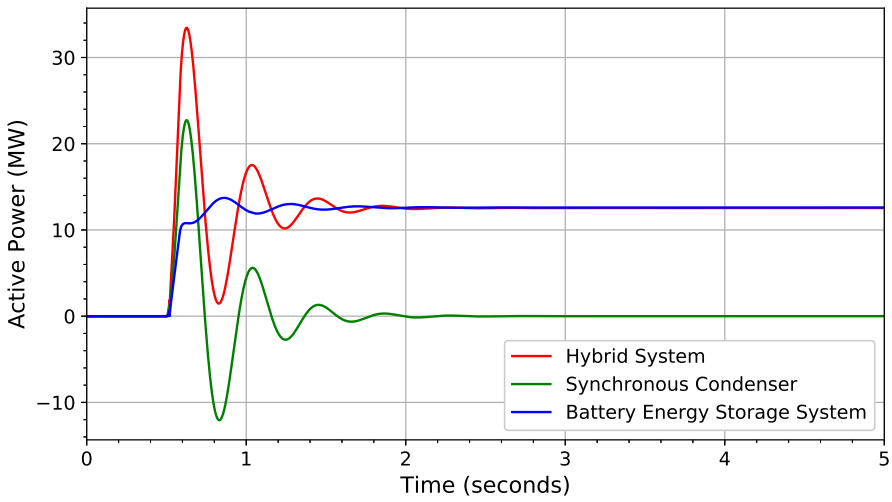

Figur 5.3: Active power output of the hybrid system when subjected to 1 Hz/s RoCoF with SC inertia of 1.34 s and only droop control active in the BESS control

5.3 Simulation Results

To study the effectiveness of the proposed controller a simulation study is conducted. The simulation setup as shown in Fig. 5.2 is implemented in the DIgSILENT PowerFactory. The simulation is conducted in an EMT environment.

Firstly, the inertia of the SC is kept at a relatively low value of 1.34 s. The active power output response of the hybrid system when subjected to a system rate of change of frequency of 1 Hz/s with only frequency droop controller implemented is shown in Fig. 5.3. The total response is oscillatory as expected due to low damped electromechanical mode of the SC. BESS control with a frequency droop, but is not enough to damp the SC oscillations quickly. The same case, with inertia maximization control activated is shown in Fig. 5.4. The out phase oscilation to the RoCoF in the active power output from SC is eliminated due to the action of inertia maximization control in the total active power output of the hybrid system.

When the inertia of the SC is increased to 6 s of inertia constant and subjected to same RoCoF of 1 Hz/s the, the response from hybrid system becomes even more oscillatory. The active power response from the hybrid system even falls below the pre event active power due to large oscillations

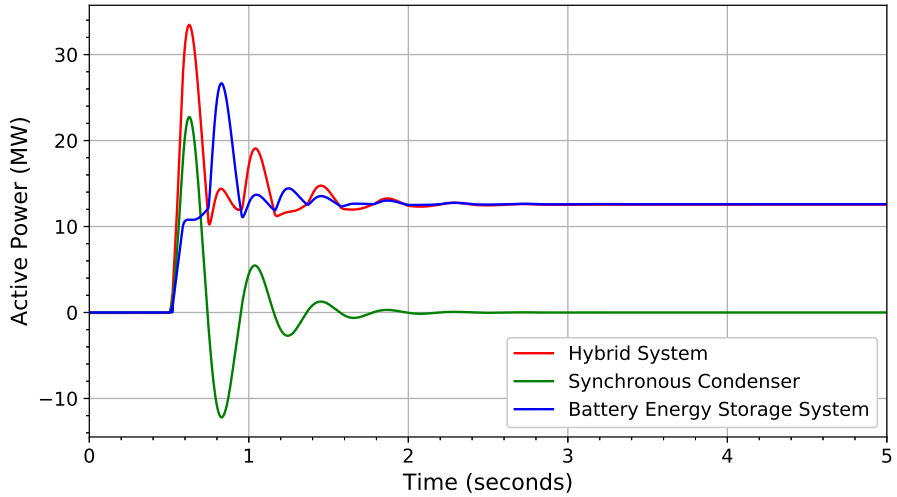

Figur 5.4: Active power output of the hybrid system when subjected to 1 Hz/s RoCoF with SC inertia of 1.34 s, with inertia maximisation loop enabled

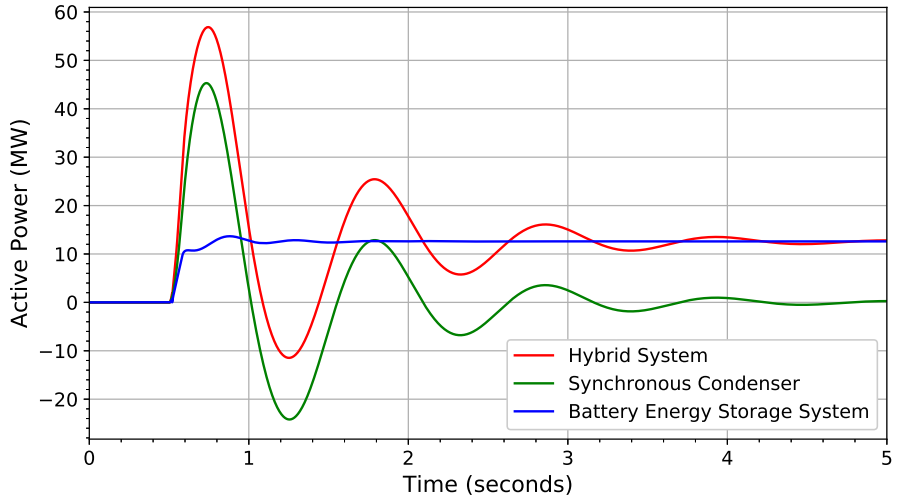

Figur 5.5: Active power output of the hybrid system when subjected to 1 Hz/s RoCoF with SC inertia constant of 6 s and only droop control active in the BESS control

in inertial active power of the SC as shown in Fig. 5.5. With the activation of the inertia maximisation loop, the oscillation in the output power is reduced because the out of phase, negative peak output power is clipped due to inertia maximisation compensation, thus increasing the net inertial power contribution from the hybrid system as shown in Fig. 5.6.

Finally, the simulations are repeated with SC inertia constant of 20 s, representing a flywheel connected SC. Without the inertia maximisation loop the output power is highly oscillatory with large negative active power in the hybrid system output due to oscillatory SC dominating the response as shown in Fig. 5.7. The inertia maximisation loop is effective in mitigating large peak to peak oscillation in the output of the hybrid system as shown in Fig. 5.8.

5.4 Conclusion

The highly oscillatory nature of the SC response, particularly when the SC inertia is boosted with coupled flywheel, can be a challenge in maintaining the quality of inertial power response from the

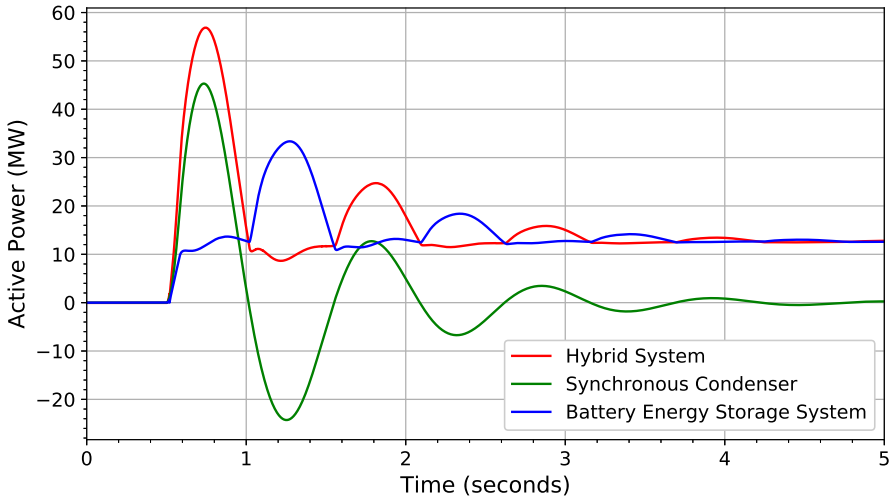

Figur 5.6: Active power output of the hybrid system when subjected to 1 Hz/s RoCoF with SC inertia constant of 6 s, with inertia maximisation loop enabled

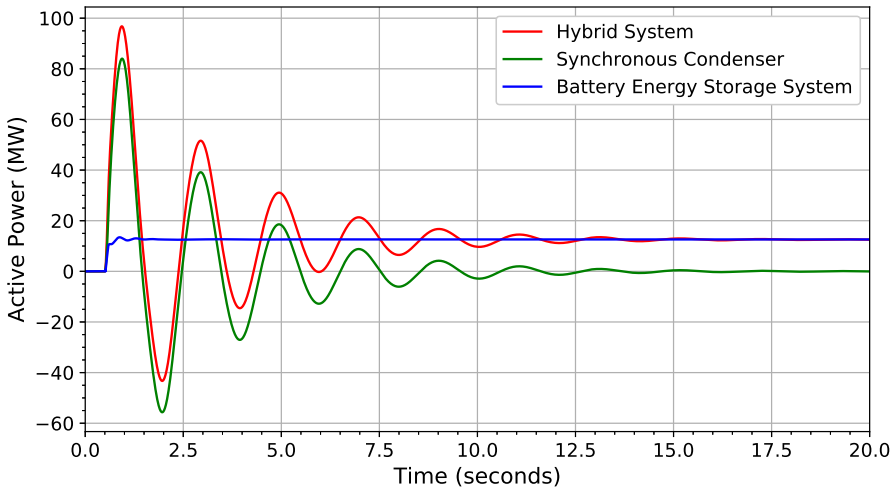

Figur 5.7: Active power output of the hybrid system when subjected to 1 Hz/s RoCoF with SC inertia constant of 20 s and only droop control active in the BESS control

hybrid system. In this chapter, a controller that can maximize the inertial contribution from HSC is proposed and reduce the oscillatory inertial response from the HSC. The inertia maximization loop implemented in BESS compensates for the out-of-phase peak oscillation in the SC, thus resulting in reduced oscillations in the inertial active power output. The proposed controller is validated using time-domain simulations performed in PowerFactory.

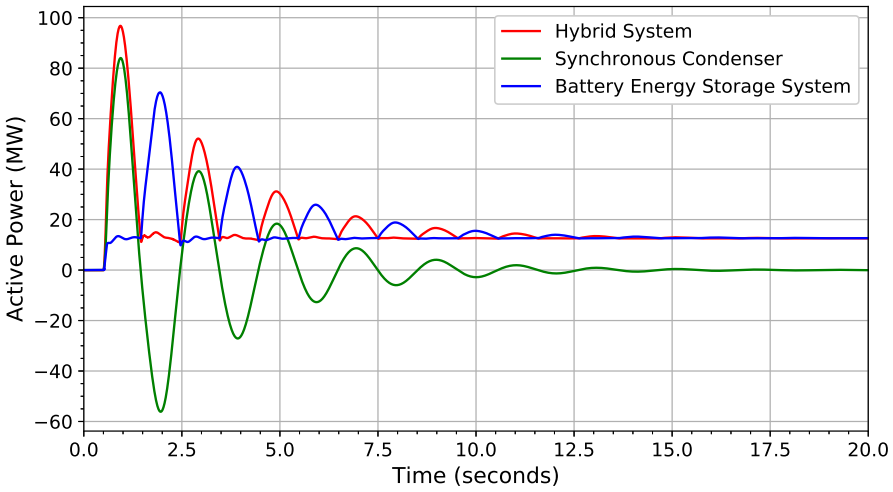

Figur 5.8: ctive power output of the hybrid system when subjected to 1 Hz/s RoCoF with SC inertia constant of 20 s, with inertia maximisation loop enabled

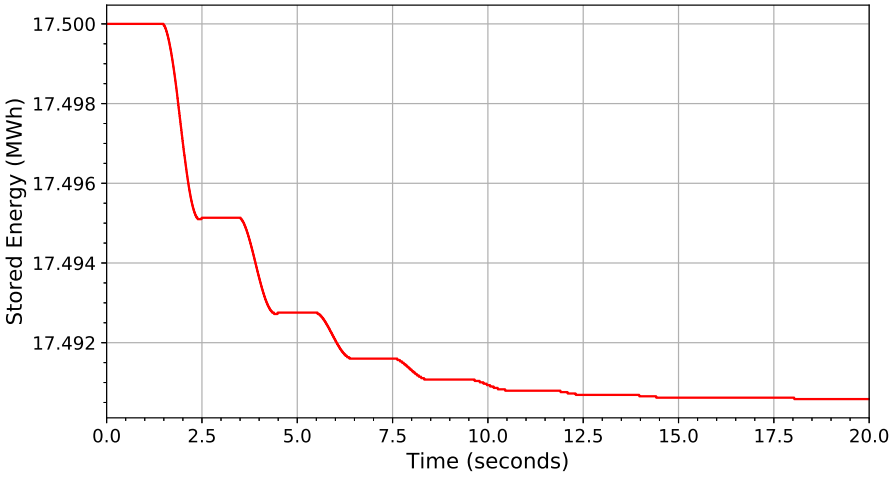

Figur 5.9: Inertia-twenty-secondsEnergy1

KAPITEL 6

Conclusion and future work

6.1 Conclusion

All current trends indicate that the future power systems will be significantly different from what we call the conventional power system with synchronous machine dominated power generation. Power converter interfaced renewable sources will potentially dominate the generation mix in the power systems which brings new challenges in terms of operation and stability. Flexibility of converter controls provides the potential to replace and replicate some of the major functions that are inherent to synchronous machines, such as inertia, short-circuit level, and voltage controllability. Special attention is being given to synchronous condensers as a possible solution to some of the major issues with converter dominated power systems. Additionally, Battery Energy Storage Systems (BESS) are being implemented across the globe with a goal of providing ancillary services that are required for stable system operation.

In this work, a new technology termed Hybrid Synchronous Condenser System (HSC) that combines the benefits of both synchronous condensers and battery energy storage systems has been investigated. A detailed description of battery modelling has been presented and an overview of possible applications of BESS. A comparison between the hybrid solution, standalone technologies, grid-following and grid forming control strategy has been conducted and evaluation of the performance of each technology presented in a summary. Hybrid synchronous condenser system is capable of providing multiple supplementary functions to the power system. Namely, a torsional oscillation damping controller was designed and included as an integral part of the HSC control system. Inertia contribution from the HSC can be highly beneficial in a converter dominated power system and in light of that, a control design is proposed to maximise the overall impact of the HSC in terms of inertial support by using battery energy storage system.

6.1.1 Hybrid Synchronous Condenser System

The inspiration for the HSC came from the Phoenix project, as explained previously. The idea was to combine the benefits of the power converter-based technology and synchronous condensers, and design a hybrid system with unique response and multiple ancillary functions. The concept involved an analysis of a possible implementation with BESS. The inertial response of the synchronous condenser in line with fast frequency response from BESS makes it possible to emulate the response of a conventional synchronous generator to a certain extent. The overloading capability of SC and fast acting response from BESS in terms of reactive power offer a significant functionality for strong voltage support.

In terms of inertia support, synchronous condensers have a typical value between 1 and 4 seconds for the inertial constant. Power converters do not inherently posses the capability to provide inertia, but there is a possibility of so-called synthetic inertia support and grid-forming control architecture that can provide and mimic a response similar to synchronous machines. If combined in a hybrid

system, the response can span over a longer time scale and include instantaneous response from SC and slower but sustainable response from converters provided by droop control. Grid-forming converters have an edge over grid-following converters as their response is almost instantaneous. The differentiating factor between the hybrid system and the standalone technologies is the time scale of the response where hybrid system provides support over longer period.

High overloading capability of synchronous condenser makes it a dominant technology in terms of voltage and reactive power support. Grid-following and grid-forming converter are both limited by the same physical constraint and can usually provide up to 1.3 pu of overcurrent. The advantage of converters over synchronous condensers is that the converter can provide full rated current in both capacitive and inductive mode. Possible instability issues related to cascaded loops make the grid-following converter less attractive than other technologies. In a hybrid system, rating of the synchronous condenser is reduced and consequently the overloading capability is affected and less than that of standalone synchronous condenser. Additionally, if HSC is compared to a power converter, the inductive current rating is reduced due to the physical limitation of the SC.

Short-circuit current contribution from the synchronous machine is well known, and can be up to 4 times higher than the rated current, peaking at the moment a short-circuit occurs due to the fact that the subtransient reactance dominates at that stage. As already mentioned, the power converter is usually limited up to 1.3 pu of overloading current. The contribution of the HSC is diminished when compared to standalone synchronous condenser due to the lower rating of SC in HSC platform. Power converter control requires current limiting function for grid-forming architecture and a fault-ride-through strategy in case of grid-following converters.

AVR of the synchronous condenser has very low bandwidth and it is slow to respond to voltage regulation setpoint change. Additionally, the settling time of SC following a disturbance is measured in seconds and in these terms cannot compare to the fast acting power converter control, which can be few cycles or less. The slow response of the SC can be compensated by the fast acting converter control and give an edge to the HSC over standalone SC.

6.1.2 Supplementary Functions of HSC - Torsional Oscillation Damping and Inertia Maximisation

A significant advantage of the HSC system is the flexibility that provides in terms of supplementary function which can be added to the control structure. Oscillation damping has always been a challenging and costly task, and by using the already existing technology to provide damping to the system is a very efficient way of solving multiple problems with one solution. The shaft of a synchronous generator is in most cases comprised of several turbine shafts with each connection point generating an oscillation mode. The solution proposed in this work is a multiple generator, multi-modal torsional oscillation damping controller. It contains a loop for each individual oscillating mode. Each loop contains a filter to extract the specific oscillating signal, gain, and the phase compensator. For parameter tuning, a platform was set up where the simulations where performed in RTDS rack, while the optimization algorithm was running in Matlab. Small signal analysis showed a significant improvement in damping around critical frequencies. A method for scanning the damping factor over a frequency range has been implemented, witch is an efficient and quick way to evaluate damping in the system without having to build a small signal model. A simulation of larger disturbance done in RTDS validated the small signal analysis and showed no or minimal interaction between the control loops. And finally, a power hardware-in-a-loop

test demonstrated the validity of the proposed controller and provided insight in how the HSC capabilities can be expanded into other applications. One of the significant advantages of the controller is that it does not require access to the plant holding the affected generators, as it uses local voltage measurement as an input.

Synchronous condensers are essentially unloaded synchronous motors and have highly oscillatory behaviour. For a larger frequency disturbance, SC will be subjected to significant oscillations which can be detrimental in a low inertia system. The oscillating behaviour of the SC means that it will inject active power following a disturbance, but it will also absorb power as it swings around the nominal value (which is 0 active power for synchronous condenser). In a hybrid solution, battery energy system can be used to compensate the power absorbed by the SC and provide improved support of HSC during frequency events. The power measured at the terminal of SC is taken as the input to the controller. Rate of change of power measured at the terminal of the SC determines the level of compensation by BESS. The controller ensures that the level of power injected by HSC does not drop below the droop setting of the battery system. It was shown that the energy levels required for stable operation of the controller are very low, which implies that this implementation can be used with flywheel, while the energy can be provided by supercapacitor.

6.2 Future work

- Battery model used in the work is a simple electrical circuit equivalent which represents the internal chemistries of a battery cell. The model is based on a single battery cell and the performance of the entire battery pack is based on that study. A more detailed study on extrapolation of performance from single battery cell is needed, as well the evaluation of a thermal battery model and does it need to be included in some of the studies performed in this thesis.
- The simulations in this work have been conducted on a small system containing only HSC and the Thevenin source and impedance, and in several cases the the Thevenin source was replaced by a large synchronous machine. This implies that all the proposed solution need to be validated in a larger realistic system in order to provide validation bur also additional insights into actual benefits of such a solution in the practical sense.
- A large number of individual controllers and functions placed in a single component can potentially lead to stability issues due to the interaction and overlapping. A detailed study and possibly a supervisory design needs to be considered in order to prevent problems with interacting control loops.
- The dynamics of load and different load types have not been considered in this thesis, which means that a study is required which includes different load types and evaluates the performance of the HSC in such environment.
- Damping of local and interarea oscillations can potentially be implemented in a similar way as the damping for torsional oscillations. A study on a larger system with remote damping is potentially very useful for gaining insights if it is possible to provide damping for several plants from a single HSC unit. Finally, a controller design with adaptive damping, meaning that it can adjust phase and gain of the control loop based on the measured signal, would be an interesting prospect with possible inclusion of machine learning algorithms.

Litteratur

[1] UK National Grid ESO. Operating a low inertia system - a system operability framework document. Technical report, UK National Grid ESO, 2020.

[2] North American Electric Reliability Corporation NERC. Reliability guideline - improvements to interconnection requirements for bps-connected inverter-based resources. Technical report, North American Electric Reliability Corporation - NERC, 2019.

[3] UK National Grid ESO John West. Phoenix - impact of sc/h-sc on existing balancing schemes and markets. Technical report, UK National Grid ESO, 2021.

[4] Kanakesh Vatta Kkuni and Guangya Yang. âco-simulation for faster prototyping for new designs and controls,â. Technical report, Phoenix project deliverable report, 2018.

[5] Hongyang Zhang, Jean Philippe Hasler, Nicklas Johansson, Lennart Angquist, and Hans Peter Nee. Frequency response improvement with synchronous condenser and power electronics converters. *2017 Ieee 3rd International Future Energy Electronics Conference and Ecce Asia, Ifeec - Ecce Asia 2017*, pages 1002–1007, 2017.

[6] Michel Maher Naguib Rezkalla, Michael Gerold Pertl, and Mattia Marinelli. Electric power system inertia: Requirements, challenges and solutions. *Electrical Engineering*, 100(4):2677–2693, 2018.

[7] Australian Energy Market Commission AEMO. Fast frequency response market ancillary service. Technical report, Australian Energy Market Commission, 2021.

[8] Oriol Gomis-Bellmunt, Jie Song, Marc Cheah-Mane, and Eduardo Prieto-Araujo. Steady-state impedance mapping in grids with power electronics: What is grid strength in modern power systems? *International Journal of Electrical Power and Energy Systems*, 136:107635, 2022.

[9] Yang Zhang, Shun Hsien Fred Huang, John Schmall, Jose Conto, Jeffrey Billo, and Ehsan Rehman. Evaluating system strength for large-scale wind plant integration. *Ieee Power and Energy Society General Meeting*, 2014-(October):6939043, 2014.

[10] Kanakesh Vatta Kkuni and Guangya Yang. Effects of current limit for grid forming converters on transient stability: analysis and solution. page 8, 2021.

[11] National Grid ESO. Noa stability pathfinder â phase 1, 2021.

[12] ABB. Abb synchronous condenser packages, 2021.

[13] *Synchronous Condensers Application in Low Inertia Systems (SCAPP).*

[14] The massive integration of power electronic devices - migrate, 2020.

[15] Hybrid synchronous condenser solution - phoenix project, 2021.

[16] Mirza Nuhic and Guangya Yang. A hybrid system consisting of synchronous condenser and battery - enhanced services for weak systems. *Proceedings of 2019 Ieee Pes Innovative Smart Grid Technologies Europe, Isgt-europe 2019*, page 8905459, 2019.

[17] Hyeondeok Jo, Jeonghyeon Choi, Kofi Afrifa Agyeman, and Sekyung Han. Development of frequency control performance evaluation criteria of bess for ancillary service: A case study of frequency regulation by kepco. *2017 Ieee Innovative Smart Grid Technologies - Asia: Smart Grid for Smart Community, Isgt-asia 2017*, pages 1–5, 2017.

[18] Paul Vincent Brogan, Robert J. Best, D. John Morrow, Kenneth McKinley, and Marek L. Kubik. Effect of bess response on frequency and rocof during underfrequency transients. *Ieee Transactions on Power Systems*, 34(1):575–583, 2019.

[19] Christian Julien, Alain Mauger, Ashok Vijh, and Karim Zaghib. *Lithium Batteries: Science and Technology*. Springer International Publishing, 2015.

[20] Dennis W. Dees, Vincent S. Battaglia, and AndrÃ© BÃ©langer. Electrochemical modeling of lithium polymer batteries. *Journal of Power Sources*, 110(2):310–320, 2002.

[21] Shuhui Li and Bao Ke. Study of battery modeling using mathematical and circuit oriented approaches. *Ieee Power and Energy Society General Meeting*, page 6039230, 2011.

[22] Hanlei Zhang and Mo Yuen Chow. Comprehensive dynamic battery modeling for phev applications. *Ieee Pes General Meeting, Pes 2010*, page 5590108, 2010.

[23] Min Chen and Gabriel A. RincÃ$^3 n - Mora. Accurateelectricalbatterymodelcapableofpredictingruntimeandi - vperformance. IeeeTransactionsonEnergyConversion, 21(2) : 504 - -511, 2006.$

[24] Evgenij Barsoukov and J. Ross Macdonald. *Impedance Spectroscopy: Theory, Experiment, and Applications*. John Wiley and Sons, 2005.

[25] Wladislaw Waag, Christian Fleischer, and Dirk Uwe Sauer. Critical review of the methods for monitoring of lithium-ion batteries in electric and hybrid vehicles. *Journal of Power Sources*, 258:321–339, 2014.

[26] DIgSILENT GmbH. *DIgSILENT PowerFactory 2018 - User Manual*. 2018.

[27] Ana Irina Stroe, Daniel Ioan Stroe, Maciej Swierczynski, Remus Teodorescu, and SÃ¸ren Knudsen KÃ¦r. Lithium-ion battery dynamic model for wide range of operating conditions. *Proceedings - 2017 International Conference on Optimization of Electrical and Electronic Equipment, Optim 2017 and 2017 Intl Aegean Conference on Electrical Machines and Power Electronics, Acemp 2017*, pages 660–666, 2017.

[28] National Grid UK. The grid code. Technical report, National Grid UK, 2019.

[29] Phoenix project, international review, 2019.

[30] Ha Thi Nguyen, Guangya Yang, Arne Hejde Nielsen, and Peter HÃ¸jgaard Jensen. Combination of synchronous condenser and synthetic inertia for frequency stability enhancement in low inertia systems. *Ieee Transactions on Sustainable Energy*, 10(3):997–1005, 2018.

[31] Y Katsuya, Y Mitani, and K Tsuji. Power system stabilization by synchronous condenser with fast excitation control. *2000 International Conference on Power System Technology, Vols I-iii, Proceedings*, pages 1563–1568, 2000.

[32] Fan Shixiong, Han Wei, Wang Wei, Luo Chaolong, Xu Guorui, Wang Wei, Zhang Peng, and Fu Jiayu. Influence of synchronous condenser transient parameters on voltage stability of hvdc. *Proceedings of the 2018 13th Ieee Conference on Industrial Electronics and Applications (iciea 2018)*, pages 2015–2020, 2018.

[33] Jundi Jia, Guangya Yang, Arne Hejde Nielsen, Peter Weinreich-Jensen, Eduard Muljadi, and Vahan Gevorgian. Synchronous condenser allocation for improving system short circuit ratio. *Proceedings of 5th International Conference on Electric Power and Energy Conversion Systems*, page 8443358, 2018.

[34] Shuaixun Chen, Tian Zhang, H. B. Gooi, Ralph D. Masiello, and Warren Katzenstein. Penetration rate and effectiveness studies of aggregated bess for frequency regulation. *Ieee Transactions on Smart Grid*, 7(1):167–177, 2016.

[35] Yongli Zhu, Bin Wang, and Kai Sun. Damping control for power systems using energy storage. *2017 29th Chinese Control and Decision Conference (ccdc)*, pages 3730–3735, 2017.

[36] Zhuang Cai, Christian Bussar, Philipp StÃ¶cker, Luiz Moraes, Dirk Magnor, Matthias Leuthold, and Dirk Uwe Sauer. Application of battery storage for compensation of forecast errors of wind power generation in 2050. *Energy Procedia*, 73:208–217, 2015.

[37] Tingting Yang, Xiangjun Li, Lei Qi, Dong Hui, and Xuecui Jia. A schedule method of battery energy storage system (bess) to track day-ahead photovoltaic output power schedule based on short-term photovoltaic power prediction. *Iet Conference Publications*, 2015(679):4, 2015.

[38] Phoenix project, 2020.

[39] R.A. Rivas, A. Owens, F. Wang, E. Arnsten, R. Rui, and C. Foote. Phoenix: The worldâs first hybrid synchronous condenser system. In *CIGRE Session 48, Paris*, 2020.

[40] Mirza Nuhic and Guangya Yang. A hybrid system consisting of synchronous condenser and battery - enhanced services for weak systems. In *2019 IEEE PES Innovative Smart Grid Technologies Europe (ISGT-Europe)*, pages 1–5, 2019.

[41] L. Zhang, L. Harnefors, and H. Nee. Power-synchronization control of grid-connected voltage-source converters. *IEEE Transactions on Power Systems*, 25(2):809–820, 2010.

[42] Mengran Yu, Richard Ierna, Adam Dyśko, Agustí Egea-Àlvarez, Andreas Avras, Can Li, Mark Horley, Campbell Booth, Helge Urdal, et al. Performance of hybrid power park technologies in future ofto networks with the aim to achieve grid-forming capability. In *19th Wind Integration Workshop*, 2019.

[43] Valentin Muenzel, Marcus Brazil, Iven Mareels, Julian De Hoog, and Doreen A. Thomas. Modeling reversible self-discharge in series-connected li-ion battery cells. *Ieee 2013 Tencon - Spring, Tenconspring 2013 - Conference Proceedings*, pages 470–474, 2013.

[44] Eduardo Redondo-Iglesias, Pascal Venet, and Serge Pelissier. Global model for self-discharge and capacity fade in lithium-ion batteries based on the generalized eyring relationship. *Ieee Transactions on Vehicular Technology*, 67(1):104–113, 2018.

[45] Ieee recommended practice for excitation system models for power system stability studies, 2016.

[46] Eli Pajuelo, Ramakrishna Gokaraju, and M. S. Sachdev. Coordination of overexcitation limiter, field overcurrent protection and generator control. *Ieee Pes General Meeting, Pes 2010*, page 5589734, 2010.

[47] Nationalgrideso. Operability strategy report 2021. Technical report, Nationalgrideso, 2021.

[48] ENTSO-E guidance document for national implementation for network codes on grid connection. Fault current contribution from ppms & hvdc. Technical report, Draft of Expert Group FFCI, 2017.

[49] Inertia2020 Working Group. Technical requirements for fast frequency reserve provision in the nordic synchronous area â external document. Technical report, ENTSO-E, 2020.

[50] National Grid Electricity System Operator. The Grid Code (Uk). (5):0–1014, 2020.

[51] Ha Thi Nguyen, Guangya Yang, Arne Hejde Nielsen, et al. Frequency stability enhancement for low inertia systems using synthetic inertia of wind power. In *2017 IEEE Power & Energy Society General Meeting*, pages 1–5. IEEE, 2017.

[52] *Phoenix â System Security and Synchronous Condenser*.

[53] Prabha Kundur. *Power System Stability and Control*. McGraw-Hill Education,, 22 Jan 1994.

[54] Xiaorong Xie, Ping Liu, Kai Bai, and Yingduo Han. Applying improved blocking filters to the ssr problem of the tuoketuo power system. *IEEE Transactions on Power Systems*, 28(1):227–235, 2012.

[55] RG Farmer, AL Schwalb, and Eli Katz. Navajo project report on subsynchronous resonance analysis and solutions. *IEEE Transactions on Power Apparatus and Systems*, 96(4):1226–1232, 1977.

[56] CEJ Bowler, DH Baker, NA Mincer, and PR Vandiveer. Operation and test of the navajo ssr protective equipment. *IEEE Transactions on Power Apparatus and Systems*, (4):1030–1035, 1978.

[57] Rajiv K Varma, Soubhik Auddy, and Ysni Semsedini. Mitigation of subsynchronous resonance in a series-compensated wind farm using facts controllers. *IEEE transactions on power delivery*, 23(3):1645–1654, 2008.

[58] Xi Wu, Shuang Feng, Ping Jiang, Gang Xu, and Xiang Yang. An ssr multichannel damping control scheme for tcsc considering multiple operating conditions. *International Transactions on Electrical Energy Systems*, 26(12):2759–2773, 2016.

[59] Xiaorong Xie, Huakun Liu, and Yingduo Han. Sedc's ability to stabilize ssr: A case study on a practical series-compensated power system. *IEEE Transactions on Power Systems*, 29(6):3092–3101, 2014.

[60] National Grid ESO. Stability pathfinder â oct 2019, draft grid code â grid forming and request for information feedback. Technical report.

Department of Electrical Engineering
Center for Electric Power and Energy (CEE)
Technical University of Denmark
Elektrovej, Building 325
DK-2800 Kgs. Lyngby
Denmark

www.elektro.dtu.dk/cee
Tel: (+45) 45 25 35 00
Fax: (+45) 45 88 61 11
E-mail: cee@elektro.dtu.dk